Modelo Coloidal para Crecimiento Epitaxial en Una Dimensión

Colloidal Model for Epitaxial Growth in One Dimension

Juan David Álvarez Cuartas
Proyecto de investigación
Maestría en Ciencias-Física (Código 7178)

Director:
Ph.D. Diego Luis González Cabrera

Grupo de Investigación:
Física Teórica del Estado Sólido

Universida del Valle
Facultad de Ciencias Naturales y Exactas
Departamento de Física
Santiago de Cali, 2024

Abstract

Through a one-dimensional colloidal model for epitaxial growth, we characterize the nucleation and aggregation processes occurring in a gap between adjacent islands. The timescales associated with deposition, diffusion, aggregation, and nucleation inside the gap are studied in terms of the parameters defining the interaction between colloidal particles. Numerical results from molecular dynamics (MD) simulations are compared with those from analytical models, and good agreement between both data sets is found. The analytical and numerical results for the timescales are used to calculate the associated rates to generate kinetic Monte Carlo (kMC) simulations, which allow exploring larger systems and longer timescales in comparison with MD simulations. The kMC simulations reproduce the global behavior of the densities of islands and monomers and the gap length distribution between adjacent islands.

Keywords: Epitaxial Growth, Two-Step Protocol, Morse potential, colloids, time scales, diffusion, aggregation, nucleation, master equation, Fokker-Planck equation, fragmentation equation, computational simulation, molecular dynamics, kinetic Monte Carlo.

Resumen

A través de un modelo coloidal unidimensional para crecimiento epitaxial, se caracterizaron los procesos de nucleación y agregación que ocurren en un espaciamiento entre islas adyacentes. Las escalas de tiempo asociadas con la deposición, difusión, agregación y nucleación dentro de un espaciamiento son estudiadas en términos de los parámetros que definen la interacción entre partículas coloidales. Los resultados numéricos de simulaciones de dinámica molecular (MD) son comparados con los dados por los modelos analíticos y se encuentra una buena concordancia entre ambos conjuntos de datos. Los resultados numéricos y analíticos para las escalas de tiempo se utilizan para calcular las tasas asociadas para generar simulaciones cinéticas de Monte Carlo (kMC), las cuales permiten explorar sistemas más grandes y escalas de tiempo más largas en comparación con las simulaciones MD. Mediante las simulaciones de kMC se logró reproducir el comportamiento global de las densidades de islas y monómeros, así como la distribución de la longitud de los espacios entre islas adyacentes.

Palabras clave: Crecimiento epitaxial, Protocol en dos pasos, potencial de Morse, partículas coloidales, escalas de tiempo, difusión, agregación, nucleación, ecuación maestra, ecuación de Fokker-Planck, ecuación de fragmentation, simulaciones computacionales, dinámica molecular, Monte Carlo cinético.

Acknowledgments

I want to express my deepest gratitude to my family, whose unwavering support and encouragement have been the foundation of my journey. To my friends, thank you for your companionship and always being there through the highs and lows. I am also immensely grateful to the faculty, staff, and administration of the University for their guidance, dedication, and the resources they provided, which have been instrumental in the completion of this work.

I want to extend my deepest gratitude to Professor Diego Luis for their exceptional guidance throughout this long journey, from the start of the first statistical mechanics course, through the bachelor thesis, until now, the end of the masters. His insightful advice, unwavering support, and commitment to excellence have been invaluable to my development as a researcher. His mentorship has not only shaped the direction of this work but has also profoundly influenced my growth, both academically and personally. Thank you for your patience, wisdom, and for always challenging me to strive for the best.

I would also like to sincerely thank Professor Manuel Camargo for his invaluable assistance with this project. Your expertise, thoughtful feedback, and willingness to collaborate have significantly contributed to the success of this work.

Contents

List of Figures

List of Symbols

Below are included the main general symbols, as Greek and Latin letters, subscripts, and abbreviations that will be used in the present document.

Symbols with Latin letters

Symbol	Term	Definition
k_BT	Energy unit	
m	Mass unit	
A, B	Denotes particle type.	
$\vec{F}$	Sedimentation field.	$\vec{F} = -F\hat{j}$
D_0	Diffusion coefficient in the suspension.	$D_0 = k_BT/\zeta_0$
L	Gap length.	$L = \sigma N$
N	Number of lattice sites.	
$\vec{n}(t)$	Stochastic force.	
$\mathcal{V}_{ij}(r)$	Potential strength between i and j colloids.	
r_{cut}	Potential cut-off distance.	$r_{cut} = 1.6\sigma$
q	Polymer-colloid size ratio.	$q = \sigma_{pol}/\sigma_{col}$
$\mathcal{A}_{AA}$	Colloid-Colloid interaction constant.	$\mathcal{A}_{AA} = 8.8\, k_BT$,
$\mathcal{A}_{AB}$	Colloid-Island interaction constant.	$\mathcal{A}_{AB} = 8.0\, k_BT$
$\mathcal{F}$	Flux of colloids towards the substrate.	
$P(y,t)$	Probability distribution function of the height y.	
a_1	Fokker-Planck equation parameter.	$a_1 = -F/\zeta_0$,
a_2	Fokker-Planck equation parameter.	$a_2 = \frac{1}{2}(\nu/\zeta_0)^2$
J	Stationary flux of colloids.	
L_x, L_y	Horizontal/Vertical length of the simulation box.	
$D(y)$	Diffusion coefficient on a periodic potential.	

$V(x,y)$	Lattice potential.	
$P(x,y,t)$	Equilibrium distribution.	$P(x,y,t) \approx C\, e^{-\beta V(x,y)}$
$p_x(x)$	Marginal probability, colloid position inside a gap.	$p_x(x) = \int_0^\infty dy\, P(x,y,t)$
$p_x(x)$	Marginal probability, colloid height relatively to the substrate.	$p_y(y) = \int_0^\infty dx\, P(x,y,t)$
D	Effective lateral diffusion coefficient.	$D \approx D(\sigma) p_y(\sigma)$
$p_n(t)$	Probability to have a single colloid to be on site n at time t on the substrate.	
$W_{m,n}$	Transition rate from site m to n.	$W_{m,n} = 1/(2\tau)$
$P_s(t)$	Survival probability at time t.	$P_s(t) = e^{-t/\tau_{\rm res}}$
$P_{\rm res}(t)$	Residence probability at time t.	$P_{\rm res}(t) = -\frac{dP_s(t)}{dt}$
q_{n+1}	Probability of having $(n+1)-$colloids simultaneously on the substrate.	
$\mathcal{R}$	Control parameter.	$\mathcal{R} = D/\mathcal{F}$
$p_{m,n}(t)$	Probability to have two colloids on site m and n, respectively, at time t on the substrate.	
$\tilde{p}_{m,n}(t)$	Auxiliary initial conditions.	
$Y_k(m)$, B_{kj}	Coefficients from two-colloid master equation.	
$\mathcal{P}(n)$	Nucleation probability at site n.	
$p_{MF}(n)$	Nucleation probability in the mean-field approximation.	
g	Conditional probability of a nucleation event inside, a gap given two colloids are already present.	$g = \sum_{n=1}^{N} \mathcal{P}(n)$
$W(t)$	Wannier process.	
$R_t(t)$	Uncorrelated Gaussian noise.	
$F(x,y)$	Breakup rate.	
$c(x,t)$	Density of fragments with size $(x, x+dx)$ at time t.	
$R(s)$	Total breakup rate.	
$P_n^{xy}(s)$	Probability that a nucleation occurs at relative position x inside a gap of length y.	
$P_n^{x}(s)$	Probability that a nucleation occurs at relative position x inside a gap of any length y.	
$P_n^{y}(s)$	Probability that a nucleation occurs at any site inside a gap of length y	.
$F_M(s)$	Number of fragments with size s given that are M	

	fragments already.	
$p^{(k)}(s)$	$k-$th order spacing distribution function.	
$\tilde{p}^{(0)}(s)$	Laplace transform of $p^{(0)}(s)$.	
$g(x)$	Pair correlation function.	$g(x) = \sum_{n=0}^{\infty} p^{(n)}(x)$
$P_{\mathrm{PV}}(s)$	Size distribution function of the Voronoi cells.	
$\mathcal{N}_1$	Density of monomers.	
$\mathcal{N}$	Density of islands.	

Symbols with Greek letters

Symbol	Term	Definition
σ	Diameter/Length unit	
	Length unit	
τ_{md}	Thermalization time	$\tau_{md} = \sqrt{m\sigma^2/(k_B T)}$
	Time unit	
α	Interaction strength	
σ_{pol}	Polymer size	
σ_{col}	Colloid size	
ζ_0	Drift constant	
η	Number of repetitions	
δ_{ij}	Kronecker delta	$\delta_{ij} = \begin{cases} 1, & \text{if} \quad i = j, \\ 0, & \text{otherwise} \end{cases}$
$\delta(t)$	Delta Dirac	$f(t) = \int_{-\infty}^{\infty} dt' f(t')\delta(t - t')$
β	Inverse temperature	$\beta = 1/(k_B T)$
ν	Stochastic force strength	
$\rho(t)$	Density of colloids in the suspension	
τ_{dep}	Time between consecutive depositions	$\tau_{\mathrm{dep}} = 1/(\mathcal{F} L_x)$
τ	Hopping rate	$\tau = 1/(2D)$
τ_{res}	Residence time	$\tau_{\mathrm{res}} = \tau \left(\frac{\epsilon N}{1-\epsilon} + \frac{(N+1)(N+2)}{6} \right)$
ρ_n	Stationary density of colloids on the substrate	$\rho_n = \frac{\tau}{N} \left(\frac{\epsilon N}{1-\epsilon} + (1+N)n - n^2 \right)$
ϵ	Colloid-Island interaction constant	$0 \leq \epsilon \leq 1$

Symbol	Term	Definition
Δt	Time-step	
ω	Nucleation rate inside a gap	$\omega = g\, q_2\, \mathcal{F}\, L,$
λ	Scaled length	$\lambda = n/N$
γ	Model parameter	$\gamma = 1, 2, 3, 4$
μ_γ	$\gamma-$th order moment of spacing distribution function	
θ	Coverage	$\theta = \mathcal{F}t$

Abbreviations

Abbreviation	Term
EG	Epitaxial Growth
kMC	Kinetic Monte Carlo
2SG	Two-Step Growth
CZ	Capture Zone
AO	Asakura-Oosawa
NP	Nanoparticles
FP	Fokker-Planck
MD	Molecular Dynamics
LAMMPS	Large-Scale Atomic/Molecular Massively Parallel Simulator
FE	Fragmentation Equation

Introduction

The study of epitaxial growth (EG) has been important due to its relevance in solid-state physics, materials science, and semiconductor technology. The understanding of the microscopic mechanisms related to the deposition and growth processes is required to achieve control of the material properties for a wide range of applications, such as, the assembly of nanostructures [3–5] for the construction of electronic devices and photosensors [6–8]; improvement of solar and fuel cells [9–12] and even development of nanowire sensors for medicine and the life sciences [13]. The main industrial interest in EG is because it offers the possibility of building nano-structures in a controlled way that allows the fabrication of high-quality semiconductors and nanodevices [14–16].

In standard EG, the basic growth units, monomers, are sequentially deposited at a controlled rate onto a substrate. The deposited monomers are captured by the potential associated with the substrate. These monomers are called adatoms, which stands for absorbed atoms, and they can freely diffuse on the substrate until they interact with other adatoms making groups of stable adatoms, called islands, or until they aggregate to other preexisting islands, which grow to form layers, as shown in Fig. 1.

The growth properties are highly depend on the microscopic nature of the substrate. In general, two types of structures are used in EG: (i) rough surfaces (stepped surfaces) or (ii) smooth surfaces (atomically flat). The latter case is the one considered in this project. Therefore, basic models to describe EG, from a microscopic perspective, must involve at least three fundamental processes, such as the transport of adatoms on the substrate (diffusion), the formation of islands (nucleation), and the growth of islands (aggregation). All these processes have been widely studied during the last two decades [17–26], using different analytical approaches like rate equations and computational simulations based on kinetic Monte Carlo (kMC) [22, 27–29].

Consequently, at least three different time scales are required to describe the relevant microscopic processes during growth. For a long time, the system reaches a quasi-steady state where the colloid density is much smaller than the island density. In this way, nucleation remains relevant in the temporal evolution of the island density. Both nucleation and aggregation must be considered simultaneously. The time scale associated with aggregation must also be included along with those mentioned earlier [30, 31].

To improve control and facilitate understanding of growth processes, Tokar and Dreyssé [31] proposed an unconventional deposition process as an alternative to the standard EG. This new process is called the two-step growth (2SG) protocol, see Fig. 1, because it consists of two

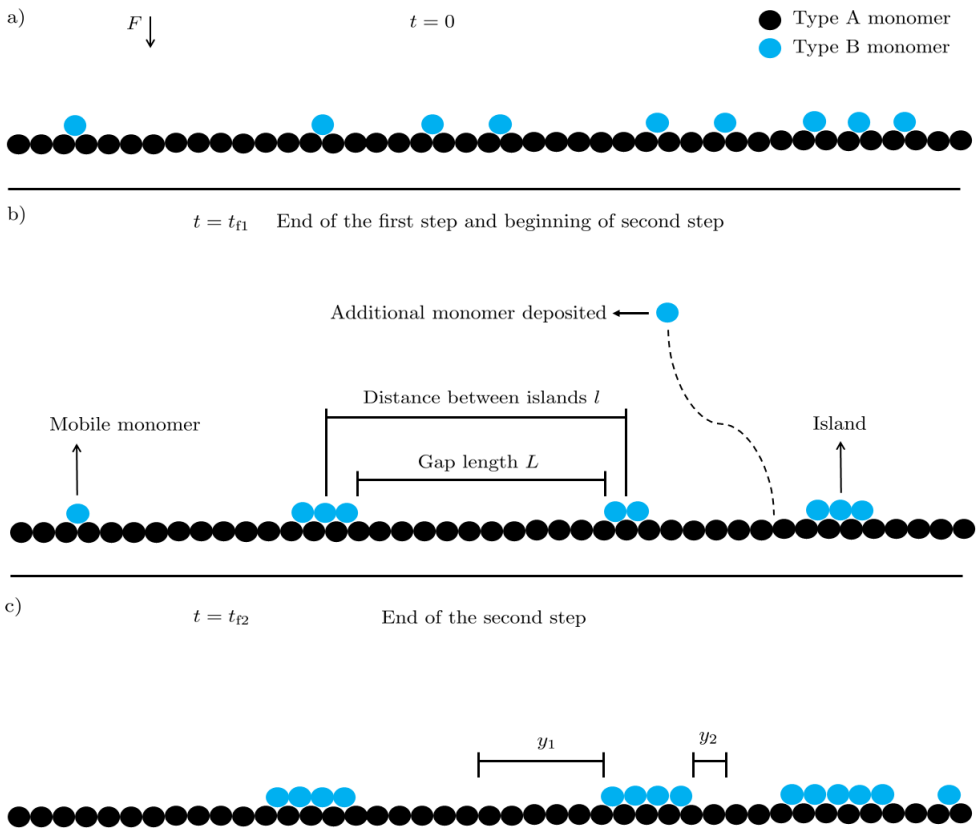

Figure 1: (a) At $t = 0$ few monomers are deposited on the substrate. (b) At the end of the first step, $t = t_{f1}$ most of the monomers are grouped in small islands and the presence of mobile monomers is unlikely. The gap length and distance between an island of size three and its neighbor of size two is indicated. During the second step, additional monomers are deposited, the time between two consecutive depositions guarantees that new nucleation processes hardly occurs. (c) At $t = t_{f2}$ the process ends. At this point, the capture zone (CZ) corresponding to the island with size four is also indicated. This figure appears as Figure 1 in Ref. [1].

phases. In the first phase, a small number of monomers are simultaneously deposited on the substrate. Experimentally, this can be achieved by rapidly depositing monomers on a substrate at low temperatures [32–34]. After deposition, the substrate temperature is raised, increasing diffusivity, and monomers start to diffuse, eventually forming islands. At the end of the first step, the system reaches an equilibrium state characterized by the absence of free colloids. In the second phase, additional colloids are sequentially deposited at a constant rate. In this way, the colloids deposited in the second step mainly aggregate to the islands formed in the first step. In the second step, only aggregation is relevant because nucleation is a rare event since the typical time between consecutive depositions is much longer than the aggregation time, making the simultaneous presence of two or more monomers at the substrate unlikely. In the 2SG protocol, nucleation and aggregation occur in two distinct stages of growth. In the first step, aggregation is negligible, whereas in the second step, nucleation is negligible. This protocol simplifies the control over the growth processes due to the separation of nucleation

and aggregation in different time regions. Regardless of the growth protocol used, it is clear that the behavior of the systems depends on the relative values of the time scales associated with each of the fundamental processes: diffusion, deposition, aggregation, and nucleation. These processes are of great interest since they determine the mechanical and electrical properties of the resulting structures [35, 36]. However, the theoretical models proposed so far have not provided a complete description of various quantities of interest, such as the critical island size, the time evolution of island density, the island size distribution, and the capture zone distribution [17–21, 25, 26, 37].

On the other hand, in the last decades the paradigm of understanding colloids as “super atoms” has emerged, motivating the study of colloidal systems as models to describe phenomena in the field of condensed matter [38]. In the particular case of the growth of crystalline layers on substrates, the term “colloidal epitaxy” was introduced, and corresponds to a process in which the slow sedimentation of the colloids [32–34] on a substrate allows the formation of colloidal crystals, allowing easy control over the structure of the lattice, such as the orientation and size of the resulting crystal [39–41]. These studies allow us to conclude that the nature of the colloidal epitaxy is similar to that found in atomic epitaxy. However, the time scales associated with each process are not necessarily of the same order of magnitude. Similarly, studies based on computational simulations of colloidal systems have given results about the role of the tension field of the substrate in the dynamics of island formation and the morphology of the resulting islands [42]. Nevertheless, most studies about the formation of ordered colloidal structures have been performed only on bulk and under equilibrium conditions. In practice, the results obtained through computational simulations of colloidal epitaxy can be reproduced experimentally, allowing a better understatement of the related processes with the growth of monolayers and the relevant interactions in the formation of the island [43, 44].

Currently, there is a wide variety of techniques aimed at producing mono or multi-layers of colloidal particles from a dilute colloid suspension. In the most commonly used growth protocol, colloids are deposited onto the substrate as a result of the action of an external field, allowing the production of monolayers with controlled coverage and structure. The deposition rate is regulated by the particle concentration in the suspension, the nature of the substrate, and the intensity of the external field. This growth method corresponds essentially to the standard EG protocol described before.

In a one-dimensional model, the islands divide the substrate into independent segments called gaps, where a gap refers to the space between two consecutive islands. Also, in one dimension, the spatial fluctuations of the density of monomers are relevant. Therefore, a detailed description of the nucleation and aggregation processes is necessary to describe the behavior of the system, more specifically, the capture kernels associated with nucleation and aggregation in a gap are directly related to the time evolution of the densities of islands and monomers. Another drawback of one dimensional systems is that the standard mean-field approaches does not work well. In that sense, from a theoretical perspective one-dimensional models are more challenging than their two-dimensional counterpart.

The relevant processes, such as, deposition, diffusion, aggregation and nucleation inside the gap allow us to define the time scales by which the system evolves and describe it in terms

of the parameters defining the interaction between colloidal particles in the submonolayer regime [23, 24, 45]. Furthermore, knowledge of the nucleation and aggregation rates, in conjunction with the appropriate fragmentation equation makes it possible to evaluate the gap length distribution between adjacent islands.

In this investigation project, we will study, theoretically and by computational simulations, the nucleation and aggregation processes inside a single gap for a colloidal model, where the interactions are modeled by means of the Morse potential. The integration of the equations of motion for the colloids is carried out using the BAOAB algorithm [46]. This algorithm provides a good balance between efficiency and precision and has already been successfully used to determine the diffusion coefficient and the deposition rate in colloidal systems [1, 23, 30, 45, 47]. The distributions associated with the relevant time scales can be measured directly in computational simulations and compared with results reported in the literature from analytical models based on reaction-diffusion systems. Finally, we use the results for a single gap to describe the behavior of a system with many gaps.

This thesis is divided as follows. In Chapter 1, the single gap system and its fundamental time scales are described. Chapter 2 is devoted to the relevant details of the MD simulations. Chapter 3 presents the obtained results along with a complete discussion of them. In Chapter 4, the results for the time scales of a single gap are used to describe the time evolution of a one-dimensional system with many consecutive gaps. Finally, in Chapter 5, some conclusions and perspectives are given. The main results of this thesis were summarized in Ref. [2] and a recent review about the one-dimensional EG written by us can be found in Ref. [48], also see Appendix D.

Chapter 1

Colloidal Dynamics in One-Dimension

This chapter provides a comprehensive analytical overview of the fundamental processes describing the behavior of one and two colloids confined in a gap. The dynamic of the colloids is explored in detail through analytical models that describe the fundamental processes: diffusion, deposition, aggregation, and nucleation.

1.1 Gap Description

Consider a section of a one-dimensional substrate, define by two adjacent islands, as shown in Fig. 1.1. The islands are considered immobile, stable, and formed by monomers of type A, while the immobile particles of the substrate are type B. All monomers have diameter σ and mass m, and they are under the influence of a constant external sedimentation field $\vec{F}$. The temperature of the suspension is T, and D_0 denotes the diffusion coefficient of a particle in the suspension. Henceforth, the parameters σ, m, k_BT, and $\tau_{\rm md}$ are defined as length, mass, energy, and time units, respectively. The time scale for the numerical simulations is defined as $\tau_{\rm md} = \sqrt{m\sigma^2/(k_BT)}$ where k_B is the Boltzmann constant.

1.1.1 The Morse Potential

In the last decade experimental results have been published indicating that the laws governing island growth in atomic and colloidal epitaxy have common characteristics [49–51]. Many of the experimental studies on colloidal epitaxy take advantage of the depletion interaction between colloidal particles, which can be caused by the presence of smaller non-adsorbing polymers in the suspension. The main feature of this attractive (effective) interaction is that its range and strength can be easily tuned by the variation of the size and the concentration of the polymers.

An analytical expression for the functional form of this interaction in terms of the polymer properties (size and concentration) is provided by the so-called Asakura–Oosawa (AO) potential [52, 53]. However, in the AO potential the repulsive contribution is considered to be a hard-core

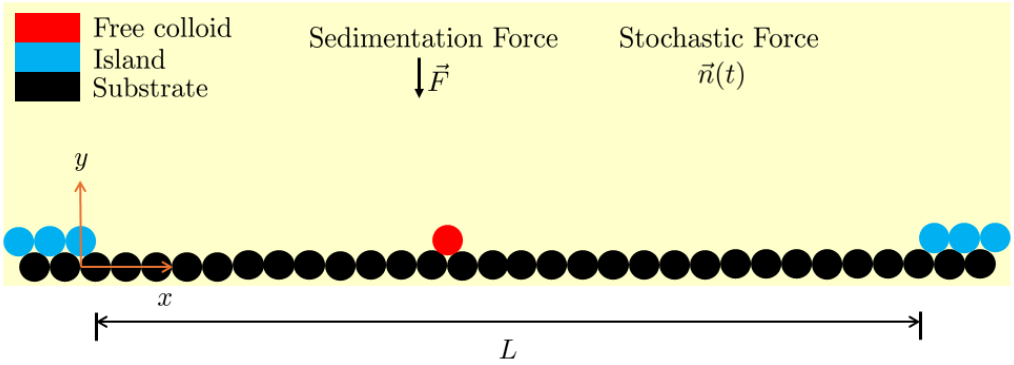

Figure 1.1: One free monomer (red circle) inside a gap of length $L = \sigma N$ between two fixed islands (blue circles). Both red and blue are A-type articles, while the substrate is formed by B-type particles (black circles). The system is subject to a constant sedimentation force $\vec{F}$ that drives the colloids towards the substrate. Also the system is immerse in a suspension (pale yellow background) which is modeled implicitly through a stochastic force $\vec{n}(t)$.

interaction. To avoid discontinuous potentials which could cause problems in MD simulations, the AO expression can be approximated by the Morse potential, $\mathcal{V}_{ij}(r)$, given by

$$\mathcal{V}_{ij}(r) = \begin{cases} \mathcal{A}_{ij}\left(e^{-2\alpha(r-\sigma)} - 2e^{-\alpha(r-\sigma)}\right) & r \leq r_{\text{cut}}, \\ 0 & r > r_{\text{cut}}, \end{cases} \tag{1.1}$$

where r is the center-to-center distance between two colloidal particles. Parameters $\mathcal{A}_{ij}$ with $i, j = A, B$; α and r_{cut} determine the strength, range, and cut-off distance of the interaction potential, respectively.

In Fig. 1.2, is shown the comparison between Eq. (1.1) and the AO potential whose attractive well extends over a range equivalent to that of a system with a polymer-to-colloid size ratio $q = \sigma_{\text{pol}}/\sigma_{\text{col}} = 0.15$. It can be seen that the Morse potential provides a good approximation to the AO potential.

In addition, experimental results in film self-assembly experiments of ligand-coated colloidal nanoparticles (NP) adsorbed at toluene-air interfaces, provided solid proof that the process of NP island nucleation and growth during drop-drying is similar to epitaxial growth [54]. In these experiments the effective representations of the potential between the NPs adsorbed at the toluene-air interface are considered. These potentials take into account the van der Waals interaction between the cores as well as the ligand-ligand and ligand-toluene interactions.

The resulting potentials display qualitative features that would be very well fitted by the Morse potential, therefore, this will be considered to model the interactions between the different types of colloids.

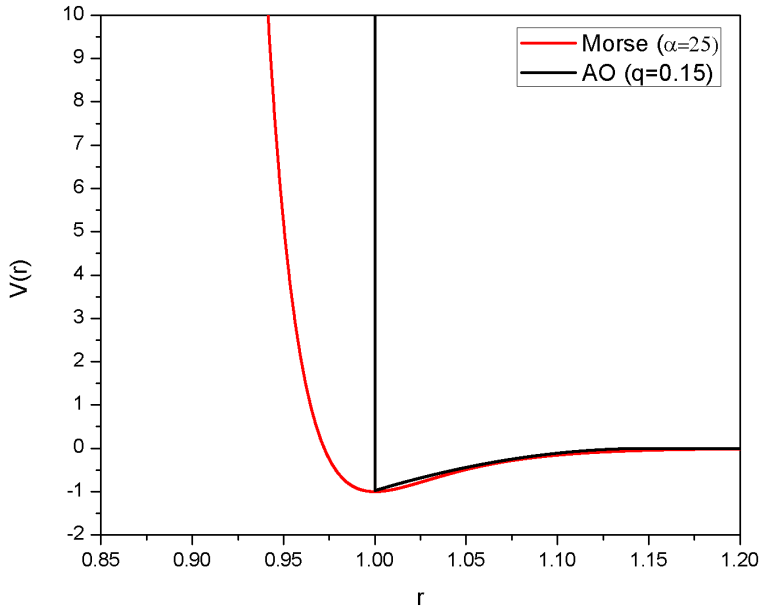

Figure 1.2: Asakura-Oosawa and Morse interaction potentials between two colloidal particles. The AO potential is calculated for a polymer-to-colloid size ratio $q = 0.15$ while the Morse potential is evaluated for $\alpha = 25$.

1.1.2 Langevin Dynamics

In our model, colloids evolve according to Langevin dynamics, in such a way that the position of the i-th colloid, $\vec{r}_i$, evolves according to

$$m\,\frac{d^2\vec{r}_i}{dt^2} = -\,\zeta_0\,\frac{d\vec{r}_i}{dt} + \nu\,\vec{n}(t) + \vec{F}_i(t), \tag{1.2}$$

where $\vec{F}_i(t)$ is the total force on the i-th colloid due to the external field and all the other colloidal particles. The interaction with the solvent is taken into account implicitly through parameters $\zeta_0 = m/\tau_{md}$ and $\nu = (2\zeta_0 k_B T)^{1/2}$, where the later is the intensity of the stochastic force and is chosen to satisfy the Fluctuation-Dissipation Theorem [55], see Appendix A. The stochastic variable $\vec{\eta}(t)$ satisfy the following conditions

$$\langle \vec{n}(t) \rangle_\eta = 0 \quad \text{and} \quad \langle n_i(t)\, n_j(t') \rangle_\eta = \delta_{ij}\,\delta(t-t'), \tag{1.3}$$

where terms $n_i(t)$ is the $i-th$ component of $\vec{n}(t)$, while $\langle\cdot\rangle_\eta$ indicates the ensemble average. Finally, δ_{ij} and $\delta(t-t')$, represent the Kronecker delta and the Dirac delta function, respectively. The relations given in Eq. (1.3) ensure that the stochastic variable follows a Gaussian distribution with zero average and that the system has a Markovian evolution.

1.1.3 System Parameters

The advantage of using colloidal particles is the possibility to control the interaction between colloids to reproduce the desired dynamics. As shown in Ref. [1], $\mathcal{A}_{AA} = 8.8k_BT$, $\mathcal{A}_{AB} = 8.0k_BT$, $\alpha = 25/\sigma$ and $r_{\rm cut} = 1.6\sigma$, allows the stable growth of islands in the submonolayer regime with a negligible detachment of colloids from the substrate. Therefore they will be those used in the simulations in this document unless otherwise specified.

1.2 Dynamics in the Suspension

The suspension parameters ζ_0 and ν together with the external constant sedimentation field $\vec{F}_s = -F\,\hat{j}$ determine the dynamics of the colloidal particles in the suspension, such as, the diffusion coefficient in the suspension D_0 and the flux of particle towards the substrate $\mathcal{F}$.

1.2.1 Diffusion Coefficient

The diffusion coefficient of a colloid moving through the suspension without external field can be calculated from the mean-square displacement, as follows:

$$\begin{aligned}\left\langle (\vec{r}(t) - \vec{r}(t_0))^2 \right\rangle_\eta &= \left\langle \left(\int_{t_0}^{t} dt'\, \vec{v}(t') \right)^2 \right\rangle_\eta , \\ &= \left\langle \int_{t_0}^{t} dt_1\, \vec{v}(t_1) \int_{t_0}^{t} dt_2\, \vec{v}(t_2) \right\rangle_\eta , \\ &= \int_{t_0}^{t} dt_1 \int_{t_0}^{t} dt_2\, \langle \vec{v}(t_1) \cdot \vec{v}(t_2) \rangle_\eta , \end{aligned} \tag{1.4}$$

The integrals given in Eq. (A.11) are discussed in Appendix A where it was found, performing the integrals, we obtain the following result

$$\begin{aligned}\left\langle (\vec{r}(t) - \vec{r}(t_0))^2 \right\rangle_\eta &= \left(\vec{v}^2(0) - \frac{\tau\,\nu^2}{m^2} \right) \tau_{md}^2 \left(1 - e^{-(t-t_0)/\tau_{md}} \right)^2 \\ &+ \frac{\tau_{md}^2\,\nu^2}{m^2}\,(t - t_0) - \frac{\tau_{md}^3\,\nu^2}{m} \left(1 - e^{-(t-t_0)/\tau_{md}} \right) . \end{aligned} \tag{1.5}$$

In equilibrium, the first term in parenthesis vanishes since we set $\nu = 2k_BT/\zeta_0$, also for $t \gg \tau_{md}$ the exponential term tends to zero, so we got left the two following terms

$$\left\langle (\vec{r}(t) - \vec{r}(t_0))^2 \right\rangle_\eta = \frac{\tau_{md}^2\,\nu^2}{m^2}\,(t - t_0) - \frac{\tau_{md}^3\,\nu^2}{m}, \tag{1.6}$$

where for long times the leading term is dominant, so the constant term can be neglected. After writing τ_{md} and g in terms of the system parameters, we finally obtain the expression for the diffusion coefficient of a colloid in the suspension for zero external field.

$$\left\langle (\vec{r}(t) - \vec{r}(t_0))^2 \right\rangle_\eta = 4D_o\, t, \quad \text{with} \quad D_0 = k_B T/\zeta_0, \tag{1.7}$$

where the factor 4 arises because each dimension contributes by a factor 2. Now, if we consider the presence of a constant sedimentation field $\vec{F}(t) = -F\,\hat{j}$, we expect that the mean squared displacement changes accordingly. In order to determine $\langle (y(t) - y(t_0))^2 \rangle_\eta$ explicitly, we perform similar calculations which lead to Eq. (1.7). Given the velocity correlation Eq. (A.9), see Appendix A, we obtain

$$\begin{aligned}
\left\langle (y(t) - y(t_0))^2 \right\rangle_\eta \;=\; & \int_{t_0}^{t} dt_1 \int_{t_0}^{t} dt_2 \left\langle \vec{v}(t_1) \cdot \vec{v}(t_2) \right\rangle_\eta \\
& + \int_{t_0}^{t} dt_1 \int_{t_0}^{t} dt_2\, \vec{v}(t_0)\, e^{-(t_1 - t_0)/\tau_{md}}\, \frac{\vec{F}_s}{m}\, \tau_{md} \left(1 - e^{-(t_2 - t_0)/\tau_{md}}\right) \\
& + \int_{t_0}^{t} dt_1 \int_{t_0}^{t} dt_2\, \vec{v}(t_0)\, e^{-(t_2 - t_0)/\tau_{md}}\, \frac{\vec{F}_s}{m}\, \tau_{md} \left(1 - e^{-(t_1 - t_0)/\tau_{md}}\right) \\
& + \int_{t_0}^{t} dt_1 \int_{t_0}^{t} dt_2 \left(\frac{\vec{F}_s}{m}\right)^2 \tau_{md}^2 \left(1 - e^{-(t_2 - t_0)/\tau_{md}}\right) \left(1 - e^{-(t_1 - t_0)/\tau_{md}}\right),
\end{aligned} \tag{1.8}$$

where the first term of Eq. (1.8) is the same as found in Eq. (1.7), the second and third terms can be neglected in the limit $t \gg t_0$, and the fourth term can be calculated by standard integration methods. Finally, we calculate the vertical mean squared displacement

$$\left\langle (y(t) - y(t_0))^2 \right\rangle_\eta = 2D_0\, t + \left(\frac{F}{\zeta_0}\right)^2 t^2, \tag{1.9}$$

where the additional quadratic term in Eq. (1.9) arises due to the presence of the external constant sedimentation field F.

1.2.2 Flux Towards the Substrate

The Fokker-Planck (FP) equation presented in Appendix B, is commonly used to describe the time evolution of probability distributions for systems undergoing stochastic processes. In order to calculate the deposition rate at which the colloids reach the substrate, we need to find a FP for a single colloid in the suspension. The starting point is the Langevin equation for the vertical position of a colloid in the suspension with a constant sedimentation field. From Eq. (1.2) we have

$$m\,\frac{d^2y}{dt^2} = -\zeta_0\,\frac{dy}{dt} + \nu\,n(t) - F. \tag{1.10}$$

In order to have control over the system, the sedimentation of the colloids should be slow; in that sense, considering the overdamped limit, it is not a mere theoretical simplification but also a desirable situation. In the overdamped limit the acceleration is negligible and the differential equation takes the form

$$\frac{dy}{dt} = \frac{\nu}{\zeta_0}n(t) - \frac{F}{\zeta_0}j. \tag{1.11}$$

As shown in Appendix B, an equation such as (1.11) has an associated FP equation

$$\frac{\partial P(y,t)}{\partial t} = \frac{\partial}{\partial y}\left(a_1 + \frac{\partial}{\partial y}a_2\right)P(y,t), \tag{1.12}$$

where $P(y,t)$ corresponds to the probability distribution function of the height y of the colloid in the suspension. The coefficients a_1 and a_2 are given by

$$a_1 = -\frac{F}{\zeta_0} \quad \text{and} \quad a_2 = \frac{1}{2}\left(\frac{\nu}{\zeta_0}\right)^2. \tag{1.13}$$

Using the results of Eq. (1.13) in Eq. (1.12) we obtain the FP equation for $P(y,t)$

$$\frac{\partial P(y,t)}{\partial t} = \frac{\partial}{\partial y}\left(\frac{F}{\zeta_0}P(y,t) + \frac{\partial}{\partial y}\left(\frac{\nu^2}{2\zeta_0^2}\right)P(y,t)\right) = \frac{\partial J}{\partial y}. \tag{1.14}$$

Note that Eq. (1.14) have the form of a continuity equation, where the term in parentheses can be interpreted as the "current probability", J. Under the appropriate set of parameters it is possible to achieve a stationary flow of particles towards the substrate, J, such as $\frac{\partial P}{\partial t} = 0$ and therefore J is a constant. In this regime, Eq. (1.14) reduces to

$$\frac{2\zeta_0^2}{\nu^2}\frac{F}{\zeta_0}P(y) + \frac{\partial P(y)}{\partial y} = \frac{2\zeta_0^2}{\nu^2}\,J. \tag{1.15}$$

The Eq. (1.15) can be easily integrated using the standard method of the integrating factor, obtaining

$$P(y) = P(y_0)\,e^{-\frac{2\zeta_0^2 F}{\nu^2}(y-y_0)} + \frac{J\zeta_0}{F}\left(1 - e^{-\frac{2\zeta_0^2 F}{\nu^2}(y-y_0)}\right). \tag{1.16}$$

Since the system parameters are set in such a way that the deposition is irreversible we have $P(y_0) = 0$, and finally we obtain the probability of finding a colloid along the y-axis

$$P(y) = \frac{J\zeta_0}{F}\left(1 - e^{-\frac{2\zeta_0 F}{\nu^2}y}\right). \tag{1.17}$$

It is clear that the normalization constant J represents the flux of particles, which can be determined from the normalization condition $\int_0^{L_y} dy P(y) = 1$, where L_y represents the maximum height at which the colloids can be from the substrate. Therefore, we have

$$J = \frac{2F^2}{2\zeta_0 F L_y + \nu^2\left(e^{-\frac{2\zeta_0 F}{\nu^2}L_y} - 1\right)}. \tag{1.18}$$

Now, in EG the deposition rate $\mathcal{F}$ is defined as the number of particles that arrive on the substrate with length L_x. Consequently, $\mathcal{F}$ is given by

$$\mathcal{F} = \frac{NJ}{L_x} = \frac{N}{L_x L_y}\left(\frac{2F^2}{2\zeta_0 F + \frac{\nu^2}{L_y}\left(e^{-\frac{2\zeta_0 F}{\nu^2}L_y} - 1\right)}\right), \tag{1.19}$$

where N corresponds to the total number of colloids in the suspension and L_x corresponds to the horizontal length of the system. The density of colloids in the suspension, $\rho = N/(L_x L_y)$, is assumed to be constant because we consider the steady-state. There is an interesting limit case, when $F\,L_y \gg k_B T$ then Eq. (1.19) reduces to a simple linear form $\mathcal{F} = \rho F/\zeta_0$.

Equation (1.19) shows that even in the absence of an external sedimentation field there is, indeed, flux of particles towards the substrate, which was expected since the colloids evolve by Brownian motion. Note that in this regime, the flux is entirely dependent on the suspension parameters.

The time between consecutive depositions τ_{dep} of colloids in a gap can be obtained using known results, since it depends on two key factors, the length L_x of the gap and the flux of colloids toward the substrate $\mathcal{F}$, as follows

$$\tau_{\mathrm{dep}} = \frac{1}{\mathcal{F}L_x}. \tag{1.20}$$

As shown in Eq. (1.20), the quantity $\mathcal{F}L_x$ gives the net flux of colloids toward the substrate, regardless of the gap length. A higher flux $\mathcal{F}L_x$ means that more colloids are arriving at the substrate within a given time interval, this results in a shorter time between consecutive depositions, conversely, a lower flux $\mathcal{F}L_x$ means fewer colloids arrive on the substrate in the same time interval, leading to a longer time between depositions.

1.3 Dynamics on the Substrate

Regardless of the protocol used for deposition, the behavior of the system depends on the relative values of the time scales associated with each of the fundamental processes. In the past section, we have described the diffusion in the suspension and the deposition on the substrate. Once a colloid is trapped by the substrate, it evolves by diffusion until either an aggregation or nucleation event occurs. In the following sections, we describe those processes in order to have a complete description of the time scales required to have control over the system.

1.3.1 Diffusion Coefficient on the Substrate

Lifson and Jackson derived a formula for the diffusion coefficient of a single particle moving along a periodic potential [56], which was originally derived for a diffusing polymer chain in a one-dimensional periodic potential. It was found to be

$$D(y) = \frac{D_0\,\sigma^2}{\int_0^\sigma dx\, e^{\beta\,\mathcal{V}(x,y)} \cdot \int_0^\sigma dx\, e^{-\beta\,\mathcal{V}(x,y)}}, \tag{1.21}$$

with $\beta = 1/(k_B T)$, and D_0 corresponds to the diffusion coefficient for $V(x,y) = 0$. Equation (1.21) can be used as an approximation for a quasi one-dimensional diffusion of particles in periodic potentials [47, 57].

However, for a colloidal particle diffusing inside a gap, Eq. (1.21) cannot be directly applied because the fluctuations on the y-coordinate, free colloids do not move along a horizontal line. In Ref. [47] it is shown that Eq. (1.21) does not agree well with the results of the MD simulations. Here, we propose a way to estimate the diffusion coefficient on the substrate taking into account the periodicity of the potential and the fluctuations in the y-coordinate.

The substrate generates a periodic potential with well-defined minima, each of which comprises a metastable site for the deposited, mobile colloid, this potential is given by

$$V(x,y) = \sum_i \mathcal{V}_{AB}(r_i), \quad \text{with} \quad r_i = \sqrt{(\sigma/2 + x - x_i)^2 + y^2}, \tag{1.22}$$

where $\mathcal{V}_{AB}$ is given by Eq. (1.1), while $(x_i, 0)$ represents the coordinates of the $i-\text{th}$ particle of the substrate, and (x, y) are the coordinates of the mobile colloid.

As shown in Fig. 1.3, the potential is, indeed, periodic and very sensitive to the y coordinate of the colloid. Because of the short-range nature of the potential, small increases in the height of the colloid greatly weaken the potential strength.

The dynamics of the colloid on the substrate is modeled by Eq. (1.2), where the term corresponding to the sedimentation field can be neglected this time, since the colloid is trapped by the lattice and the force due to the substrate is much larger than F. Since $\tau_{\text{dep}} \gg \tau_{md}$ we can

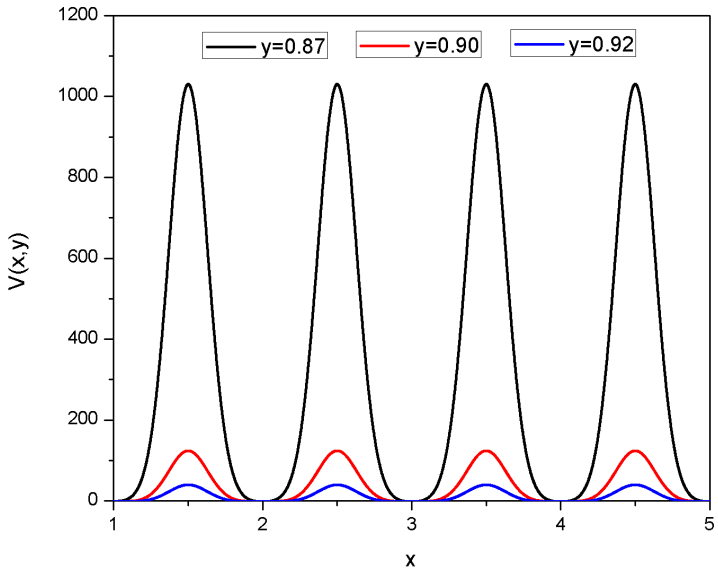

Figure 1.3: Periodic potential generated by the lattice, $\mathcal{V}(x,y)$, using $\mathcal{A}_{AB} = 8.0$ and $\alpha = 25$, for different heights y. Due to the short-range nature of the interaction the potential is very sensitively to y-coordinate fluctuation.

work in the over-damping limit. Thus, in the overdamped regime the equation of motion for the colloid on the substrate is as follows

$$\frac{d\vec{r}}{dt} = \left(\frac{\nu}{\zeta_0}\,\vec{n}(t) - \frac{1}{\zeta_0}\nabla\mathcal{V}(x,y) \right). \tag{1.23}$$

In this case, the system dynamics is two-dimensional, so the FP equation associated to Eq. (1.23) depends on the coordinates x and y. The FP associated to Eq. (1.23) is given by

$$\frac{\partial P(x,y,t)}{\partial t} = \left[\frac{\partial}{\partial x}\left(\frac{1}{\zeta_0}\frac{\partial \mathcal{V}}{\partial x} + \frac{\nu^2}{2\zeta_0^2}\frac{\partial}{\partial x} \right) + \frac{\partial}{\partial y}\left(\frac{1}{\zeta_0}\frac{\partial \mathcal{V}}{\partial y} + \frac{\nu^2}{2\zeta_0^2}\frac{\partial}{\partial y} \right) \right] P(x,y,t). \tag{1.24}$$

Note that Eq. (1.24) is not separable due to the form of the interaction potential $\mathcal{V}(x,y)$, making it difficult to find an exact solution for $P(x,y,t)$ with the Morse potential. However, for the set of parameters chosen, the colloids will diffuse on the substrate by infrequent events. Therefore, the probability distribution function for finding a colloid close to a potential minimum can be approximated by the equilibrium distribution given by

$$P(x,y,t) \approx C\, e^{-\beta\, V(x,y)}, \tag{1.25}$$

where C is the normalization constant of the distribution. Through Eq. (1.25) we can define the marginal probability distributions to find the colloid close to the positions x and y, $p_x(x)$ and $p_y(y)$, respectively. By definition, these distributions are given by

$$p_x(x) = \int_0^\infty dy\, P(x,y,t) \quad \text{and} \quad p_y(y) = \int_{-\sigma/2}^{\sigma/2} dx\, P(x,y,t). \tag{1.26}$$

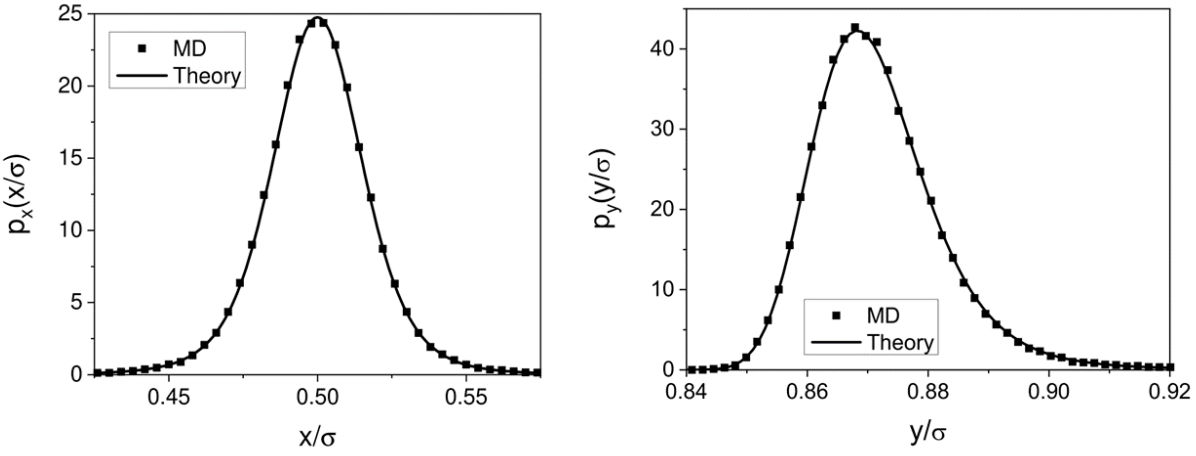

Figure 1.4: Marginal distributions $p_x(x)$ (left) and $p_y(y)$ (right) given by Eqs. (1.26). As expected, $p_y(y)$ has a well-defined peak at $y \simeq (\sqrt{3}/2)\sigma$ while $p_x(x)$ has its maximum at the midpoint between the center of two consecutive colloids of the substrate.

The marginal probabilities of Eq. (1.26) were evaluated using MD simulations for the set of parameters chosen. In Fig. 1.4, the lines correspond to the analytical results of Eq. (1.26), while the dots represent the MD simulation; the details of the computational simulations are provided in Chapter 2. As can be seen in Fig.1.4 the agreement between numerical and analytical results is excellent.

As shown in Fig. 1.4 (left), the most probable position to find the colloid is around 0.50σ which corresponds to the one minimum of the potential $\mathcal{V}(x,y)$. In Fig. 1.4 (right) can be seen that the probability of find the colloid at a height greater than 0.876σ decays rapidly. Then, as presumed, the hopping of a colloid to other potential minimum is, indeed, an infrequent event.

Figure. 1.5 shows the behavior of the function $D(y)p_y(y)$ as function of height y. Note that in the region $y > \sigma$, $D(y)$ becomes equal to the diffusion constant at the suspension. Due to the finite size of the colloids, the transitions between metastable states only occur for $y \gtrsim \sigma$. As shown in the right panel of Fig. 1.5 , the probability of finding the particle in this region is quite small. Consequently, the distribution $D(y)p_y(y)$ decays rapidly as y exceeds σ, as can be seen in the main panel of Fig. 1.5. Then, the effective lateral diffusion coefficient, D, can be estimated as follows

$$D \approx D(\sigma)p_y(\sigma), \tag{1.27}$$

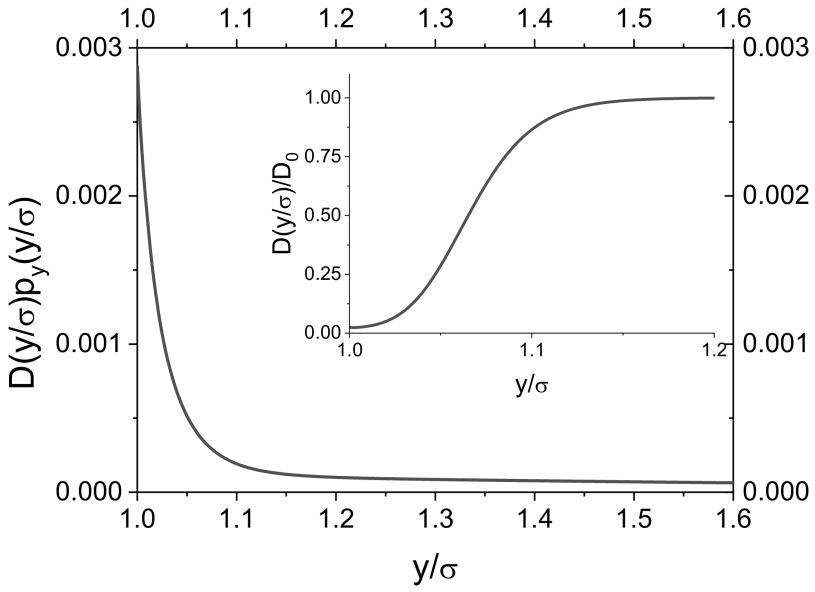

Figure 1.5: Behavior of the distribution $D(y)\,p_y(y)$ as function of y. The inset shows how $D(y)$ increases with y until it equals the value of the diffusion constant in the suspension D_0.

where $D(\sigma)$ correspond to the diffusion coefficient provided by the Lifson-Jackson formula Eq. (1.21), and $p_y(\sigma)$ the marginal probability, Eq. (1.26). Note that we assume that the hops between potential minima occur only at $y = \sigma$.

1.3.2 Residence Time

The traversal time, $\tau_{\rm tr}$, is defined as the average time after deposition required for a monomer to reach one of the edges of the gap, while the residence time $\tau_{\rm res}$ measures the survival time of a monomer before it aggregates to one of the islands of the gap.

The diffusion on the substrate occurs by infrequent events constituting a random walk, which can be analytically described by a master equation; see Appendix C for a general derivation. For a Markovian process the general master equation is given by

$$\frac{\partial}{\partial t}P_1(n,t) = \sum_{m=1}^{N}\left[P_1(m,t)W_{m,n} - P_1(n,t)W_{n,m}\right], \tag{1.28}$$

where $P_1(n,t)$ represents the probability for a single particle to be on site n of the lattice at time t, and $W_{m,n}$ corresponds to the transition rate from m to n. Since all the calculation will be made for one particle we can relax the notation a simply define $P_1(n,t) \equiv p_n(t)$ as the probability to find the colloid on the site n at time t. In Fig.1.6 it is show a diagrammatic representation of the possible jump processes for a colloid on the substrate indicating the respective transition rates.

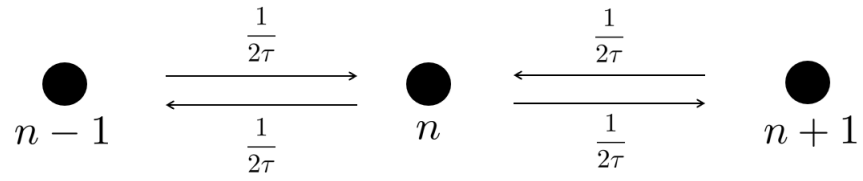

Figure 1.6: Diagrammatic representation of the incoming and outcoming probability flux to/from site n. Since all processes have the same probability to occur and the hopping rate is the same regardless the site, all four possible processes have the same transition rate, $1/(2\tau)$.

A colloid can hop to the left or the right with the same probability (1/2) and the average time between consecutive hops is τ. Therefore, we have $W_{m,n} = W_{n,m} = 1/(2\tau)$. Using these rates, from Eq. (1.28) we can obtain the master equation for a colloid executing a random walk on the substrate, as follows

$$\frac{dp_n(t)}{dt} = \frac{1}{2\tau}\left[p_{n+1}(t) + p_{n-1}(t) - 2p_n(t)\right], \tag{1.29}$$

where the first and second terms of Eq. (1.29) correspond to the flux incoming from site $n+1$ and $n-1$ to n, respectively, while the third term represents the flux outgoing from n to $n+1$ and $n-1$. Note that the hopping rate $1/\tau$ and the diffusion coefficient on the substrate D are related as $D = \sigma^2/(2\tau)$, see Appendix C.

1.3.2.1 Density of monomers

In order to have control over the growth process, we have to be able to describe the density of colloids on the substrate $\rho(t)$ as well as the time it takes a colloid to execute a random walk on the substrate until it aggregates to an island, the so-called residence time $\tau_{\rm res}$.

From $p_n(t)$, we can find the density of colloids on site n regardless the time, i.e., the stationary density of colloids ρ, as follows:

$$\rho_n = \int_0^\infty dt\, p_n(t). \tag{1.30}$$

Using Eqs (1.29) and (1.30) we can obtain the stationary density of colloids ρ_n in the gap, as follows:

$$\begin{aligned} \frac{d\rho_n}{dt} &= \frac{d}{dt}\int_0^\infty dt\, p_n(t), \\ \frac{1}{2\tau}\left(\rho_{n+1}(t) + \rho_{n-1}(t) - 2\rho_n(t)\right) &= p_n(\infty) - p_n(0) \\ \rho_{n+1}(t) + \rho_{n-1}(t) - 2\rho_n(t) &= -2\tau p_n(0), \end{aligned} \tag{1.31}$$

with boundary conditions $p_{N+1} = \epsilon\, p_N$ and $p_0 = \epsilon\, p_1$, see appendix C. The constant $0 \leq \epsilon \leq 1$ takes account for the interaction between islands and the mobile colloid. Since the deposition of colloids is completely random, without loss of generality we can assume the initial condition $p_n(0) = 1/N$. Equation (1.31) is a second order nonhomogeneous linear difference equation which can be solved by proposing a solution of the type $\rho_n = \sum_{j=0}^{2} c_j n^j$ [58], obtaining

$$\rho_n = \frac{\tau}{N}\left(\frac{\epsilon\, N}{1-\epsilon} + (1+N)n - n^2\right). \tag{1.32}$$

1.3.2.2 Residence time

We define the survival probability $P_s(t)$, as the probability that the colloid is somewhere on the substrate at time t, as follows

$$P_s(t) = \sum_{n=1}^{N} p_n(t). \tag{1.33}$$

Then, the probability for a colloid to be captured in the time interval $[t, t+\Delta t]$ can be calculated from the residence probability distribution $P_{res}(t)$, as follows

$$P_{res}(t)\Delta t = -P_s(t+\Delta t) + P_s(t), \tag{1.34}$$

and in order to obtain a continuous equation we take the limit $\Delta t \to 0$, obtaining

$$P_{res}(t) = -\frac{dP_s(t)}{dt}. \tag{1.35}$$

The residence time $\tau_{\rm res}$ is the average time that a colloid spends in the gap before being captured by an island. Therefore, it is given by

$$\tau_{\rm res} = \int_0^\infty dt\, t\, P_{res}(t), \tag{1.36}$$

replacing Eq. (1.35) into Eq. (1.36), and by doing integration by parts we obtain

$$\tau_{\rm res} = \int_0^\infty dt\, P_s(t). \tag{1.37}$$

Finally using the definition of $P_s(t)$, Eq. (1.33) in Eq. (1.37) we obtain

$$\tau_{\rm res} = \sum_{n=1}^{N} \int_0^\infty dt\, p_n(t), \tag{1.38}$$

where the integral term of Eq. (1.38) can be interpreted as the stationary density of colloids on the substrate ρ_n

$$\tau_{\rm res} = \sum_{n=1}^{N} \rho_n, \tag{1.39}$$

Now, replacing Eq. (1.32) into Eq. (1.39) and developing the sums we obtain,

$$\tau_{\rm res} = \tau \left(\frac{\epsilon\, N}{1-\epsilon} + \frac{(N+1)(N+2)}{6} \right), \tag{1.40}$$

where $\tau = 1/(2D)$, see Appendix C for more details. For the case where the island behaves as perfect traps $\epsilon = 0$, i.e., once a free colloid reaches the interaction range of an island the aggregation occurs instantaneously. In this limit, the time of the interaction colloid-island is negligible and $\tau_{\rm tr} \approx \tau_{\rm res}$. Therefore, for large gaps Eq. (1.41) simplifies takes the simple form

$$\tau_{\rm res} = \frac{(N+1)(N+2)}{12D} \approx \frac{N^2}{12D}. \tag{1.41}$$

As expected, the residence time depends on the diffusion coefficient. Low diffusivity implies long times expended by the colloids executing random walks on the substrate. On the contrary, high diffusivity leads to a fast aggregation of colloids after deposition. Also, note that the residence time scales quadratically with the gap length.

1.4 Spatial Description of the Nucleation

For a nucleation event to occur in a gap, at least two colloids are required simultaneously in the gap. Thus, nucleation depends on $\mathcal{F}$, which controls colloid deposition, and D, which determines the colloid's residence time in the gap. The relationship between $\mathcal{F}$ and D is crucial, as the first colloid must remain in the gap long enough without aggregating into an island until the second colloid arrives. As a control parameter we define the quotient $\mathcal{R} = D/\mathcal{F}$. For small densities of colloidal particles in the suspension, the deposition rate of monomers satisfies $\mathcal{R} \gg 1$. In this regime, for a gap of length L, $\tau_{\rm res} \ll \tau_{\rm dep}$ and the probability of simultaneously finding more than one colloid inside a gap is small.

1.4.1 Probability of Having Two Colloids on the Substrate

In order to describe explicitly the nucleation process, we start by calculating the probability q_{n+1}, of finding $n+1$ non-interacting colloids simultaneously on the substrate [59].

Let t_i be the time interval between the arrival of colloids i and $i+1$, and let τ_i be the residence time of colloid i, where $i = 1, 2, ..., n$. The first colloid arrives at time $t = 0$, the second at time

$t = t_1$, and so on. For all n colloids to remain on the substrate when the $(n+1)$-st colloid arrives, the residence times must satisfy $\tau_i > t_i + t_{i+1} + \cdots + t_n$.

The variables t_i and τ_i are exponential random variables with mean $\tau_{\rm dep}$ and $\tau_{\rm res}$, respectively. In order to described the probability distribution function for the arrival of colloid to the substrate consider the following process: The i-th colloid is deposited on the substrate at time $t = 0$ and we want to calculated the probability that it survives until time t. In order to calculate that probability we divide the time period into n small segments of equal length Δt, such as, $\Delta t = t/n$. Then, in each segment Δt, the probability of survival can be approximated as

$$P_s(\Delta t) \approx 1 - \frac{\Delta t}{\tau_{res}}. \tag{1.42}$$

The total survival probability over the entire time interval t is the product of the survival probabilities in each of the n small segments, given by

$$P_s(\Delta t) = \left(1 - \frac{\Delta t}{\tau_{res}}\right)^n = \left(1 - \frac{t}{n\,\tau_{res}}\right)^n. \tag{1.43}$$

Taking the limit when the number of division of the time interval tends to infinity we obtain the continuous limit of the survival probability given by Eq. (1.44), as follows

$$P_s(t) = \lim_{n\to\infty}\left(1 - \frac{t}{n\,\tau_{res}}\right)^n = e^{-t/\tau_{res}}. \tag{1.44}$$

In the same way as in Eq. (1.44), we can obtain a similar expression for the probability of deposition at time t, $P_{dep}(t) = e^{-t/\tau_{dep}}$. Therefore, the probability q_{n+1} can be written as follows

$$q_{n+1} = \frac{1}{(\tau_{\rm dep})^n}\prod_{i=1}^{n}\int_0^\infty dt_i\, e^{-t_i/\tau_{\rm dep}}\,\frac{1}{\tau_{res}^n}\prod_{i=1}^{n}\int_{t_i+t_{i+1}+\cdots+t_n}^\infty d\tau_i\, e^{-\tau_i/\tau_{\rm res}}, \tag{1.45}$$

the first term enclosed in parenthesis in Eq. (1.45) represents the probability of a colloid being deposited, while the second term enclosed in parenthesis represents the probability of having n colloids on the substrate at time t_n. Since these two probabilities are independent, their product gives the probability of a colloid being deposited given that there are already n colloids on the substrate.

The second term of Eq. (1.45) can be simplified as follows

$$\frac{1}{\tau_{\rm res}^n}\prod_{i=1}^{n}\int_{t_i+t_{i+1}+\cdots+t_n}^\infty d\tau_i\, e^{-\tau_i/\tau_{\rm res}} = \frac{1}{\tau_{\rm res}^n}\prod_{i=1}^{n}\tau_{\rm res}\, e^{-(t_i+t_{i+1}+\cdots+t_n)/\tau_{\rm res}} = \prod_{j=1}^{n} e^{-j\,t_j/\tau_{\rm res}}. \tag{1.46}$$

Using Eq. (1.46) in Eq. (1.45) we found

$$q_{n+1} = \frac{1}{(\tau_{\rm dep})^n} \prod_{i=1}^{n} \int_0^\infty dt_i e^{-t_i\left(\frac{1}{\tau_{\rm dep}} + \frac{i}{\tau_{\rm res}}\right)}, \tag{1.47}$$

the last integral of Eq. (1.47) can be performed easily obtaining

$$q_{n+1} = \frac{1}{(\tau_{\rm dep})^n} \prod_{i=1}^{n} \frac{1}{\left(\frac{1}{\tau_{\rm dep}} + \frac{i}{\tau_{\rm res}}\right)} = \prod_{i=1}^{n} \frac{1}{\left(1 + i\frac{\tau_{\rm dep}}{\tau_{\rm res}}\right)}, \tag{1.48}$$

since $\tau_{\rm dep} \gg \tau_{\rm res}$, the probability of finding two colloids in a gap simultaneously is quite small and the product term in Eq. (1.45) can be approximated by a first-order expansion, leading to

$$q_{n+1} \approx \prod_{i=1}^{n} \frac{1}{i} \frac{\tau_{\rm res}}{\tau_{\rm dep}} = \frac{1}{n!} \left(\frac{\tau_{\rm res}}{\tau_{\rm dep}}\right)^n. \tag{1.49}$$

Replacing in Eq. (1.49) the explicit expression found for $\tau_{\rm res}$ and $\tau_{\rm dep}$, see Eqs. (1.41) and (1.20), respectively, we obtain

$$q_{n+1} = \frac{1}{n!} \left[\frac{N}{2\mathcal{R}} \left(\frac{\epsilon\, N}{1-\epsilon} + \frac{(N+1)(N+2)}{6}\right)\right]^n. \tag{1.50}$$

As expected, q_{n+1} depends on ϵ, N and $\mathcal{R}$. In our MD simulations, we set $\mathcal{A}_{AA} = 8.8 k_B T$, which makes dimers stable, i.e., clusters of two monomers can be considered as immobile and stable islands. Also, for the parameters used in the simulations we can guarantee $\epsilon = 0$, thus, for large gaps Eq. (1.50) simplifies as follows

$$q_{n+1} \approx \frac{1}{n!} \left[\frac{N^3}{12\mathcal{R}}\right]^n. \tag{1.51}$$

1.4.2 Nucleation Probability

Given that for the parameters used, $\tau_{\rm res} \ll \tau_{\rm dep}$, if two monomers coincide in the gap, the first monomer probably has already reached steady state by the time the second arrives. This scenario is equivalent to having both monomers deposited simultaneously at random sites within the gap. The first monomer is deposited at the site n with a uniform probability of $1/N$, while the second is deposited with a probability of $\rho_n / \sum_n \rho_n$. The time evolution of two free colloids is described by the master equation

$$\frac{dp_{m,n}(t)}{dt} = \frac{1}{4\tau}\left[p_{m+1,n}(t) + p_{m-1,n}(t) + p_{m,n+1}(t) + p_{m,n-1}(t) - 4p_{m,n}\right], \tag{1.52}$$

where, for $\epsilon = 0$, $p_{0,n}(t) = p_{N+1,n}(t) = p_{m,0}(t) = p_{m,N+1}(t) = 0$. The interaction between free colloids is represented by the boundary condition $p_{n,n} = 0$. In the following, we assume that nucleation occurs once the colloids are separated by a distance smaller than the interaction range, which is a reasonable assumption since we set the $\mathcal{A}_{AB}$ value to make detachment negligible.

The solution of Eq. (1.52) can be found using the auxiliary initial condition [60–62]

$$\tilde{p}_{m,n}(0) = \begin{cases} -p_{n,m}(0) & \text{for} \quad m > n \\ 0 & \text{for} \quad m = n \\ p_{m,n}(0) & \text{for} \quad m < n, \end{cases} \tag{1.53}$$

where the symmetrized $p_{m,n}(0)$ can be written as

$$p_{m,n}(0) = \frac{\rho_n + \rho_m}{2L\sum_n \rho_n}. \tag{1.54}$$

In this way, the probability of having two colloids at sites m and n at time t in the gap, see Appendix C, has the form

$$p_{m,n}(t) = \frac{1}{2^t}\sum_{k,j=1}^{N} B_{kj}\left[\cos\left(\frac{k\pi}{N+1}\right) + \cos\left(\frac{j\pi}{N+1}\right)\right]^t Y_k(m)Y_j(n), \tag{1.55}$$

where the coefficients $Y_k(m)$ and B_{kj} are given by

$$Y_k(m) = \sin\left(\frac{mk\pi}{N+1}\right) \quad \text{and} \quad B_{kj} = \left(\frac{2}{N+1}\right)^2 \sum_{m,n=1}^{N} p_{m,n}(0)Y_k(m)Y_j(n). \tag{1.56}$$

The probability that nucleation occurs at site n, $\mathcal{P}(n)$, is given by [63]

$$\mathcal{P}(n) = \frac{1}{4}\int_0^\infty dt\, \left[p_{n+1,n}(t) + p_{n-1,n}(t) + p_{n,n+1}(t) + p_{n,n-1}(t)\right], \tag{1.57}$$

where the integral is made over the all times where the dynamics occurs, but since outside that lapse the probabilities describing the process simply vanish we can extend the integration domain to infinity.

From Eq. (1.56) it is easy to see that $Y_k(n)Y_j(n+1) = Y_k(n+1)Y_j(n)$, leading to the fact that $p_{n+1,n}(t) = p_{n,n+1}(t)$, reducing the size of the integrand of Eq. (1.57) from four to two terms. Also, the sum over time can be done easily, since the time-dependent terms form a geometric progression. Then, the probability of nucleation at site n can be written as

$$\mathcal{P}(n) = \frac{1}{2}\sum_{k,j=1}^{N} \frac{B_{kj}\ \left(Y_k(n)Y_j(n+1) + Y_k(n)Y_j(n-1)\right)}{1 - \frac{1}{2}\left[\cos\left(\frac{k\,\pi}{N+1}\right) + \cos\left(\frac{j\,\pi}{N+1}\right)\right]}. \tag{1.58}$$

1.4.3 Mean-Field Approach

An excellent mean-field approximation for Eq. (1.55) is given by the Walton's relation, which assumes that $\mathcal{P}(n)$ is proportional to the squared density. In this way, using Eq. (1.32) with $\epsilon = 0$, it can be found [23, 24, 64], that

$$\mathcal{P}_{MF}(n) \approx \frac{30n^2(N-n+1)^2}{(N+1)^5}. \tag{1.59}$$

As shown in the next chapter, for the set of parameters used in this thesis the MF approximation gives an excellent description of the nucleation sites. The main advantage of Eq. (1.59) is that it is much easier to evaluate than the exact expression given by Eq. (1.58).

1.4.4 Nucleation Rate

The nucleation rate inside the gap, ω, indicates the number of nucleation events per time unit. Let g be the conditional probability for a nucleation within a gap, given that there is one monomer inside the gap at the time of the second deposition. Consequently, ω can be written as

$$\omega = g\, q_2\, \mathcal{F}\, L, \tag{1.60}$$

where q_2 is given by Eq. (1.51) and g and $\mathcal{P}(n)$ are related according to

$$g = \sum_{n=1}^{N} \mathcal{P}(n). \tag{1.61}$$

where $\mathcal{P}(n)$ is given by Eq. (1.55). Using Eqs. (1.51) and (1.58), and taking into account that $g \approx 0.47$, it is not difficult to show that for large gaps

$$\omega \sim L^4, \tag{1.62}$$

while in the MF approximation $\omega \sim L^5$. The nucleation rate depends algebraically on the length of the gap.

Chapter 2

Molecular Dynamics (MD) Simulations

In this chapter, we present the formalism for the Molecular Dynamics (MD) simulations conducted to numerically reproduce the behavior of the system. We utilized the BAOAB algorithm as the integrator for the equations of motion, and details of the code implementation are provided. The MD simulations were performed to calculate various quantities of interest, including the diffusion coefficient on the substrate, flux toward the substrate, time between consecutive depositions, residence time, and the density of colloids on the gap. The details of the simulations and the results are discussed. In addition, a description of the nucleation process is provided, with simulations carried out using LAMMPS, and the corresponding results are presented.

2.1 Langevin Dynamics

In our problem, the use of a stochastic differential equation model, such as the Langevin equation, introduces random fluctuations into the force component, the advantage of this formalism is that the Langevin dynamics is well known to be ergodic [65, 66].

The problem regarding the perturbations due to the discretization error has to be addressed in each particular case, and, since almost every computational work relying on MD algorithms lies in force calculations, most existing methods require only one force evaluation per time step. For time-stepping methods that achieve an accurate sampling of the canonical distribution, the adequate timescales for the simulation depend on the system itself. Large time steps provide faster simulations at the cost of precision in the measurements. In comparison, a quite short time step will surely give a detailed sampling of the phase space at the expense of consuming more computational resources and longer simulation time. The ideal scenario is to choose a time step small enough to avoid drastic perturbations in the measurements but still large enough to ensure a thorough exploration of the configuration space.

The potential energy function in MD determines the maximum allowed step size. Most numerical methods, Langevin dynamics included [67], have similar limitations in the maximum time-step size since the potential energy determines the forces acting on the particles, and how sensitive

the force function is to changes over time determines the stability of the systems, and therefore, provides a threshold for the time-step of the MD simulation.

2.2 The BAOAB Algorithm

Without loss of generality, we can break down the Langevin dynamics in the following equations [46]

$$dq = M^{-1}\,p\,dt, \tag{2.1}$$
$$dp = -\nabla U(q)\,dt - \zeta_0\,p\,dt + \sigma\,M^{1/2}\,dW, \tag{2.2}$$

where q, $p \in \mathbb{R}^{3N}$ are vectors of instantaneous position and momentum, respectively, $W = W(t)$ is a vector of $3N$ independent Wiener processes [68], $\zeta_0 > 0$ is a free scalar parameter, M is a constant diagonal mass matrix and $\sigma = \sqrt{2\zeta_0/\beta}$.

The objective is to integrate Eqs. (2.1) and (2.2) effectively and with minimal computational cost. The so-called splitting methods provide a simple way for integrating the Langevin dynamics equations [69–71]. In this approach, the right-hand side of Eqs. (2.1) and (2.2) is divided into pieces, where each piece is solved exactly in sequence. In our problem, the Langevin dynamics can be split into three parts, as follows

$$\begin{bmatrix} dq \\ dp \end{bmatrix} = \underbrace{\begin{bmatrix} M^{-1}p \\ 0 \end{bmatrix} dt}_{A} + \underbrace{\begin{bmatrix} 0 \\ -\nabla U(q) \end{bmatrix} dt}_{B} + \underbrace{\begin{bmatrix} 0 \\ -\zeta_0\,p\,dt + \sigma\,M^{1/2}\,dW \end{bmatrix}}_{O}, \tag{2.3}$$

where A describes the Newtonian dynamics of the system, B accounts for the contribution of the potential to the dynamics, and O holds the terms related to drift and noise. The term O has been widely studied in the literature since is associated with an Ornstein-Uhlenbeck equation [68] with exact solution of the form

$$q(t) = q(0), \tag{2.4}$$
$$p(t) = e^{-\zeta_0 t}p(0) + \frac{\sigma}{\sqrt{2\zeta_0}}\sqrt{1 - e^{-2\zeta_0 t}M^{1/2}}R_t, \tag{2.5}$$

where $R_t \sim \mathcal{N}(0,1)$ is a vector of uncorrelated Gaussian noise processes. Equations (2.4) and (2.5) are said to be exact since they define a random map that generates the probability distribution $\rho(q,p,t)$ defined by the solutions of the Ornstein-Uhlenbeck equation.

Leimkuhler and Matthews [46] proposed a method to integrate the system described by Eq. (2.3) using the so-called “BAOAB” algorithm. The sequence of integration, as indicated by the algorithm’s name, follows the order of the splitting given in Eq. (2.3) from left to right.

The integration process can be divided into three parts. The first part, represented by the string “BA”, involves solving the “B” part first and then the “A” part, updating the momentum and position, respectively, both for a half time step $\Delta t/2$. The second part, the “O” part, is time independent and updates the momentum by incorporating all stochastic processes. Finally, the “AB” part updates the position based on the contributions of the stochastic processes, followed by updating the momentum again based on the potential contribution, both for a half time step $\Delta t/2$. Therefore, the whole integration “BAOAB” gives the dynamic evolution of one single colloid for a whole time-step Δt.

In the case of our system, the equations associated to the integration algorithm given by Eqs. (2.3), (2.4) and (2.5) can be written as

$$\text{B} \quad \begin{cases} v_x(t) = v_x(t_0) + \dfrac{\Delta t}{2} a_x(t), \\ v_y(t) = v_y(t_0) + \dfrac{\Delta t}{2} a_y(t). \end{cases} \tag{2.6}$$

$$\text{A} \quad \begin{cases} x(t) = x(t_0) + \dfrac{\Delta t}{2} v_x(t), \\ y(t) = y(t_0) + \dfrac{\Delta t}{2} v_y(t). \end{cases} \tag{2.7}$$

$$\text{O} \quad \begin{cases} v_x(t) = v_x(t)\, e^{-\Delta t\, \zeta_0} + R_t \sqrt{\dfrac{k_B T}{m}\,(1 - \Delta t\, e^{-2\zeta_0})}, \\ v_y(t) = v_y(t)\, e^{-\Delta t\, \zeta_0} + R_t \sqrt{\dfrac{k_B T}{m}\,(1 - \Delta t\, e^{-2\zeta_0})}. \end{cases} \tag{2.8}$$

We remark that to carry out the integration process according to the BAOAB algorithm, the first step is to calculate the instantaneous acceleration components of each mobile colloid, $a_x(t)$ and $a_y(t)$, which can be done using Eq. (1.1), as follows

$$a_x(t) = -\frac{\partial \mathcal{V}_{AB}(x,y)}{\partial x}, \tag{2.9}$$

$$a_y(t) = -\frac{\partial \mathcal{V}_{AB}(x,y)}{\partial y} - F, \tag{2.10}$$

where the additional term in Eq. (2.10) includes the presence of the constant sedimentation field which helps to drive the colloids towards the substrate. Once the acceleration components are calculated for the given time, the algorithm can be performed as indicated. First, the BA part, given by Eqs. (2.6) and (2.7), in that specific order, which gives us the updated velocity and position components for the first half time step. Then, the O part of the algorithm is performed using Eq. (2.8), where the contribution of the stochastic terms to the velocity is included. Finally, the AB part of the algorithm is performed using Eqs. (2.7) and (2.6) in that order.

Chapter 3

MD Simulations Results and Discussion

In this chapter, we discuss the scheme used to perform the MD simulations implemented to measure the desired quantities such as the diffusion coefficient on the substrate D, the flux towards the substrate $\mathcal{F}$, the time between consecutive depositions τ_{dep}, the density of monomers on the substrate ρ_n and the residence time τ_{res}. The procedure used to determine the distribution of nucleation sites is also presented.

3.0.1 Diffusion Coefficient on the Substrate

We are interested in calculating the diffusion coefficient of a free colloid executing a random walk on the substrate. By definition, the diffusion coefficient D is directly related to the mean squared displacement, as follows

$$\left\langle (x(t) - x(t_0))^2 \right\rangle_\eta = 2Dt, \tag{3.1}$$

where $x(t_0)$ corresponds to the initial position of the monomer at the beginning of the simulation at $t_0 = 0$, and $x(t)$ the position at time t. Since we are interested in studying the diffusion process there is no need for islands on the ends of the substrate. However, the substrate has to be long enough so that the colloid does not reach one of the ends during the simulation. The physical system setup for the MD simulation can be seen in Fig. 3.1

As shown in Fig. 3.1, the colloid is released at $y = 1.56\,\sigma$, measured from the center of mass of the colloids that form the substrate. The initial $x(t_0)$ coordinate is chosen such that the colloids arrive close to the center of the substrate. Once a colloid is trapped by the potential of the substrate executes a random walk until the physical time t_f is reached. The free colloid evolves according to the equations of motion, Eqs. (2.4) and (2.5), which are integrated using the BAOAB algorithm.

Since the dynamics of the colloid is slow, it is not necessary to record the quantity $x(t) - x(0)$ for each time step, but rather every set amount of time steps. In our simulation, we use a time step $\Delta t = 0.0001\,\tau_{md}$. We found that recording the mean squared displacement, Eq. (3.1),

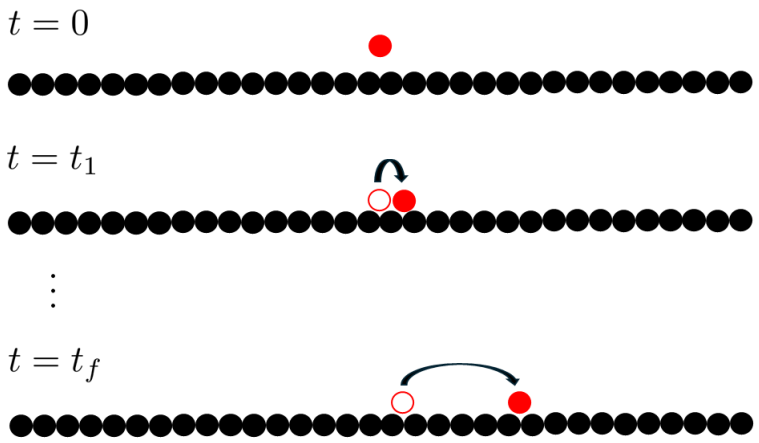

Figure 3.1: Diffusion of a colloid on a substrate. The colloid is deposited at a fixed height near the substrate at a initial time $t = 0$, as time evolves the colloids executes a random walk on the substrate by hopping between near sites.

every second, that is, every 10,000 steps, is enough to obtain accurate results, with a simulation time $t_f = 500\,\tau_{md}$. The simulation is carried out until 5000 repetitions are made and the quantity $x(t) - x(0)$ is accumulated for each t to obtain a smooth distribution after taking the average over the realizations $\langle\cdot\rangle_\eta$.

For a simulation as the one described above and using the parameters presented in Chapter 1, we obtain the mean-square-displacement as a function of time shown in Fig. 3.2

According to Eq. (3.1), the long-time behavior corresponds to a linear function. However, as shown in Fig. 3.2, there is a small non-linear part just at the beginning of the simulation. This result can be understood by taking into account that the colloid is released at a small height from the substrate and not exactly on the substrate. Furthermore, the colloid requires a short time for thermalization. From a linear fit for large time, we obtain the diffusion coefficient on the substrate $D = 0.314\,\sigma^2/\tau_{md}$.

Figure 3.3 displays the results for the diffusion coefficient D obtained by numerically evaluating Eq. (1.27) at $y = \sigma$ for different values of $\mathcal{A}_{AB}$.

The theoretical results are compared to those from MD simulations estimated from the long-time behavior of the mean squared displacement. The diffusion constant $D = D(\sigma)p_y(\sigma)$ strongly depends on $\mathcal{A}_{AB}$ as it decreases two orders of magnitude as $\mathcal{A}_{AB}$ increases from $7.5k_BT$ to $9.0k_BT$. The inset shows that our approximation reproduces the exponential decay of D as a function of $\mathcal{A}_{AB}$ but overestimates the decay rate. As reported in Refs. [1, 2], taking $A_{AB} = 8.0k_BT$ guarantees the mobility of the free colloids on the substrate but makes unlikely their detachment from the substrate.

A simulation, similar to the one described above, can be used to obtain the marginal distributions given by Eq. (1.26) and shown in Fig. 1.4. The simulation algorithm is the same used to calculate the diffusion coefficient but in this case, the spatial coordinates of the colloid are recorded. To

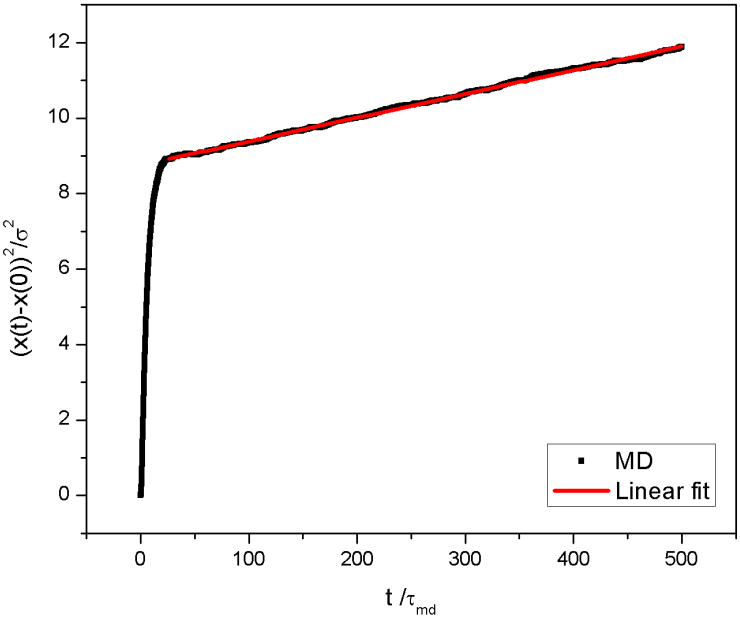

Figure 3.2: Results from the MD simulation for Mean-square-displacement in function of time. The simulation was made with a time step $\Delta t = 0.0001\tau_{md}$, for a physical time of $t = 500\tau_{md}$, gathering data every $10,000$ steps and averaged for $5,000$ realizations. This figure appears as FIG. 4 in Ref. [2].

obtain the distribution $p_y(y)$, the height of the colloid needs to be recorded, while to obtain $p_x(x)$ the position of the colloid relative to the nearest minimum point needs to be recorded.

3.0.2 Time Between Consecutive Depositions

To calculate the flux of colloids towards the substrate or, equivalently, the time between consecutive depositions τ_{dep}, we define a simulation box, as shown in Fig. 3.6. The vertical boundaries satisfy periodic boundary conditions, the upper one reflective boundary conditions, and the lower limit determines the region where the substrate can trap the colloids. Once a colloid surpasses the lower limit of the simulation box, we assume that the particle is trapped by the substrate, and another colloid is added to the top of the simulation box. In this way, the number of particles in the simulation box is conserved.

However, as shown before, for large values of $\mathcal{A}_{AB}$ the diffusion coefficient D becomes comparable to the deposition rate $\mathcal{F}$. This is not a desired situation because it leads to an evolution in which nucleation and aggregation occur simultaneously, which decreases the chance of controlling the formed structure. To avoid this issue, we set the density in the suspension as $\rho = 0.004/\sigma^2$, such as $\mathcal{F} \simeq 2 \times 10^{-6}/(\sigma\tau_{md})$, which gives $\mathcal{R} = D/\mathcal{F} \approx 1.6 \times 10^3\sigma^3$ [2]. Once the simulation starts each particle evolves according to the BAOAB

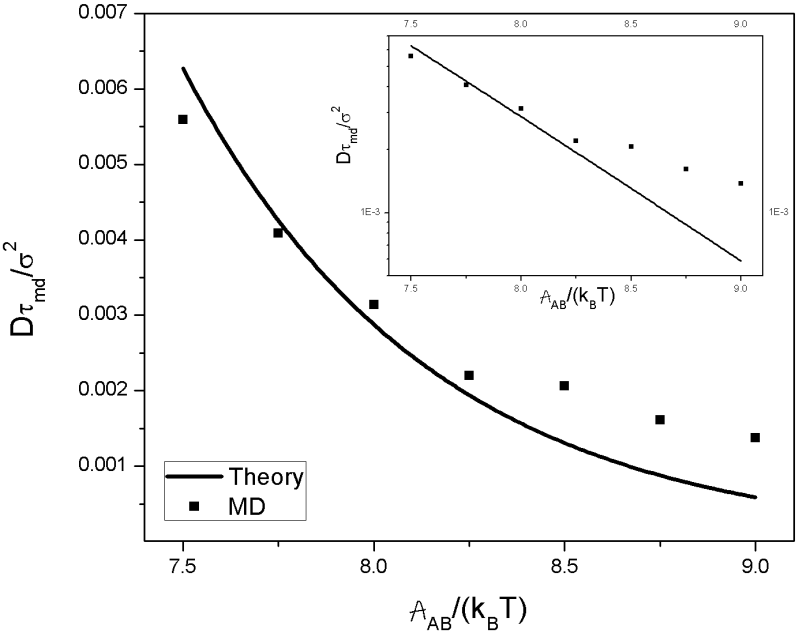

Figure 3.3: Behavior of the distribution $D(y)\,p_y(y)$ as function of y. The inset shows how $D(y)$ increases with y until it equals the value of the diffusion constant in the suspension. $D(y)$ is given by Eq. (1.27) with system parameters taken from Ref. [1].

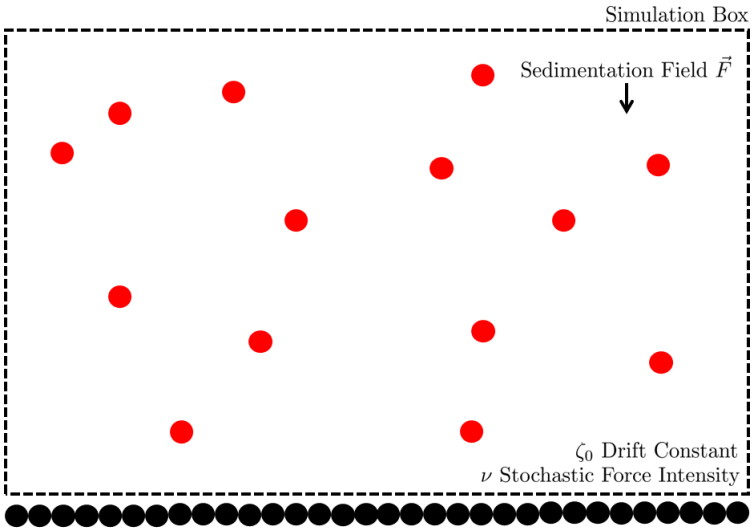

Figure 3.4: The flux of colloids towards the substrate. The colloids are initially put inside a suspension with drift coefficient ζ_0 and stochastic force intensity ν. The presence of a constant sedimentation field $\vec{F}$ directed towards the substrate drives the colloids towards it. The simulation box defines the boundaries of the system, with periodic boundary conditions on the vertical boundaries and a reflective boundary in the upper limit.

algorithm until a colloid reaches the lower limit of the simulation box, then, the time of the event is stored and when a second deposition occurs, the arrival time is also stored, and through the difference of times, we calculate and record the time between two consecutive depositions, as a function of the system parameters.

The simulation runs for a finite time but long enough so that plenty of colloids reach the substrate. This guarantees sufficient data to calculate accurate averages. We found that a simulation time of $t_{sim} = 10,000\,\tau_{md}$ with a time step $\Delta t = 0.0001\,\tau_{md}$ is enough to obtain excellent results.

Figures 3.5 and 3.6 show the behavior of τ_{dep} and $\mathcal{F}$ as function of F, respectively. In both cases, good agreement is found between MD results and those from the analytical model. As expected, the linear approximation for the deposition rate gives good results for large values of F.

3.0.3 Residence Time

Once the particle has reached the substrate, it executes a random walk until it eventually aggregates to one of the islands; see Fig.3.7, either the one on the left or right. The simulation continues until the mobile colloid reaches one of the islands. The side limits of the simulation box determine the region in which the colloid can be trapped by the island. Since the aggregation is instantaneous for the parameter used, the transversal time, i.e., the time a colloid spends on the substrate before reaching one of the islands, is equal to the residence time.

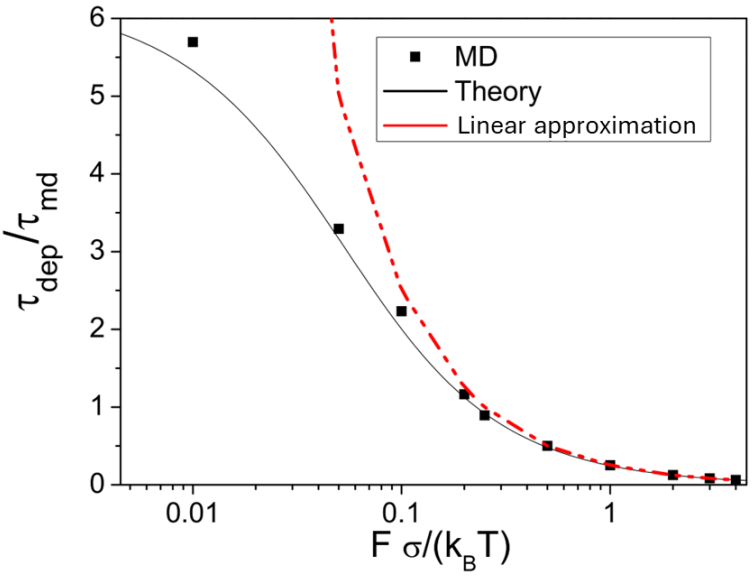

Figure 3.5: Deposition time as a function of F calculated from MD simulations and from the analytical result given by Eq. (1.20). This figure appears as FIG. 5 in Ref. [2].

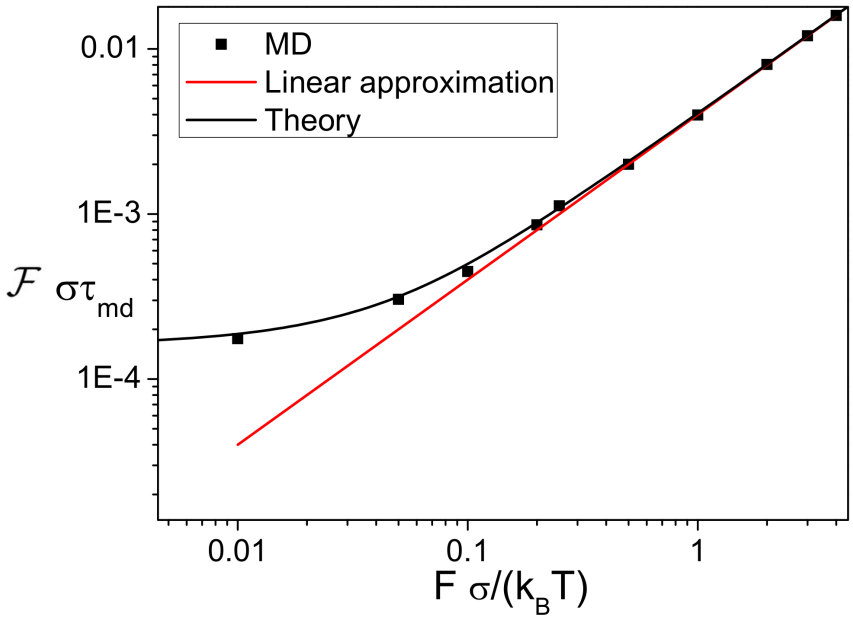

Figure 3.6: Flux towards the substrate as a function of F from MD simulations and from analytical results given by Eq. (1.19). As predicted, for large values of F the flux increases linearly. This figure appears as FIG. 6 in Ref. [2].

Figure 3.7: A colloid trapped by the field generated by the substrate evolves by random walk until it either aggregates to the island on the left or right end of the simulation box.

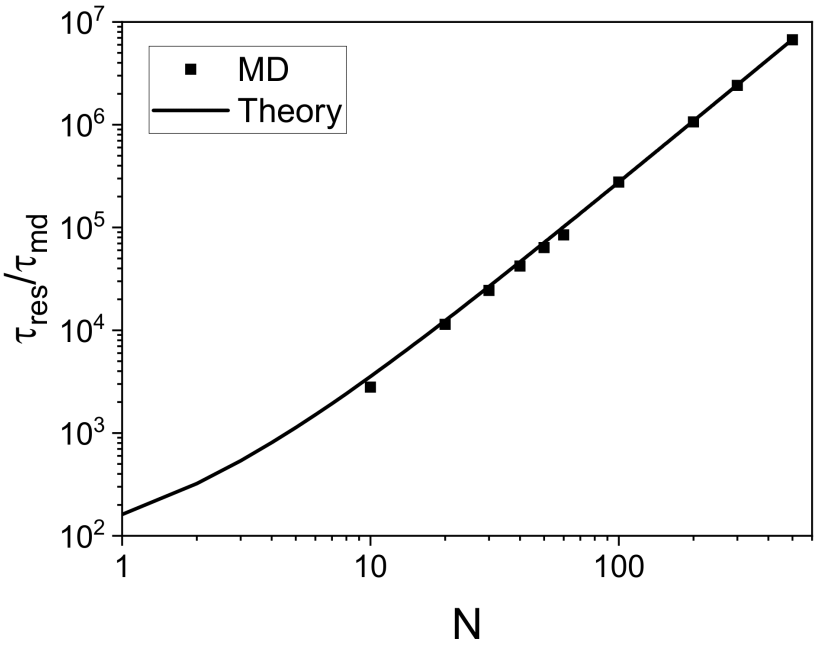

Figure 3.8: The behavior of $\tau_{\rm res}$ as a function of N. Symbols correspond to MD results and the analytical curve to Eq. (1.41). The discrepancies due to the assumption of $\epsilon = 0$ become negligible for large gaps, i.e., $(N > 20)$. This figure appears as FIG. 9 in Ref. [2].

The simulation proceeds as follows. A colloid is deposited at a random site, inside the gap, and the time is set to $t = 0$. The colloid then evolves according to the BAOAB algorithm until it crosses one of the side limits of the simulation box, and the aggregation time is recorded. Then, another colloid is deposited at a random site inside the gap and the process is repeated until there is enough data to obtain good averages. We found that around 10,000 repetitions are enough to reproduce the expected results.

The behavior of $\tau_{\rm res}$ as function of N with $\epsilon = 0$ is shown in Fig. 3.8. The agreement with Eq. (1.41) is excellent, especially for large gaps where $\tau_{\rm res} \approx \tau_{md} N^2/6$.

3.0.4 Density of Colloids

The density of colloids at each site of the gap can be obtained through a simulation setup similar to the one used for the aggregation time. Although both simulations can be run simultaneously, for the sake of simplicity, we run them separately.

The simulation box is the same as the one shown in Fig. 3.7, and the colloid evolves according to the BAOAB algorithm. In this case, every second (10,000 steps, since $\Delta t = 0,0001\tau_{md}$), the exact position of the colloid is not recorded, but the position of the nearest minimum, following the criteria shown in Fig. 3.9.

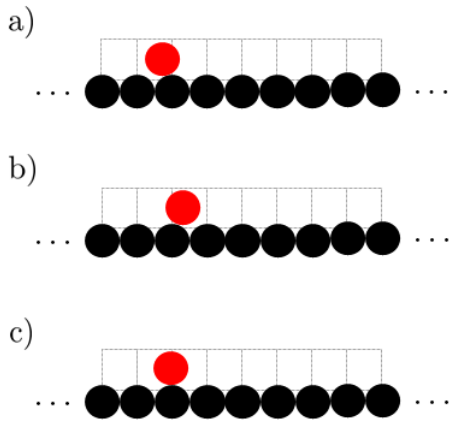

Figure 3.9: To determine the density of monomers, the position of the colloid is recorded, based on the nearest minimum position. There are three different cases: a) the nearest minimum is the left one, b) the nearest minimum is the right one, c) when the colloid is exactly in the middle between two minimums no position is recorded, which is an unlikely case.

The simulation runs for a time longer than the typical aggregation time, which depends on the gap length. In this way, most of the sites of the gap would be occupied at least once. Once the simulation ends, the whole process is repeated to obtain good averages. We found that 10,000 repetitions would reproduce the expected results.

Figure 3.10 shows the density for gaps with different lengths ($N = 10$, 20, 30, 40, and 50). The numerical evidence suggests that the islands can be considered perfect traps for the employed parameters and then the system is limited by diffusion.

Despite ϵ being finite for this interaction strength [2], taking $\epsilon = 0$ in Eqs. (1.32) and (1.41) gives an excellent approximation to evaluate both ρ_n and τ_{res}.

3.1 LAMMPS

LAMMPS [72,73] stands for Large-scale Atomic/Molecular Massively Parallel Simulator. LAMMPS is a classical molecular dynamics simulation code focusing on materials modeling. It was developed at *Sandia National Laboratories*, a US Department of Energy facility, but now LAMMPS

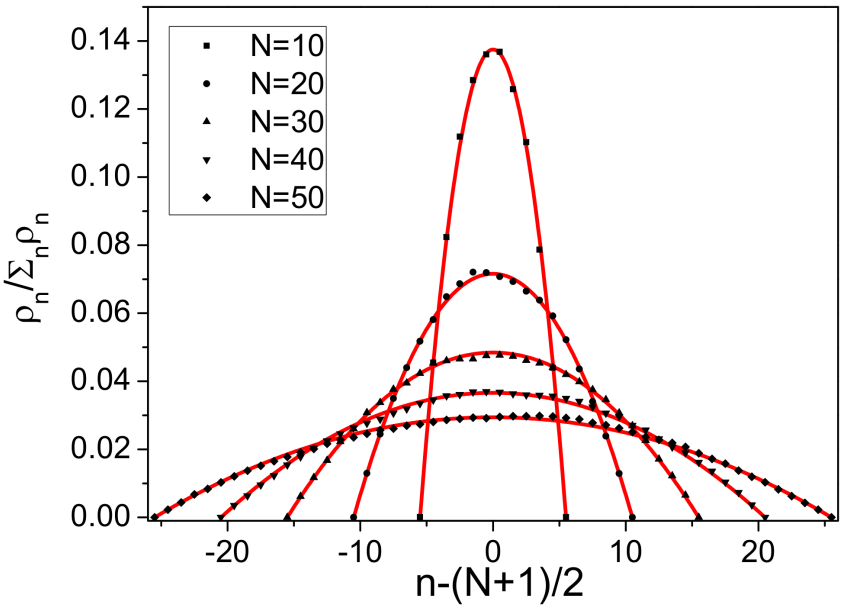

Figure 3.10: Density ρ_n for five different gap lengths. Symbols correspond to MD results and lines to analytical results from Eq. (1.32) with $\epsilon = 0$. This figure appears as FIG. 8 in Ref. [2].

includes contributions from many research groups and individuals from many institutions. LAMMPS is open-source software distributed under the terms of the GNU Public License Version 2 (GPLv2).

We use LAMMPS to run the simulations regarding the nucleation processes since they are costly in terms of computational resources. LAMMPS, as a joint work of several investigation groups, provides a robust enough tool to run such simulations at the expense of reasonable resources.

3.1.1 Nucleation Description

Given that the simulation parameters are such that $\tau_{res} \ll \tau_{dep}$, if two colloids coincide in the gap, the first colloid likely has already reached a steady state by the time the second arrives. This situation is equivalent to having the two colloids simultaneously in the gap, one of them is deposited at a site with an uniform probability $1/N$, and the remaining one is deposited with a probability $\rho_n / \sum_n \rho_n$ where ρ_n is the density of colloids for large time. This procedure is illustrated in Fig. 3.11.

The simulation continues until either one of the colloids aggregates to one of the islands, at the left or right of the gap, or when the two colloids reach the interaction range between them. For the parameters used, the latter case means that a nucleation event occurs. If a nucleation occurs, the simulation time and the position inside the gap of the nucleation event are recorded.

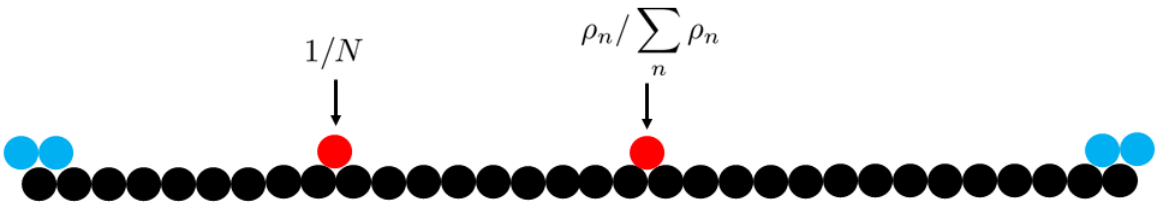

Figure 3.11: Setup for the computational simulation for the nucleation process using LAMMPS. Two colloids are deposited simultaneously, the first one with uniform probability $1/N$ and the second one with probability $\rho_n / \sum_n \rho_n$.

Then, the simulation is repeated until there is enough data to obtain good averages. It is worth mentioning that around 47% of the experiments end up with a nucleation event.

For the sake of simplicity at the time of analyzing the behavior of the nucleation probability function for different gap lengths, we defined the scaled nucleation probability distribution according to $\lambda = n/N$ and $p(\lambda) = N\,\mathcal{P}(\lambda)$. In the case of the mean-field approximation, the scaled for of p_{MF} given by Eq. (1.59), can be rewritten as

$$p_{MF}(\lambda) \approx 30\lambda^2(1-\lambda)^2. \tag{3.2}$$

In this way, Eq. (3.2) can be used to visualize MD data for all gaps on the same scale. Figure 3.12 shows the scaled distribution of the nucleation sites for gaps of different lengths ($N = 10$ to 100). Both $\mathcal{P}(n)$ and $\mathcal{P}_{MF}(n)$ provide an adequate description of the simulation results for the lengths considered.

These results also support the approximation $\epsilon = 0$, since for $\epsilon > 0$, $\mathcal{P}(n)$ should be flatter and $\mathcal{P}(0) > 0$. The main differences between the analytical and numerical results are due to the assumption that a nucleation occurs when a colloid hops on top of the other used in the former, whereas in the simulations, a nucleation occurs when the centers of two colloids are closer than the interaction cutoff distance, which leads to a more pronounced distribution peak. On the other hand, the initial condition given by Eq. (1.53) is formally fulfilled in the limit $\mathcal{R} \to \infty$, which cannot be easily achieved for colloids; as mentioned previously, in this work $\mathcal{R} \approx 1.6 \times 10^3$ is far from the desired limit.

The numerical evaluation of Eq. (1.61) using the result of Eq. (1.58) leads to $g \approx 0.47$ regardless of the length of the gap, as shown in the inset of Fig. 3.12. This is a consequence of the chosen interaction parameters, which make dimers stable. For a different set of interaction parameters, the critical nucleus size can be larger than $i = 1$, and g would depend on L [74].

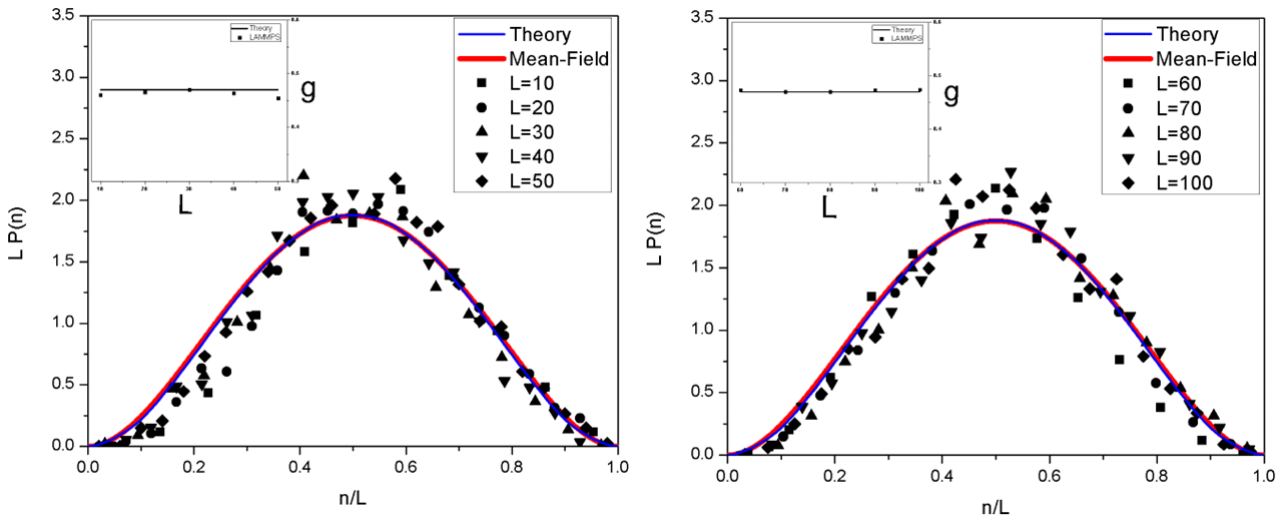

Figure 3.12: Probability distribution of the nucleation sites inside a gap with length L. Symbols correspond to MD simulation results, black lines to theoretical results from Eq. (1.57), and the red line to the mean-field approximation given by Eq. (3.2). Inset: The nucleation rate inside the gap ($g \simeq 0.47$) is found to be independent of the gap length.

Chapter 4

Fragmentation Equation (FE): From Local to Global Behavior

In this chapter, we extend the results obtained from studying the dynamics of one and two colloids in a single gap to develop a global description for a system that evolves by EG. In this case, our system consists of an ensemble of gaps. We derive a fragmentation equation (FE) using the analytical and numerical results for nucleation and aggregation found previously. The results from the FE are compared with those found by a kinetic Monte Carlo simulation that uses as input the time scales for diffusion, deposition, aggregation, and nucleation. Using kMC simulation we can explore larger and more complex systems.

4.1 Fragmentation Equation (FE)

A fragmentation process can be understood as a reaction in which a gap of length $x + y$ breaks into two smaller gaps of lengths x and y. The rate at which such a process occurs is $F(x, y)$, and the reaction can be represented as follows [75]

$$[x + y] \xrightarrow{F(x,y)} [x] + [y]. \tag{4.1}$$

The determination of $F(x, y)$ is a separate physical problem and depends on the particular system under study. In our case, $F(x, y)$ depends on the distribution of nucleation sites inside a gap. In contrast to the complementary phenomenon of aggregation, it is natural to treat the cluster sizes as continuous, but similarly to the aggregation process, the objective is to understand the emergent gap-length distribution. The number of fragments grows with no limits, and the initial number of fragments is large in most physical settings. The simplest approach is a statistical framework that focuses on average densities and ignores fluctuations; such kind of approach should give a progressively better approximation as the system evolves.

We define $c(x, t)$ as the density of fragments with size in the range $(x, x + dx)$ at time t. This quantity evolves in time according to [75]

$$\frac{\partial c(x,t)}{\partial t} = -c(x,t)\int_0^x F(y,x-y)\,dy + 2\int_x^\infty c(y,t)F(x,y-x)\,dy. \tag{4.2}$$

The first term in Eq. (4.2) accounts for the loss of fragments of mass x due to their breakup. Similarly, then, the second term of Eq. (4.2) accounts for the gain of such fragments due to the breakup of a cluster of mass greater than x, and the 2 in front of the term is to take into account the possibility that either one of the two resulting fragments from the breakup of a y-fragment has size x. A useful way to verify the correctness of the master equation is to verify that the total mass, $\int x\,c(x,t)\,dx$, is conserved.

In general, the master equation of the fragmentation process Eq. (4.2) is constructed in such a way that the following conditions are satisfied [75]

- Linearity: external driving leads to fragmentation instead of interactions between fragments, making the breakup of a fragment independent of the states of other fragments.
- Binary fragmentation: each breaking event produces two fragments.
- Spatial homogeneity: fragment densities are independent of spatial position.
- Shape independence: fragment shape play no role in the system evolution.

The above properties are satisfied by our one-dimensional system. However, if the fragmentation rate $F(x,y)$ depends only on the initial length and not on the lengths of the daughter gaps, then $F(x,y) = \bar{F}(x+y)$ is a function exclusively of the total initial length. Consequently, the following conditions are also satisfied:

$$F(y,x-y) = \bar{F}(y+x-y) = \bar{F}(x), \tag{4.3}$$

and

$$F(x,y-x) = \bar{F}(x+y-x) = \bar{F}(y). \tag{4.4}$$

Replacing equations (4.3) and (4.4) in Eq. (4.2) we obtain

$$\begin{aligned}\frac{\partial c(x,t)}{\partial t} &= -c(x,t)\bar{F}(x)\int_0^x dy + 2\int_x^\infty c(y,t)\bar{F}(y)\,dy,\\ &= -c(x,t)\,x\,\bar{F}(x) + 2\int_x^\infty y^{-1}\,c(y,t)\,y\,\bar{F}(y)\,dy.\end{aligned} \tag{4.5}$$

Defining the function $R(s) = s\bar{F}(s)$, then Eq. (4.5) can be written as follows

$$\frac{\partial c(x,t)}{\partial t} = -c(x,t)R(x) + 2\int_x^\infty y^{-1}\,R(y)\,c(y,t)\,dy, \tag{4.6}$$

where the function $R(s)$ measures how much each site contributes to the overall occurrence rate of the fragmentation process. Therefore, $R(s)$ can be understood as the total breakup rate of a fragment with length s.

4.2 Breakup Rate

In one-dimensional EG the substrate is fragmented into several gaps due to the formation of islands through a nucleation events. In one-dimensional systems, a nucleation inside a gap can be interpreted as a bar breaking into two pieces. The gap distribution between adjacent islands evolves through the fragmentation of gaps by consecutive nucleation events. Therefore, it is possible to use the nucleation description to determine $F(x, y)$. The analogy between fragmentation an nucleation events is shown in Fig. (4.1).

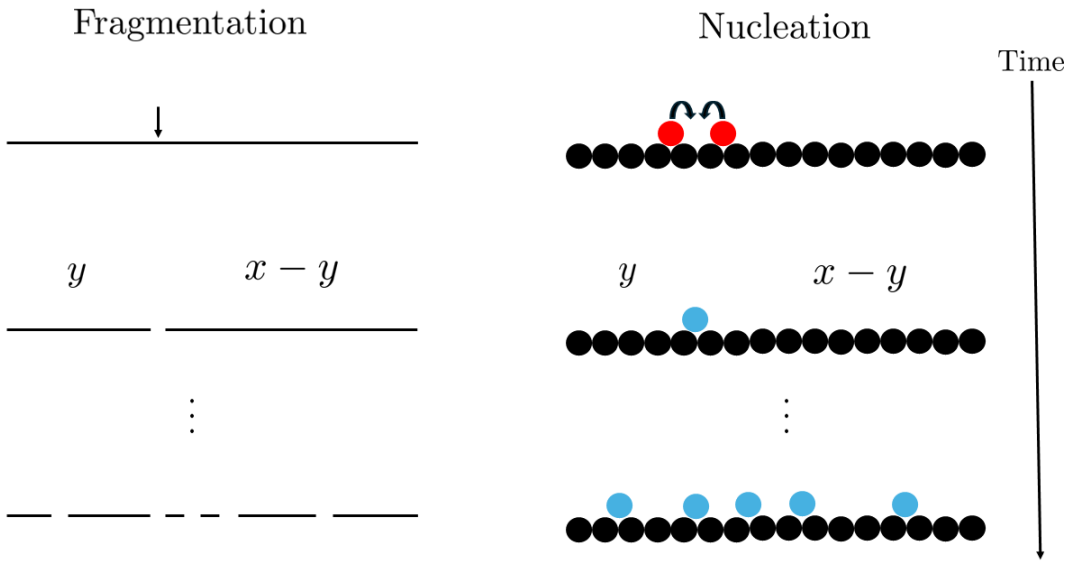

Figure 4.1: Parallel representation and comparison of the fragmentation (left) and nucleation process (right). In both processes, a segment or gap with length x breaks into two sections.

In this way, the formalism used to describe the fragmentation processes in one dimension can be extrapolated and used to describe the formation of islands on a substrate through nucleation events.

We define $P_n^{xy}(s)$ as the probability that a nucleation occurs at the relative position x inside a gap of length y. Similarly, $P_n^{x}(s)$ is the probability density that a nucleation event occurs at the relative position x inside a gap of any length. The retation between $P_n^{x}(s)$ and $P_n^{xy}(s)$ is given by [23]

$$P_n^x(x) = \int_x^\infty dy\, P_n^{xy}(x, y). \tag{4.7}$$

On the other hand, $P_n^y(S)$ is defined as the probability density that a nucleation event occurs in any site of a gap of length y, i.e., it is the probability density of fragmentation of a gap of size y. Consequently, we have

$$P_n^y(x) = \int_0^y dx\, P_n^{xy}(x, y). \tag{4.8}$$

In order to obtain a fragmentation equation in terms of the probabilities defined above, Eqs. (4.7) and (4.8), consider process shown in Fig. 4.2.

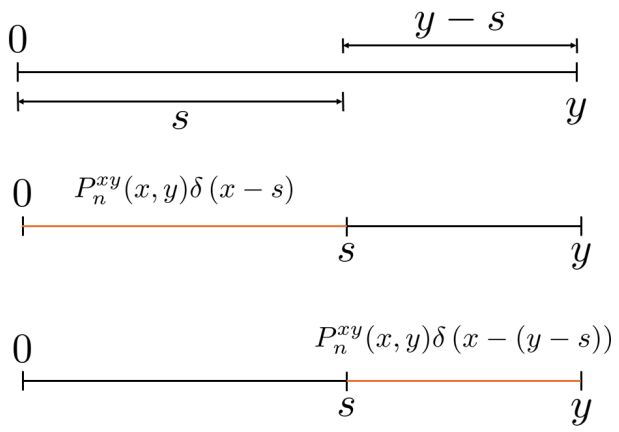

Figure 4.2: Graphical representation of a fragmentation process at site s inside a gap of length y. Using the probability $P_n^{xy}(x, y)$ and delta functions it is possible to write the probability to obtain either of the two possible fragments.

As shown in Fig. 4.2, a gap of length y can break up in position $x = s$, relative to the system of coordinates of the gap, in two possible ways. The first one is giving origin to a fragment of size s (left side of the fragmentation), with probability $P_n^{xy}(x, y)\delta(x - s)$, or the complementary case, giving origin to a fragment of size $y - s$ (right side of the fragmentation), with probability $P_n^{xy}(x, y)\delta(x - (y - s))$. The delta function guarantees that the nucleation event occurs in a way that the gap fragments giving origin to two smaller gaps of exact length s and $y - s$.

The total breakup rate, $R(n)$, can be calculated from the probability $P_n^{xy}(x, y)$ by summing over all possible sites inside the gap and also summing over all gaps lengths as follows

$$R_n(s) = \int_x^\infty dy \int_0^y dx\, P_n^{xy}(x, y)\left[\delta(x - S) + \delta(x - y + S)\right], \tag{4.9}$$

where the inner integral of Eq. (4.9) corresponds to the sum over the nucleation positions x, while the outer integral accounts for all possible gap lengths in which the fragmentation occurs. Note that $y > x$, because to have a fragmentation event which generates a fragment daughter of size x, the original fragment has to be larger than the resulting ones.

Due to the symmetry of the nucleation probability distribution around its maximum, we have $P_n^{xy}(s,y) = P_n^{xy}(s-y,y)$. Then, the total breakup rate $R(n)$, Eq. (4.9), can be simplified to [23]

$$\begin{aligned} R_n(s) &= \int_x^\infty dy \int_0^y dx\, P_n^{xy}(x,y)\,[\delta(x-s)+\delta(x-y+s)] \\ &= \int_x^\infty dy\, [P_n^{xy}(s,y)+P_n^{xy}(s-y,y)] \\ &= 2\int_x^\infty dy\, P_n^{xy}(s,y) \\ &= 2P_n^x(s). \end{aligned} \tag{4.10}$$

4.3 Fragmentation Approach for Island Formation

In order to find a probability distribution for the fragment lengths we define $F_M(s)$ as the number of fragments with size s given that there are M fragments. The quantity $F_{M+1}(s) - F_M(s)$ describes the probability of having a single fragment of size s, therefore that quantity describes the creation of a fragment of size s via a fragmentation event.

The spatial distribution of the islands, i.e., the distribution of the lengths of the gaps, is described by the spacing distribution functions $p^{(k)}(s)$, which in our problem can be interpreted as the probability distribution function of having a gap of size s with k islands in between [23]. The simplest case corresponds to the nearest-neighbor distribution $p^{(0)}(s)$, which represents the probability density to find a gap with an scaled size s between two islands with no additional island in between.

$F_M(s)$ is related to $p^{(0)}(s)$ [23,24], according to, $F_M(S) = (M^2/L)\,p^{(0)}(s)$. In order to determine the nearest-neighbor distribution $p^{(0)}(s)$ in terms of $F_M(s)$ we calculate the probability that describes the creation of a gap with scaled length $s = (M/L)S$, via a nucleation event, as follows

$$F_{M+1}(s) - F_M(s) = \frac{(M+1)^2}{L} p^{(0)}\left(\frac{(M+1)}{L}S\right) - \frac{M^2}{L}p^{(0)}(\frac{M}{L}S), \tag{4.11}$$

from Eq. (4.11) we can identify the step at which the gap size changes as $\Delta s = S/L$, then, Eq. (4.11) can be written as follows

$$\begin{aligned} F_{M+1}(s) - F_M(s) &= \frac{(M+1)^2}{L}p^{(0)}(s+\Delta s) - \frac{M^2}{L}p^{(0)}(s), \\ &= \frac{M^2}{L}\left[p^{(0)}(s+\Delta s) - p^{(0)}(s)\right] + \frac{2M+1}{L}p^{(0)}(s+\Delta s). \end{aligned} \tag{4.12}$$

Note that the first term of Eq. (4.12) resemblance to a finite difference first derivative, so, after some algebra we can obtain a scaled differential equation for $p^{(0)}(s)$, as follows

$$\begin{aligned} F_{M+1}(s) - F_M(s) &= \frac{M^2}{L}\Delta s\left(\frac{p^{(0)}\left(s+\Delta s\right) - p^{(0)}\left(s\right)}{\Delta s}\right) + \frac{2M+1}{L}p^{(0)}(s+\Delta s) \\ &= \frac{M^2}{L^2}S\lim_{\Delta s\to 0}\left(\frac{p^{(0)}\left(s+\Delta s\right) - p^{(0)}\left(s\right)}{\Delta s}\right) + \frac{2M+1}{L}\lim_{\Delta s\to 0}p^{(0)}(s+\Delta s) \\ &= \frac{M^2}{L^2}S\,\frac{dp^{(0)}(s)}{ds} + \frac{(2M+1)}{L}\,p^{(0)}(s) \end{aligned} \tag{4.13}$$

Finally, from the definition of scaled size s it is easy to see that the non-scaled mean length is $\langle S\rangle = L/M$; and we finally obtain the scaled version of Eq.(4.13), as follows

$$F_{M+1}(s) - F_M(s) = \frac{s}{\langle S\rangle}\,\frac{dp^{(0)}(s)}{ds} + 2\,\frac{p^{(0)}(s)}{\langle S\rangle}. \tag{4.14}$$

Regarding the left-hand-side of Eq. (4.14), it is possible to find an analytical expression for $p^{(0)}(s)$ in terms of $p_n^y(s)$ and $p_n^x(s)$ [23, 24], as follows

$$F_{M+1}(s) - F_M(s) = -P_n^y(s) + R_n(s). \tag{4.15}$$

Using (4.10), the Eq. (4.15) takes the form

$$F_{M+1}(s) - F_M(s) = -P_n^y(s) + 2\,P_n^x(s). \tag{4.16}$$

Finally, replacing Eq. (4.16) in Eq. (4.14), we obtain a differential equation for $p^{(0)}(s)$ in terms of the probabilities p_n^x and p_n^y.

$$-P_n^y(s) + 2\,P_n^x(s) = \frac{s}{\langle S\rangle}\,\frac{dp^{(0)}(s)}{ds} + 2\,\frac{p^{(0)}(s)}{\langle S\rangle} \tag{4.17}$$

The distribution $p_n^{xy}(x,y)$ can be approximated as the independent product of the probability $p_n^y(y)$ to nucleate inside a gap with size y and the conditional probability $p_{MF}(y)/y$, see Ref. [23]. In this approach $p_n^{xy}(x,y)$ is given by

$$P_n^{xy}(x,y) = \frac{p_{MF}(y)}{y}P_n^y(y), \tag{4.18}$$

where $p_{MF}(y)$ corresponds to the nucleation probability previously calculated in the mean-field approximation and given by Eq. (3.2). The explicit form of $P_{MF}(y)$ is

$$p_{MF}(x,y) = 30\left(\frac{x}{y}\right)^2\left[1-\left(\frac{x}{y}\right)\right]^2 = \frac{30}{y^4}x^2\,(y-x)^2\,. \tag{4.19}$$

It is reasonable to propose that $p_y^n(y)$ is proportional to product between the rate of nucleation within the gap, ω, and the number of gaps with length y. This functional form is supported by numerical results from the works of Blackman and Mulheran [24] and González et al. [23, 45]. Therefore, we assume

$$P_n^y(y) = \frac{y^\gamma}{\mu_\gamma}p^{(0)}(y), \tag{4.20}$$

where μ_γ is used as a normalization constant and corresponds to the γ-th moment of the distribution $p^{(0)}(s)$. The form of Eq. (4.20) assumes that $P_n^y(y)$ is proportional to the number of gaps with size y times a factor y^γ. Then, using Eqs. (4.19) and (4.20) in Eq. (4.21), we obtain

$$P_n^{xy}(x,y) = \frac{30}{\mu_\gamma}x^2\,(y-x)^2\,y^{\gamma-5}p^{(0)}(y). \tag{4.21}$$

It is easy to demonstrate that by using Eq. (4.21) along with Eq. (4.8), we recover the expression presented in Eq. (4.20). Using Eqs. (4.21) and (4.7) we obtain an expression for $p_n^x(x)$, as follows:

$$P_n^x(x) = \frac{30s^s}{\mu_\gamma}\int_s^\infty dy\,p^{(0)}(y)\frac{(y-s)^2}{y^{5-\gamma}}. \tag{4.22}$$

Finally, Eq. (4.20) into Eq. (4.17), we obtain

$$\frac{dp^{(0)}(s)}{ds} + \frac{\langle S\rangle}{s}\left(\frac{2}{\langle S\rangle}+\frac{s^\gamma}{\mu_\gamma}\right)p^{(0)}(s) = 2\frac{\langle S\rangle}{s}P_n^x(s). \tag{4.23}$$

Note that Eq. (4.23) corresponds to a first order linear integro-differential equation, which can be partially solved by the integrating factor method [76], obtaining a solution of the form

$$p^{(0)}(s) = e^{-\int ds\,\frac{\langle S\rangle}{s}\left(\frac{2}{\langle S\rangle}+\frac{s^\gamma}{\mu_\gamma}\right)}\int ds\,e^{\int ds\,\frac{\langle S\rangle}{s}\left(\frac{2}{\langle S\rangle}+\frac{s^\gamma}{\mu_\gamma}\right)}2\frac{\langle S\rangle}{s}P_n^x(s), \tag{4.24}$$

where the integral in the exponential term of Eq. (4.24) can be easily evaluated. Finally we have

$$p^{(0)}(s) = \frac{2}{s^2}\,e^{-\frac{\langle S\rangle s^\gamma}{\gamma\mu_\gamma}}\int_0^s dy\,y\,e^{-\frac{\langle Y\rangle y^\gamma}{\gamma\mu_\gamma}}\,\langle Y\rangle\,P_n^x(y). \tag{4.25}$$

The exponential tail of $p^{(0)}(s)$ depends on the value of γ and the ratio $\frac{P_n^y(s)}{p^{(0)}(s)} \propto s^\gamma$ regardless the form of $P_n^{xy}(s)$ [23, 24, 77]. This means that the fragmentation process for large values of s depends on the probability of choosing the gap to fragment; while for small values of s if depends in the probability of choosing the place of fragmentation.

4.4 Statistical Solution of the Fragmentation Equation (FE)

As mentioned in the work of Blackman [24] and González [23], Eq. (4.23) corresponds to an integro-differential equation which is hard to fully solve analytically and even numerically. However, Eq. (4.23) can be solved using a simple statistical algorithm [23].

A line of length L is used to generate an array of points along it. A point in deposited at a random site giving origin to a two independent gaps or fragments. Then a fragments is selected through weighted random probability, of the form y^γ/μ_γ, given that the fragment have size y. If fragment selection is accepted, then the position in which the fragment will break up is selected according to the conditional probability of the form $p_{MF}(y)/y$. The process goes on until the desired coverage θ is achieved.

4.4.1 Poisson Fragmentation

Consider a one-dimensional substrate divided in several gaps. For a totally random fragmentation, the normalized gap length distribution is given by $p^{(0)}(s) = e^{-x}$. Because sizes of the adjacent gaps are not correlated, it is possible to write the normalized spacing distributions for arbitrary values of n in Laplace space as [78]

$$\tilde{p}^{(n)}(l) = \left(\tilde{p}^{(0)}(l)\right)^{n+1}, \tag{4.26}$$

where $\tilde{p}^{(0)}(l) = \int_0^\infty de\, e^{-xl}\, p^{(n)}(x)$ is the Laplace transform of $p^{(0)}(x)$ [79]. Consequently, the normalized spacing distributions between centers are given by

$$p^{(n)}(x) = \frac{1}{n!} x^n e^{-x}. \tag{4.27}$$

As expected, the pair correlation function is given by

$$g(x) = \sum_{n=0}^{\infty} p^{(n)}(x) = 1. \tag{4.28}$$

The size distribution of Voronoi cells $P_{\text{Poisson}}(s)$ is related to the next-nearest-neighbor distribution according to [23]

$$P_{\text{Poisson}}(s) = 2\, p^{(1)}(2s), \tag{4.29}$$

Equation (4.29) is a consequence of the one-dimensional nature of the system. Therefore, this simple relation between $P_{\text{Poisson}}(s)$ and $p^{(1)}(s)$ is not valid for higher dimensions. Explicitly, in one dimension, the distribution of the lengths of Voronoi cells, $P_{\text{Poisson}}(s)$, is given by

$$P_{\text{Poisson}}(s) = 4\, s\, e^{-2s}. \tag{4.30}$$

Therefore, Eq. (4.30) can be used to compare the results obtained from the statistical solution of the FE equation proposed to numerically evaluate Eq. (4.25), for $\gamma = 1$, as show in Fig. 4.3.

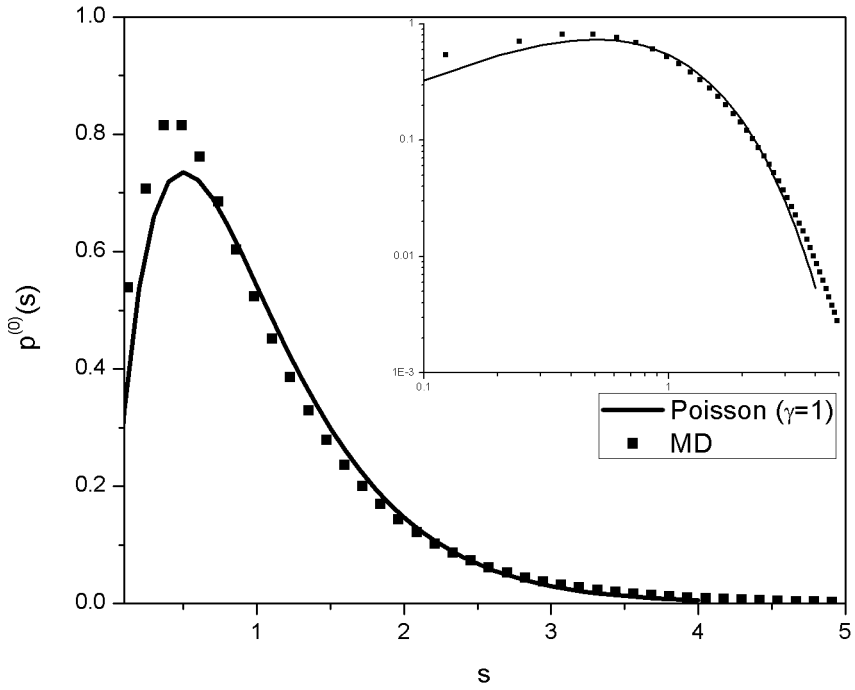

Figure 4.3: arrglar label, FE debería ser ec.(4.30). Nearest-neighbor spacing distribution function $p^{(0)}(s)$ results from a MD simulation (dots) compared to the Poisson distribution function $P_{\text{Poisson}}(s)$ given by Eq. (4.30).

4.4.2 Gap Length Distributions For Adjacent Islands

For the island formation process, the nucleation sites are correlated and the distribution is different from that found in Poisson fragmentation. We run simulations for $\gamma = 2, 3,$ and 4, as shown in Fig. (4.4). We remark that for long substrates it is not necessary to start the simulation by placing a single island, but instead, the simulation can start with a small coverage (around 10% of the desired final coverage) and then evolve from there until the desired coverage θ is

achieved. In the simulations we use a substrate of length $L = 10,000$ with a variable initial coverage θ, and gather data for $50,000$ realizations.

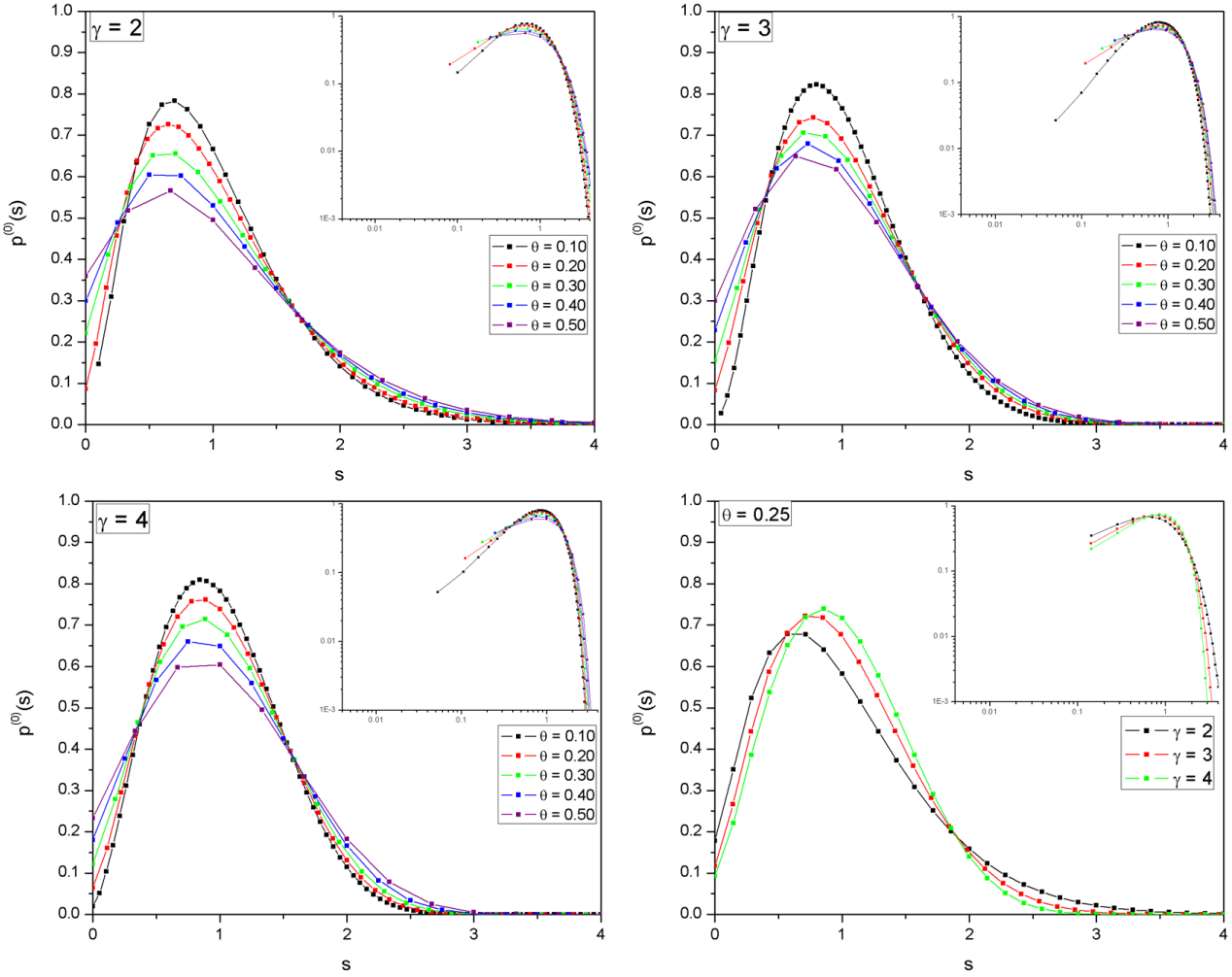

Figure 4.4: Nearest-neighbor spacing distribution function $p^{(0)}(s)$ for different initial coverage values θ. The inset in each respective figure corresponds to the log-scaled distribution. The top-left figure corresponds to a simulation made with $\gamma = 2$; the top-right figure corresponds to $\gamma = 4$; and the bottom-left one corresponds to $\gamma = 3$. The final, bottom-right, figure is a comparison of the distribution functions for $\gamma = 2, 3,$ and 4 for the same final coverage $\theta = 0.25$.

As shown in Fig. 4.4 independent of the value of the parameter γ, we note that the functional form of $p^{(0)}(s)$ does not depend on the initial coverage θ. The only notable difference is a change in the scaling of the distribution function, where the bigger the initial coverage, the smaller the probability of finding larger gaps at early stages of the simulation, which is to be expected. We found that $\theta = 0.25$ as initial coverage is a good initial coverage value, which allows us to speed up the simulations.

A direct evaluation of Eq. (1.60) suggest a value of the parameter $\gamma = 4$, which agrees with

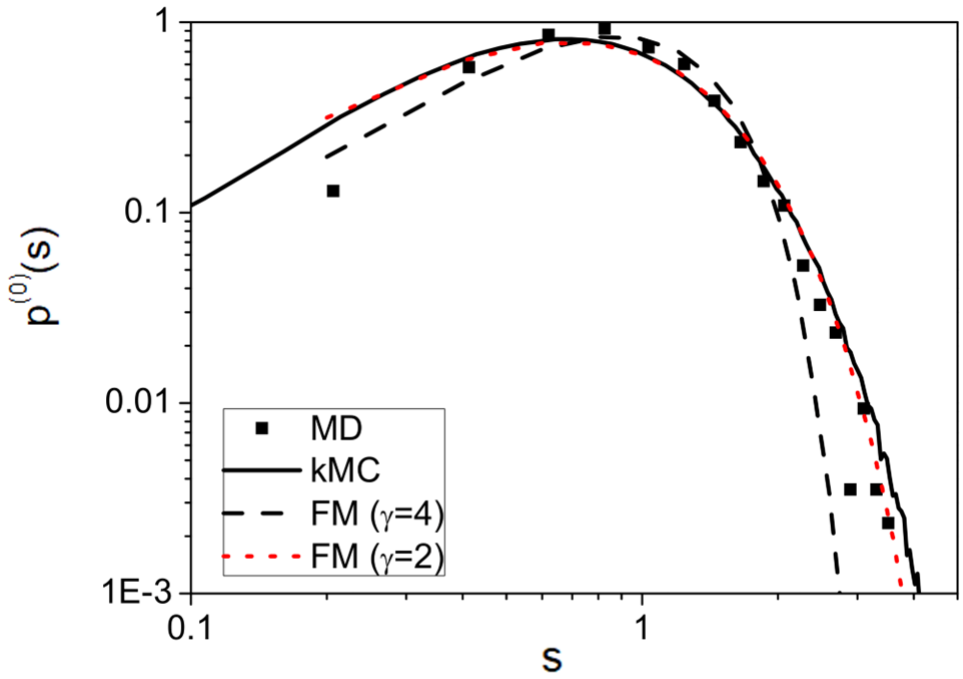

Figure 4.5: Gap length distribution for adjacent islands for a coverage $\theta = 0.25$. Symbols and the solid line correspond to MD and kMC results, respectively. Dashed and dotted lines are obtained from the solution of the fragmentation model given by Eq. (4.17) with different values of γ. This figure appears as FIG. 12 in Ref. [2].

numerical evidence reported in past works [74, 80]. It is found that for large values of s, $p^0(s) \propto s^{-2} \exp\left(-s^\gamma/(\gamma\,\mu_\gamma)\right)$, with γ being the exponent of L in the nucleation rate ω, and therefore, its behavior is completely determined by $P_n^x(s)$. Furthermore, in the limit $s \ll 1$ we have $p(\lambda) \sim \lambda^2$, which in turn implies $p^0(s) \sim s^2$ and $P_n^x(s) \sim s^2$.

Figure 4.5 displays the behavior of $p^{(0)}(s)$ evaluated for coverage $\theta = 0.25$. As expected, the kMC, see Ref. [81] for a brief overview of the numerical method, results coincide with those from MD, especially for large values of x. However, the fragmentation model, given by Eqs. (4.17)) and (4.20)) fails to describe the simulation results for $p^{(0)}(s)$ at large s. This discrepancy can be understood considering that Eq. (4.17) implicitly assumes that the system has reached a quasi-steady state, in which nucleation and aggregation balance each other; this assumption is reasonable for $\mathcal{R} \to \infty$. In this limit $p^{(0)}(s)$ reaches a scaling regime, but for the set of parameters used in our simulations, $\mathcal{R}$ is not large enough to meet this requirement.

Additionally, the fragmentation approach assumes that the colloidal density of the gaps reaches the long-time behavior which is true for small gaps but not necessarily for large gaps if $\mathcal{R}$ is not large enough. The statistical behavior of the system for large values of s is dominated by the breakup of the largest gaps, and under the steady-state assumption, Eq. (4.20) predicts $\gamma = 4$. However, for small values of $\mathcal{R}$, we can expect a smaller γ. The numerical evidence suggests that for our system $\gamma = 2$. For this empirical value, the fragmentation approach gives excellent

results for describing $p^{(0)}(s)$ when compared to simulations, as can be seen in Fig. 4.5.

4.4.3 Density of Monomers and Islands

Two typical quantities used in EG to describe the time evolution of the growing monolayer are the monomer (N_1) and islands (N) densities. Using our results for the rates of the relevant process which were obtained form analytical and numerical calculations, we perform a kinetic Monte Carlo (kMC) simulation for monolayer growth. For the interaction parameters considered in this work $\mathcal{R} = D/\mathcal{F} \simeq 1.6 \times 10^3$. In our simulations, we consider a one-dimensional substrate with $N = 1000$ sites on which colloids are deposited at random. On average, $2\,\mathcal{R}\,\mathcal{N}_1$ random moves are made by the free colloids on the lattice between two consecutive depositions. In this way, the hopping time is guaranteed to be $\tau = \sigma^2/(2D)$, and the time between consecutive depositions is $(\mathcal{F}L)^{-1}$. For the set of parameters used in the MD simulations, once two colloids are in consecutive lattice sites they form a stable island. Therefore, if a free colloid moves onto a site that is adjacent to one already occupied by another colloid, then either an aggregation or a nucleation event is considered to occur.

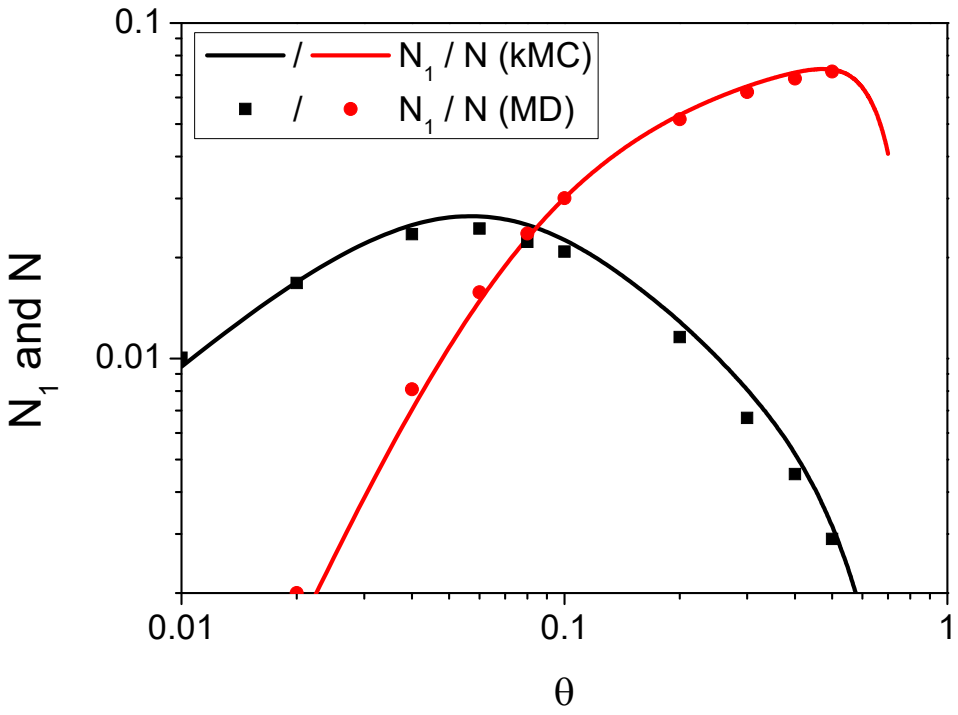

Figure 4.6: Evolution of monomer $\mathcal{N}_1$ and island $\mathcal{N}$ densities as function of the coverage $\theta = \mathcal{F}t$. Symbols correspond to MD simulations while lines to the kMC results. This figure appears as FIG. 11 in Ref. [2].

As shown in Fig. 4.6, the agreement between the MD and kMC simulations for the island and monomer densities is excellent. Nevertheless, using the time scales calculated as function

of the interation parameters allow us to explore bigger systems at a lower computational cost.

Chapter 5

Conclusions and Perspectives

In one-dimensional structures, various parameters such as temperature, pressure, deposition rate, and lattice constants are critical in determining their nature and properties. The growth protocol is particularly influential, with the two-step growth (2SG) protocol offering a promising alternative to the standard simultaneous nucleation and aggregation process. By separating the nucleation and aggregation stages, the 2SG protocol enhances control and understanding of the growth process, presenting a valuable opportunity for further experimental exploration. Although the interplay between deposition, diffusion, nucleation, and aggregation remains complex, recent advances in analytical methods and numerical simulations, including kinetic Monte Carlo (kMC) and molecular dynamics (MD), have provided increasingly valuable insights. Our understanding about the gap-dependent nature of nucleation and the impact of energy barriers on island size distribution has grown in recent years. These aspects laid the groundwork for more precise control over layer growth. With continued progress, the challenges of linking microscopical parameters as the interaction parameters between colloids to measurable quantities are being steadily overcome, moving us closer to a comprehensive understanding of processes associated with the EG.

Analytical tools, including master equations, Fokker-Planck equations, and fragmentation equations, were successfully employed to estimate the relevant time scales—specifically those governed by diffusion, aggregation, and nucleation—based on the interaction parameters between colloids. The strong agreement between theory and computational simulations in our work underscores the validity our calculations for the rates associated to relevant processes. We use the Morse potential but the approach presented can be applied for arbitrary interaction potentials.

Initially, our study focused on the analytical and numerical examination of a single gap. Computational simulations, particularly molecular dynamics (MD) using the BAOAB algorithm and analytical calculations were presented. Our simulations allowed us to accurately estimate the time scales associated with nucleation and aggregation from the interaction parameters between particles. By analyzing the local behavior of monomers within a gap, we gained valuable insights into the time evolution of both monomer and island densities. This local understanding, in turn, contributes to a broader comprehension of the global behavior of epitaxial monolayer

growth.

Furthermore, the results for the time scales were be used as input for a fragmentation model (Eq. (4.17)) to calculate the gap length distribution, $p(0)^(s)$, and consequently, the capture zone distribution and the effective interaction between islands [23]. Our results numerical results for $p(0)^(s)$, suggest an exponent $\gamma = 2$, i.e., $p_g(x) \sim x^{-2}\exp(-x^2)$, which differs from the analytical result given by the Castellano-Politi and MF approaches which gibe $\gamma = 4$ and $\gamma = 5$, respectively. This is not an unexpected result because the exponent γ determines the right tail of the gap length distribution, i.e., determines the behavior for large gaps. However, for small values of $\mathcal{R}$ the steady-state assumption used for the nucleation description does not apply to large gaps. Additionally, the simultaneous presence of more than two colloids inside a gap is not negligible for large gaps, which is one of the assumptions used to formulate Eq. (**??**). In our case, the deposition rate is not small enough ($\mathcal{R} \approx 1.6 \times 10^3$) and therefore, nucleation in large gaps can occur before the monomer density reaches the steady-state regime. In principle, $\mathcal{R}$ can be arbitrarily large, implying a very long time between depositions and, therefore, deposition times that in practice cannot be achieved by MD simulations due the large associated simulation times. Consequently, for colloidal EG, the typical values of $\mathcal{R}$ are much smaller than those found for molecular beam epitaxy.

It is possible to extrapolate the procedure discussed in this work to higher dimensions. However, for $d > 1$, space is not divided into gaps, and it is necessary to consider the concept of capture zone (CZ) and the fragmentation equation is written to describe the effect of a single nucleation in the CZ distribution. Finally, we highlight that linking the interaction parameters between colloids with the relevant times scales of the system allows more control of the size and form of the structure formed, which is one of the main goals in epitaxial growth.

Bibliography

[1] M. Camargo and D. L. González, "Colloidal model of two-step protocol for epitaxial growth in one dimension," Journal of Physics: Condensed Matter, vol. 34, p. 144006, feb 2022.

[2] J. D. Álvarez-Cuartas, M. Camargo, and D. L. González-Cabrera, "Colloidal model for nucleation and aggregation in one dimension: Accessing the interaction parameters," Phys. Rev. E, vol. 109, p. 064604, Jun 2024.

[3] D. Zhu, X. Wang, P. Jia, C. Cai, J. Huang, and G. Zhou, "One-dimensional -al2o3 growth from the oxidation of nial," Corrosion Science, vol. 216, p. 111069, 2023.

[4] C. Volk, J. Schubert, K. Weis, S. Estévez Hernández, M. Akabori, K. Sladek, H. Hardtdegen, and T. Schäpers, "Improved gate-control in inas nanowire structures by the use of gdsco3 as a gate dielectric," Applied Physics A, vol. 100, pp. 305–308, Jul 2010.

[5] J. Becdelievre, X. Guan, I. Dudko, P. Regreny, N. Chauvin, G. Patriarche, M. Gendry, A. Danescu, and J. Penuelas, "Growing self-assisted gaas nanowires up to 80 m long by molecular beam epitaxy," Nanotechnology, vol. 34, p. 045603, nov 2022.

[6] C. Thelander, P. Agarwal, S. Brongersma, J. Eymery, L. Feiner, A. Forchel, M. Scheffler, W. Riess, B. Ohlsson, U. Gösele, and L. Samuelson, "Nanowire-based one-dimensional electronics," Materials Today, vol. 9, no. 10, pp. 28–35, 2006.

[7] K. N. V. S. V. L. D. Ajitha and K. B. Lakshmi, "Nanowire transistors: A next step for the low-power digital technology," IETE Journal of Research, vol. 69, no. 8, pp. 5549–5565, 2023.

[8] B. Alhalaili, E. Peksu, L. N. Mcphillips, M. M. Ombaba, M. S. Islam, and H. Karaagac, "4 - nanowires for photodetection," in Photodetectors (Second Edition) (B. Nabet, ed.), Woodhead Publishing Series in Electronic and Optical Materials, pp. 139–197, Woodhead Publishing, second edition ed., 2023.

[9] U. Mehmood, A. Ul Haq Khan, A. Ali Qaiser, S. Bashir, and M. Younas, "Nanocomposites of carbon allotropes with tio2 as effective photoanodes for efficient dye-sensitized solar cells," Materials Letters, vol. 228, pp. 125–128, 2018.

[10] J. Kim, J. Lim, M. Kim, H.-s. Lee, Y. Jun, and D. Kim, "Fabrication of carbon-coated silicon nanowires and their application in dye-sensitized solar cells," ACS Applied Materials & Interfaces, vol. 6, pp. 18788–18794, Nov 2014.

[11] A. F. Abdelaal, M. Younas, R. N. Iman, A. Damdam, A. M. Al-Amri, and T. N. Baroud, "Fabrication of efficient and economical dye-sensitized solar cells using carbon-coated nanotextured silicon wafers counter electrodes," Synthetic Metals, vol. 301, p. 117537, 2024.

[12] W. Wang, F. Lv, B. Lei, S. Wan, M. Luo, and S. Guo, "Tuning nanowires and nanotubes for efficient fuel-cell electrocatalysis," Advanced Materials, vol. 28, no. 46, pp. 10117–10141, 2016.

[13] F. Patolsky, G. Zheng, and C. M. Lieber, "Nanowire sensors for medicine and the life sciences," Nanomedicine, vol. 1, no. 1, pp. 51–65, 2006. PMID: 17716209.

[14] T. Li, W. Guo, L. Ma, W. Li, Z. Yu, Z. Han, s. Gao, L. Liu, D. Fan, Z. Wang, Y. Yang, W. Lin, Z. Luo, X. Chen, N. Dai, X. Tu, D.-F. Pan, Y. Yao, P. Wang, and X. Wang, "Epitaxial growth of wafer-scale molybdenum disulfide semiconductor single crystals on sapphire," Nature Nanotechnology, 11 2021.

[15] N. Nguyen, H. C. Lee, K. Baek, M. Yoo, H. Lee, H. Lim, S. Choi, C. Kim, S. Nam, and K. Cho, "Atomically smooth graphene-based hybrid template for the epitaxial growth of organic semiconductor crystals," Advanced Functional Materials, vol. 31, p. 2008813, 03 2021.

[16] J. Yang and D. Yan, "Weak epitaxy growth of organic semiconductor thin films," Chem. Soc. Rev., vol. 38, pp. 2634–2645, 2009.

[17] A. Pimpinelli and T. L. Einstein, "Capture-zone scaling in island nucleation: Universal fluctuation behavior," Phys. Rev. Lett., vol. 99, p. 226102, Nov 2007.

[18] A. Pimpinelli and T. L. Einstein, "Pimpinelli and einstein reply:," Phys. Rev. Lett., vol. 104, p. 149602, Apr 2010.

[19] M. Li, Y. Han, and J. W. Evans, "Comment on "capture-zone scaling in island nucleation: Universal fluctuation behavior"," Phys. Rev. Lett., vol. 104, p. 149601, Apr 2010.

[20] T. J. Oliveira and F. D. A. Aarão Reis, "Scaling of island size and capture zone distributions in submonolayer growth," Phys. Rev. B, vol. 83, p. 201405, May 2011.

[21] J. W. Evans and M. C. Bartelt, "Nucleation, adatom capture, and island size distributions: Unified scaling analysis for submonolayer deposition," Phys. Rev. B, vol. 63, p. 235408, May 2001.

[22] J. G. Amar, M. N. Popescu, and F. Family, "Self-consistent rate-equation approach to irreversible submonolayer growth in one dimension," Surface Science, vol. 491, no. 1, pp. 239–254, 2001.

[23] D. González, A. Pimpinelli, and T. Einstein, "Spacing distribution functions for the one-dimensional point-island model with irreversible attachment," Physical review. E, Statistical, nonlinear, and soft matter physics, vol. 84, p. 011601, 07 2011.

[24] J. A. Blackman and P. A. Mulheran, "Scaling behavior in submonolayer film growth: A one-dimensional model," Phys. Rev. B, vol. 54, pp. 11681–11692, Oct 1996.

[25] K. P. O'Neill, M. Grinfeld, W. Lamb, and P. A. Mulheran, "Gap-size and capture-zone distributions in one-dimensional point-island nucleation and growth simulations: Asymptotics and models," Phys. Rev. E, vol. 85, p. 021601, Feb 2012.

[26] J. G. Amar and M. N. Popescu, "Asymptotic capture number and island size distributions for one-dimensional irreversible submonolayer growth," Phys. Rev. B, vol. 69, p. 033401, Jan 2004.

[27] V. I. Tokar and H. Dreyssé, "Universality in size distributions of irreversibly grown epitaxial islands: Kinetic monte carlo simulations and the rate equations study," Phys. Rev. B, vol. 80, p. 161403, Oct 2009.

[28] M. N. Popescu, J. G. Amar, and F. Family, "Self-consistent rate-equation approach to transitions in critical island size in metal (100) and metal (111) homoepitaxy," Phys. Rev. B, vol. 58, pp. 1613–1619, Jul 1998.

[29] M. Popescu, J. Amar, and F. Family, "Rate-equation approach to island size distributions and capture numbers in submonolayer irreversible growth," Physical Review B - PHYS REV B, vol. 64, 10 2001.

[30] J. A. Sánchez, D. L. González, and T. L. Einstein, "Two-step unconventional protocol for epitaxial growth in one dimension with hindered reactions," Phys. Rev. E, vol. 100, p. 052805, Nov 2019.

[31] V. I. Tokar and H. Dreyssé, "Universality and scaling in two-step epitaxial growth in one dimension," Phys. Rev. E, vol. 92, p. 062407, Dec 2015.

[32] P. Tong, X. Ye, B. J. Ackerson, and L. J. Fetters, "Sedimentation of colloidal particles through a polymer solution," Phys. Rev. Lett., vol. 79, pp. 2363–2366, Sep 1997.

[33] C. Allain, M. Cloitre, and M. Wafra, "Aggregation and sedimentation in colloidal suspensions," Phys. Rev. Lett., vol. 74, pp. 1478–1481, Feb 1995.

[34] D. Langevin and F. Rondelez, "Sedimentation of large colloidal particles through semidilute polymer solutions," Polymer, vol. 19, no. 8, pp. 875–882, 1978.

[35] T. L. Einstein, "Applications of ideas from random matrix theory to step distributions on "misoriented" surfaces," Annales Henri Poincaré, vol. 4, pp. 811–824, 2003.

[36] H. Ibach, Physics of Surfaces and Interfaces. Springer Berlin Heidelberg, 2006.

[37] F. Shi, Y. Shim, and J. G. Amar, "Capture-zone areas in submonolayer nucleation: Effects of dimensionality and short-range interactions," Phys. Rev. E, vol. 79, p. 011602, Jan 2009.

[38] W. C. K. Poon, "Colloids as big atoms: the genesis of a paradigm," Journal of Physics A: Mathematical and Theoretical, vol. 49, p. 401001, sep 2016.

[39] A. Blaaderen, R. R. Ruel, and P. Wiltzius, "Template-directed colloidal crystallization," Nature, vol. 385, pp. 321–324, 1997.

[40] M. Heni and H. Löwen, "Surface freezing on patterned substrates," Phys. Rev. Lett., vol. 85, pp. 3668–3671, Oct 2000.

[41] A. van Blaaderen, J. P. Hoogenboom, D. L. J. Vossen, A. Yethiraj, A. van der Horst, K. Visscher, and M. Dogterom, "Colloidal epitaxy: Playing with the boundary conditions of colloidal crystallization," Faraday Discuss., vol. 123, pp. 107–119, 2003.

[42] D. Deb and H. H. von Grünberg, "Colloidal model system for island formation," Journal of Physics: Condensed Matter, vol. 21, p. 245102, may 2009.

[43] M. Einax, W. Dieterich, and P. Maass, "Colloquium: Cluster growth on surfaces: Densities, size distributions, and morphologies," Rev. Mod. Phys., vol. 85, pp. 921–939, Jul 2013.

[44] J. Evans, P. Thiel, and M. Bartelt, "Morphological evolution during epitaxial thin film growth: Formation of 2d islands and 3d mounds," Surface Science Reports, vol. 61, no. 1, pp. 1–128, 2006.

[45] D. L. González, "Island nucleation inside a one-dimensional gap with hindered aggregation," Journal of Physics A: Mathematical and Theoretical, vol. 50, p. 035001, dec 2016.

[46] B. Leimkuhler and C. Matthews, "Robust and efficient configurational molecular sampling via langevin dynamics," The Journal of chemical physics, vol. 138, p. 174102, 05 2013.

[47] D. L. González, M. Camargo, and J. Sanchez, "Tasas de difusión y de deposición en un modelo de epitaxia coloidal," Revista de Ciencias, vol. 21, p. 37–52, abr. 2018.

[48] J. D. Álvarez Cuartas, D. L. González-Cabrera, and M. Camargo, "Epitaxial growth in one dimension," Journal of Physics: Condensed Matter, vol. 36, p. 463001, aug 2024.

[49] R. Ganapathy, M. R. Buckley, S. J. Gerbode, and I. Cohen, "Direct measurements of island growth and step-edge barriers in colloidal epitaxy," Science, vol. 327, no. 5964, pp. 445–448, 2010.

[50] J. R. Savage, S. F. Hopp, R. Ganapathy, S. J. Gerbode, A. Heuer, and I. Cohen, "Entropy-driven crystal formation on highly strained substrates," Proceedings of the National Academy of Sciences, vol. 110, no. 23, pp. 9301–9304, 2013.

[51] J.-L. Barrat, E. Del Gado, S. U. Egelhaaf, X. Mao, M. Dijkstra, D. J. Pine, S. K. Kumar, K. Bishop, O. Gang, A. Obermeyer, et al., "Soft matter roadmap," Journal of Physics: Materials, vol. 7, no. 1, p. 012501, 2023.

[52] S. Asakura and F. Oosawa, "Interaction between particles suspended in solutions of macromolecules," Journal of polymer science, vol. 33, no. 126, pp. 183–192, 1958.

[53] K. Miyazaki, K. Schweizer, D. Thirumalai, R. Tuinier, and E. Zaccarelli, "The asakura–oosawa theory: Entropic forces in physics, biology, and soft matter," The Journal of Chemical Physics, vol. 156, no. 8, 2022.

[54] B. C. Hubartt and J. G. Amar, "Critical island-size, stability, and morphology of 2d colloidal au nanoparticle islands," The Journal of Chemical Physics, vol. 142, no. 2, 2015.

[55] R. Kubo, "The fluctuation-dissipation theorem," Reports on progress in physics, vol. 29, no. 1, p. 255, 1966.

[56] S. Lifson and J. L. Jackson, "On the Self-Diffusion of Ions in a Polyelectrolyte Solution," The Journal of Chemical Physics, vol. 36, pp. 2410–2414, 05 1962.

[57] G. Pavliotis and A. Vogiannou, "Diffusive transport in periodic potentials: underdamped dynamics," Fluctuation and noise letters, vol. 8, no. 02, pp. L155–L173, 2008.

[58] S. B. Maurer and A. Ralston, Discrete algorithmic mathematics. CRC Press, 2005.

[59] J. Krug, P. Politi, and T. Michely, "Island nucleation in the presence of step-edge barriers: Theory and applications," Phys. Rev. B, vol. 61, pp. 14037–14046, May 2000.

[60] P. Politi and J. Villain, "Ehrlich-schwoebel instability in molecular-beam epitaxy: A minimal model," Physical Review B, vol. 54, no. 7, p. 5114, 1996.

[61] C. Castellano and P. Politi, "Spatiotemporal distribution of nucleation events during crystal growth," Phys. Rev. Lett., vol. 87, p. 056102, Jul 2001.

[62] P. Politi and C. Castellano, "Process of irreversible nucleation in multilayer growth. ii. exact results in one and two dimensions," Phys. Rev. E, vol. 66, p. 031606, Sep 2002.

[63] P. Politi and C. Castellano, "Process of irreversible nucleation in multilayer growth. ii. exact results in one and two dimensions," Physical review. E, Statistical, nonlinear, and soft matter physics, vol. 66, p. 031606, 10 2002.

[64] D. Walton, "Nucleation of vapor deposits," The journal of chemical physics, vol. 37, no. 10, pp. 2182–2188, 1962.

[65] G. Milstein and M. Tretyakov, "Computing ergodic limits for langevin equations," Physica D: Nonlinear Phenomena, vol. 229, no. 1, pp. 81–95, 2007.

[66] H. Risken and H. Risken, Fokker-planck equation. Springer, 1996.

[67] F. Fang and P. Zhu, Molecular Dynamics, pp. 1236–1239. Berlin, Heidelberg: Springer Berlin Heidelberg, 2019.

[68] D. S. Lemons and P. Langevin, An introduction to stochastic processes in physics. JHU Press, 2002.

[69] T. Shardlow, "Splitting for dissipative particle dynamics," SIAM Journal on Scientific computing, vol. 24, no. 4, pp. 1267–1282, 2003.

[70] F. Thalmann and J. Farago, "Trotter derivation of algorithms for brownian and dissipative particle dynamics," The Journal of chemical physics, vol. 127, no. 12, 2007.

[71] D. A. Sivak, J. D. Chodera, and G. E. Crooks, "Using nonequilibrium fluctuation theorems to understand and correct¡? format?¿ errors in equilibrium and nonequilibrium simulations¡? format?¿ of discrete langevin dynamics," Physical Review X, vol. 3, no. 1, p. 011007, 2013.

[72] A. P. Thompson, H. M. Aktulga, R. Berger, D. S. Bolintineanu, W. M. Brown, P. S. Crozier, P. J. in 't Veld, A. Kohlmeyer, S. G. Moore, T. D. Nguyen, R. Shan, M. J. Stevens, J. Tranchida, C. Trott, and S. J. Plimpton, "LAMMPS - a flexible simulation tool for particle-based materials modeling at the atomic, meso, and continuum scales," Comp. Phys. Comm., vol. 271, p. 108171, 2022.

[73] "Lammps molecular dynamics simulator." `https://www.lammps.org`.

[74] D. L. González, A. Pimpinelli, and T. L. Einstein, "Fragmentation approach to the point-island model with hindered aggregation: Accessing the barrier energy.," Physical Review E, vol. 96, no. 1, p. 012804, 2017.

[75] P. L. Krapivsky, S. Redner, and E. Ben-Naim, A Kinetic View of Statistical Physics. Cambridge University Press, 2010.

[76] D. G. Zill, M. R. Cullen, and W. S. Wright, Differential equations with boundary-value problems. Brooks/Cole Publishing Company, 1997.

[77] V. I. Tokar and H. Dreyssé, "Rigorous approach to fragmentation equation for irreversible epitaxial growth in the one-dimensional point island model," Journal of Physics A: Mathematical and Theoretical, vol. 50, p. 375002, aug 2017.

[78] D. L. González and T. L. Einstein, "Voronoi cell patterns: Theoretical model and applications," Physical Review E—Statistical, Nonlinear, and Soft Matter Physics, vol. 84, no. 5, p. 051135, 2011.

[79] D. L. González and G. Téllez, "Statistical behavior of domain systems," Phys. Rev. E, vol. 76, p. 011126, Jul 2007.

[80] P. A. Mulheran, K. P. O'Neill, M. Grinfeld, and W. Lamb, "Distributional fixed-point equations for island nucleation in one dimension: A retrospective approach for capture-zone scaling," Phys. Rev. E, vol. 86, p. 051606, Nov 2012.

[81] A. F. Voter, "Introduction to the kinetic monte carlo method," in Radiation Effects in Solids (K. E. Sickafus, E. A. Kotomin, and B. P. Uberuaga, eds.), (Dordrecht), pp. 1–23, Springer Netherlands, 2007.

Appendix A

Mean values on the Suspension

In order to determine the dependence of the dynamics of the colloidal particles on the suspension parameters it is necessary to determine some quantities as the average position and velocity and the velocity correlation.

A.1 Velocity Average

For low densities the interaction between colloids can be neglected, at least, at first approximation, the interaction between colloids in the suspension, i.e., $\mathcal{A}_{AA}$-like interaction. First, it is necessary to find the ensemble average of the velocity of colloids in the suspension, in order to do so we write the Langevin Eq. (1.2), for a single colloid, as follows

$$\begin{aligned} m\,\frac{d^2\vec{r}}{dt^2} &= -\zeta_0\,\frac{d\vec{r}}{dt} + \nu\,\vec{n}(t) + \vec{F}_T(t), \\ \frac{d\vec{v}}{dt} + \frac{\zeta_0}{m}\,\vec{v} &= \frac{1}{m}\left(\nu\,\vec{n}(t) + \vec{F}(t)\right), \end{aligned} \tag{A.1}$$

where $\vec{F}(t)$ is the total force which is the sum of the force due to the $\mathcal{A}_{AB}$-like interaction and the stochastic forces due to the suspension. Eq. (A.1) can be solved by proposing an integration factor, as follows

$$\begin{aligned} \left(\frac{d\vec{v}}{dt} + \frac{\vec{v}}{\tau_{md}}\right) e^{t/\tau_{md}} &= \frac{e^{t/\tau_{md}}}{m}\left(\nu\,\vec{n}(t) + \vec{F}(t)\right), \\ \int_{t_0}^{t} dt'\,\frac{d}{dt'}\left(\vec{v}(t')\,e^{t'/\tau_{md}}\right) &= \frac{1}{m}\int_{t_0}^{t} dt'\,e^{t'/\tau_{md}}\left(\nu\,\vec{n}(t') + \vec{F}(t')\right), \end{aligned} \tag{A.2}$$

so, from Eq. (A.2) we obtain an expression for the velocity of the colloid in the suspension, given by

$$\vec{v}(t) = \vec{v}(t_0)\, e^{-(t-t_0)/\tau_{md}} + \frac{1}{m}\int_{t_0}^{t} dt' \left(\nu\, \vec{n}(t') + \vec{F}(t')\right) e^{-(t-t')/\tau_{md}}. \tag{A.3}$$

Taking the average $\langle\cdot\rangle_\eta$ on Eq. (A.3) we note that the contribution of the stochastic force vanishes for Eq. (1.3), and since by the short range nature of the potential, Eq. (1.1), if the colloids are not near the substrate the only force acting upon it will be the sedimentation force $\vec{F} = -F\hat{j}$, so we Eq. (A.3) transforms as follows

$$\begin{aligned} \langle\vec{v}(t)\rangle_\eta &= \vec{v}(t_0)\, e^{-(t-t_0)/\tau} + \frac{\vec{F}}{m}\int_{t_0}^{t} dt'\, e^{-(t-t')/\tau_{md}}, \\ &= \vec{v}(t_0)\, e^{-(t-t_0)/\tau} + \frac{\vec{F}}{\zeta_0}\left(1 - e^{-(t-t_0)/\tau_{md})}\right). \end{aligned} \tag{A.4}$$

In the long times limit, i.e., $(t-t_0)/\tau_{md} \gg 1$ we obtain

$$\langle\vec{v}(t)\rangle_\eta = \frac{\vec{F}_s}{\zeta_0} = -\frac{F\hat{j}}{\zeta_0}. \tag{A.5}$$

Therefore, for long time, the sedimentation field makes the colloidal particles move towards the substrate with constant average velocity. If $F = 0$, the system evolves by unbiased Brownian motion.

A.2 Velocity Correlation

The velocity correlation for different times can be used to determine the intensity of the stochastic force ν. Starting from Eq. (A.3), let be $t_2 > t_1$, the correlation velocity is defined as follows

$$\begin{aligned} \vec{v}(t_1)\cdot\vec{v}(t_2) = &\left(\vec{v}(t_0)\, e^{-(t_1-t_0)/\tau_{md}} + \frac{1}{m}\int_{t_0}^{t_1} dt' \left(\nu\, \vec{n}(t') + \vec{F}(t')\right) e^{-(t_1-t')/\tau_{md}}\right)\times\cdots \\ &\cdots\times\left(\vec{v}(t_0)\, e^{-(t_2-t_0)/\tau_{md}} + \frac{1}{m}\int_{t_0}^{t_2} dt'' \left(\nu\, \vec{n}(t'') + \vec{F}(t'')\right) e^{-(t_2-t'')/\tau_{md}}\right), \end{aligned} \tag{A.6}$$

Using Eq. (A.6) and taking the average $\langle\cdot\rangle_\eta$ we obtain

$$
\begin{aligned}
\langle \vec{v}(t_1)\cdot\vec{v}(t_2)\rangle_\eta \;=\;& \vec{v}^2(t_0)\cdot\, e^{-(t_1+t_2-2t_0)/\tau_{md}} \\
&+ \vec{v}(t_0)\cdot\, e^{-(t_1-t_0)/\tau_{md}}\,\frac{1}{m}\int_{t_0}^{t_2} dt''\left\langle \nu\,\vec{n}(t'')+\vec{F}_s(t'')\right\rangle_\eta e^{-(t_2-t'')/\tau_{md}} \\
&+ \vec{v}(t_0)\cdot\, e^{-(t_2-t_0)/\tau_{md}}\,\frac{1}{m}\int_{t_0}^{t_1} dt'\left\langle \nu\,\vec{n}(t')+\vec{F}_s(t')\right\rangle_\eta e^{-(t_1-t'')/\tau_{md}} \\
&+ \left(\frac{\nu}{m}\right)^2\int_{t_0}^{t_1}dt'\int_{t_0}^{t_2}dt''\left\langle \vec{n}(t')\cdot\vec{n}(t'')+\vec{n}(t')\cdot\vec{F}(t'')+\cdots\right. \\
&\qquad \left.\cdots+\vec{n}(t'')\cdot\vec{F}(t')+\vec{F}(t')\cdot\vec{F}(t'')\right\rangle_\eta e^{-(t_1-t')/\tau_{md}}\, e^{-(t_2-t'')/\tau_{md}}.
\end{aligned}
\tag{A.7}
$$

From Eq. (1.3) all the terms involving $\langle\vec{n}\rangle_\eta$ vanish and terms of the form $\langle\vec{n}(t)\cdot\vec{n}(t')\rangle_\eta$ produce a Dirac delta, and the resulting integral can be perform by standard methods, obtaining

$$
\begin{aligned}
\langle \vec{v}(t_1)\cdot\vec{v}(t_2)\rangle_\eta \;=\;& \vec{v}^2(t_0)\, e^{-(t_1+t_2-2t_0)/\tau_{md}} \\
&+ \vec{v}(t_0)\cdot e^{-(t_1-t_0)/\tau_{md}}\,\frac{\vec{F}}{m}\int_{t_0}^{t_2} dt''\, e^{-(t_2-t'')/\tau_{md}} \\
&+ \vec{v}(t_0)\cdot e^{-(t_2-t_0)/\tau_{md}}\,\frac{\vec{F}}{m}\int_{t_0}^{t_1} dt'\, e^{-(t_1-t'')/\tau_{md}} \\
&+2\,\frac{\nu^2}{m^2}\int_{t_0}^{t_1} dt'\, e^{-(t_1+t_2-2t')/\tau_{md}}\,\Theta(t_2-t_1) \\
&+2\,\frac{\nu^2}{m^2}\int_{t_0}^{t_2} dt'\, e^{-(t_1+t_2-2t')/\tau_{md}}\,\Theta(t_1-t_2) \\
&+\frac{\vec{F}^2}{m^2}\int_{t_0}^{t_1}dt'\int_{t_0}^{t_2}dt''\, e^{-(t_1-t')/\tau_{md}}\, e^{-(t_2-t'')/\tau_{md}}.
\end{aligned}
\tag{A.8}
$$

Note that the first, fourth and fifth terms do not depend on the sedimentation field $\vec{F}$, so those are the terms that we should get in a calculation without external field which can be written in a single term $\langle\vec{v}(t_1)\cdot\vec{v}(t_2)\rangle_\eta^{(\vec{F}=0)}$. The remaining terms can be calculated using standard integration methods, obtaining

$$\begin{aligned}\langle \vec{v}(t_1)\cdot\vec{v}(t_2)\rangle_\eta &= \langle \vec{v}(t_1)\cdot\vec{v}(t_2)\rangle_\eta^{(\vec{F}=0)} \\ &+ \vec{v}(t_0)\cdot e^{-(t_1-t_0)/\tau_{md}}\,\frac{\vec{F}}{m}\,\tau\left(1-e^{-(t_2-t_0)/\tau_{md}}\right) \\ &+ \vec{v}(t_0)\cdot e^{-(t_2-t_0)/\tau_{md}}\,\frac{\vec{F}}{m}\,\tau\left(1-e^{-(t_1-t_0)/\tau_{md}}\right) \\ &+ \frac{\vec{F}_s^2}{m^2}\,\tau^2\left(1-e^{-(t_2-t_0)/\tau_{md}}\right)\left(1-e^{-(t_1-t_0)/\tau_{md}}\right). \end{aligned} \tag{A.9}$$

As a particular case of the Fluctuation-Dissipation theorem [55] we can obtain an explicit expression for the magnitude of the stochastic force, consider the field free terms of Eq. (A.9)

$$\begin{aligned}\langle \vec{v}(t_1)\cdot\vec{v}(t_2)\rangle_\eta^{(\vec{F}_s=0)} = \vec{v}^2(t_0)\,e^{-(t_1+t_2-2t_0)/\tau_{md}} &+ 2\left(\frac{\nu}{m}\right)^2\int_{t_0}^{t_1} dt'\,e^{-(t_1+t_2-2t')/\tau_{md}}\,\Theta(t_2-t_1) \\ &+ 2\left(\frac{\nu}{m}\right)^2\int_{t_0}^{t_2} dt'\,e^{-(t_1+t_2-2t')/\tau_{md}}\,\Theta(t_1-t_2).\end{aligned} \tag{A.10}$$

Performing the remaining integral using standard methods and we get

$$\begin{aligned}\langle \vec{v}(t_1)\cdot\vec{v}(t_2)\rangle_\eta &= \left(\vec{v}^2(t_0)-\frac{\tau\nu^2}{m^2}\right)e^{-(t_1+t_2-2t_0)/\tau_{md}} \\ &+ \frac{\tau\nu^2}{m^2}\left(e^{-(t_2-t_1)/\tau_{md}}\,\Theta(t_2-t_1)+e^{-(t_1-t_2)/\tau_{md}}\,\Theta(t_1-t_2)\right).\end{aligned} \tag{A.11}$$

In order to reach an stationary state the correlation function must depend only on time difference functions, such as, the third and fourth terms of Eq. (A.11), so we have to guarantee that the first term vanishes. In equilibrium we can take the thermal average $\langle\cdot\rangle_T$

$$\left\langle \vec{v}^2(t_0)-\frac{\tau_{md}\,\nu^2}{m^2}\right\rangle_{\eta,T}=0, \tag{A.12}$$

and since in equilibrium for the energy equipartition theorem we have $\langle\vec{v}^2(t_0)\rangle_{\eta,T}=2k_BT/m$ we can derive the intensity of the stochastic force in terms of the parameters of the system from Eq. (A.12), obtaining $\nu=(2\zeta_0k_BT)^{1/2}$.

A.3 Average Position

To calculate the average position of the colloid in its trajectory from the suspension to the substrate due to the action of the sedimentation field $\vec{F}(t) = -F\hat{j}$, we start integrating Eq. (A.3), obtaining

$$\vec{r}(t) = \vec{r}(t_0) + \vec{v}(t_0)\int_{t_0}^{t} dt' e^{-(t'-t_0)/\tau_{md}} + \frac{1}{m}\int_{t_0}^{t} dt' \int_{t_0}^{t'} dt'' \left(\nu\,\vec{n}(t'') + \vec{F}\right) e^{-(t'-t'')/\tau_{md}}. \quad \text{(A.13)}$$

As before, the terms concerning averages of the stochastic force vanish for Eq. (1.3), so we obtain

$$\langle \vec{r}(t) \rangle_\eta = \vec{r}(t_0) + \vec{v}(t_0)\int_{t_0}^{t} dt' e^{-(t'-t_0)/\tau_{md}} + \frac{\vec{F}}{m}\int_{t_0}^{t} dt' \int_{t_0}^{t'} dt'' e^{-(t'-t'')/\tau_{md}}. \quad \text{(A.14)}$$

The remaining integrals can be performed using standard methods, so we finally get

$$\langle \vec{r}(t) \rangle_\eta = \vec{r}(t_0) + \tau_{md}\left(1 - e^{-(t-t_0)/\tau_{md}}\right)\vec{v}(t_0) + \frac{\vec{F}\tau_{md}}{m}(t-t_0) - \frac{\vec{F}}{m}\tau_{md}^2\left(1 - e^{-(t-t_0)/\tau_{md}}\right). \quad \text{(A.15)}$$

Appendix B

Fokker-Planck Equation Method

A complete description of a macroscopic system consists of solving all the microscopic equations of the system. For many particle systems, this can only be done for a few special systems. In most cases, this kind of solution is impossible, both analytically and numerically. As an alternative, a stochastic description is used, i.e., the system is described by macroscopic variables that fluctuate in a stochastic way. The Fokker-Planck equation is just an equation of motion for the distribution function of fluctuating macroscopic variables [66].

Consider a system that evolves accordingly to a stochastic variable $\xi(t)$ that satisfies the following stochastic differential equation

$$\frac{d\xi(t)}{dt} = f(\xi, t) + g(\xi, t)\, n(t), \tag{B.1}$$

where, $f(\xi, t)$ and $g(\xi, t)$ are arbitrary functions and $n(t)$ is a noise source. The Fokker-Planck (FP) equation associated with Eq. (B.1) is given by

$$\frac{\partial P(\xi, t)}{\partial t} = \left(-\frac{\partial}{\partial \xi}\, a_1 + \frac{\partial^2}{\partial \xi^2}\, a_2 \right) P(\xi, t), \tag{B.2}$$

where, $P(\xi, t)$ corresponds to the probability distribution function of the stochastic variable ξ. The parameters a_1 and a_2 are given by

$$a_1 = f(\xi, t) + \rho\, g(\xi, t)\, \frac{\partial g}{\partial \xi} \quad \text{and} \quad a_2 = \frac{1}{2}\, g^2(\xi, t), \tag{B.3}$$

for a detailed description of the procedure to go from Langevin to Fokker-Planck equations, see Ref. [66].

B.1 Brownian Motion

In order to show how the FP equation method works we solve the problem of Brownian motion, which is also of our interest since the colloids in the suspension, in the absence of the sedimentation field, evolve by pure Brownian motion. The Langevin equation for a free colloid in the suspension is given by

$$\frac{dv}{dt} = -\frac{\zeta_0}{m}\, v + \frac{\nu}{m}\, n(t). \tag{B.4}$$

From the comparison between Eqs. (B.1) and (B.4), it is possible to identify the functions $f(v,t)$ and $g(v,t)$. Using Eq. (B.3) we calculate the parameters of the FP equation, a_1 and a_2, as follows

$$f(v,t) = -\frac{\zeta_0}{m}\, v \quad \longrightarrow \quad a_1 = -\frac{\zeta_0}{m}\, v, \tag{B.5}$$

$$g(v,t) = -\frac{\nu}{m}\, v \quad \longrightarrow \quad a_2 = \frac{\nu^2}{2m}. \tag{B.6}$$

Now, using Eqs. (B.5) and (B.6) in Eq. (B.2) we obtain the corresponding FP equation

$$\frac{\partial P(v,t)}{\partial t} = \frac{\partial}{\partial v}\left[\frac{\zeta_0}{m}\, v\, P(v,t) + \frac{\nu^2}{2m}\frac{\partial}{\partial v} P(v,t)\right]. \tag{B.7}$$

Note that Eq. (B.7) has the form of a continuity equation, where the term inside the square brackets corresponds to the "probability current" J. At equilibrium $\frac{\partial J}{\partial v} = 0$, therefore $J \equiv S$, where S is a constant. Thus, for equilibrium conditions, Eq. (B.7) takes the form

$$\frac{\zeta_0}{m}\, v\, P(v,t) + \frac{\nu^2}{2m}\frac{\partial}{\partial v} P(v,t) = S. \tag{B.8}$$

The differential equation (B.8) can be solved by using the integration factor. Taking $\nu = (2\zeta_0 k_B T)^{1/2}$ we obtain the stationary probability distribution function of velocities

$$P(v) = c\, e^{-\beta \frac{m}{2} v^2}, \tag{B.9}$$

where c is a normalization constant and $\beta = 1/(k_B T)$. Equation (B.9) corresponds to the well-known Boltzmann velocity distribution.

Appendix C

Master Equation

The Master Equation provides a powerful tool for describing the behavior of a system evolving by stochastic processes, e.g. the random walk of a colloid on a substrate.

C.1 General derivation of the Master Equation

Now, let us consider processes where the transition times between states are much smaller than the evolution time of the system. In this limit, time can be considered as a continuous variable. Thus, the equation for the evolution of the probability $p_1(n,t)$ in a time interval Δt is given by

$$\begin{aligned} p_1(n,t+\Delta t) &= \sum_{m=1}^{M} p_1(m,t) p_{1|1}(n,t+\Delta t|m,t) \\ &= \sum_{m=1,m\neq n}^{M} p_1(m,t) p_{1|1}(n,t+\Delta t|m,t) + p_1(n,t) p_{1|1}(n,t+\Delta t|m,t). \end{aligned} \tag{C.1}$$

Taking into account that

$$\sum_{m=1,m\neq n}^{M} p_{1|1}(n,t+\Delta t|m,t) + p_{1|1}(n,t+\Delta t|n,t) = 1, \tag{C.2}$$

the master equation can be written as

$$
\begin{aligned}
p_1(n,t+\Delta t) &= \sum_{m=1,m\neq n}^{M} p_1(m,t)p_{1|1}(n,t+\Delta t|m,t) \\
&+ p_1(n,t)\left(1-\sum_{m=1,m\neq n}^{M} p_{1|1}(n,t+\Delta t|m,t)\right). \qquad \text{(C.3)}
\end{aligned}
$$

Equation C.3 can be written as

$$
\begin{aligned}
\frac{p_1(n,t+\Delta t)-p_1(n,t)}{\Delta t} &= \frac{1}{\Delta t}\sum_{m=1,m\neq n}^{M} p_1(m,t)p_{1|1}(n,t+\Delta t|m,t) \\
&- \frac{1}{\Delta t}\sum_{m=1,m\neq n}^{M} p_1(n,t)p_{1|1}(n,t+\Delta t|m,t), \qquad \text{(C.4)}
\end{aligned}
$$

where a factor $1/\Delta t$ was included. Taking the limit $\Delta t \to 0$ and defining the transition rates $w_{m,n}(t)$ according to

$$
w_{m,n}(t) = \lim_{\Delta t\to 0}\frac{p_{1|1}(n,t+\Delta t|m,t)}{\Delta t}, \qquad \text{(C.5)}
$$

it is easy to find

$$
\frac{\partial p_1(n,t)}{\partial t} = \sum_{m=1}^{M}\left[p_1(m,t)w_{n,m}(t)-p_1(n,t)w_{m,n}(t)\right]. \qquad \text{(C.6)}
$$

The first term on the right-hand side of Eq. (C.6) represents the flux probability towards state n while the second is the flux probability from state n to the other states. A system is said to satisfy detailed balance if the following is true:

$$
\lim_{t\to\infty} p_1(m,t)w_{n,m}(t) = \lim_{t\to\infty} p_1(n,t)w_{m,n}(t), \qquad \text{(C.7)}
$$

for every pair of states m and n. If this condition is satisfied, then, for large times the probabilities are independent of time since

$$
\lim_{t\to\infty}\frac{\partial p(n,t)}{\partial t} = 0. \qquad \text{(C.8)}
$$

All systems that satisfy detailed balance reach equilibrium; however, not all systems that reach equilibrium satisfy detailed balance.

C.2 Diffusion equation

The interpretation of Eq. (C.6) in terms of fluxes leads to the idea of a diffusion equation. Writing the master equation, Eq. (C.6), for the system shown in Fig. 1.6 we obtain

$$\frac{\partial}{\partial t}p_n(t) = \frac{1}{2\tau}\left[p_{n+1}(t) + p_{n-1}(t) - 2\,p_n(t)\right]. \tag{C.9}$$

Introducing the minimum length unit $\Delta n \equiv \sigma$, which corresponds to the diameter of a colloid of the lattice, Eq. (C.9) can be written as

$$\frac{\partial}{\partial t}p_n(t) = \frac{\sigma^2}{2\tau}\left[\frac{p_{n+1}(t) + p_{n-1}(t) - 2\,p_n(t)}{(\Delta n)^2}\right]. \tag{C.10}$$

The term in square brackets in Eq. (C.10) corresponds to a discrete version of a second derivative. Taking the limit $\Delta n \to 0$ and defining the ratio $D \equiv \sigma^2/(2\tau)$ as the diffusion coefficient, we obtain an equation of the form

$$\frac{\partial}{\partial t}p_n(t) = D\,\frac{\partial^2}{\partial n^2}p_n(t). \tag{C.11}$$

C.3 Derivation of the boundary conditions

In the system shown in Fig. 1.1 the interaction between free colloids and islands can be included in the boundary conditions associated with the respective FP equation. In order to derive the appropriate boundary condition for our system, it is necessary to write the corresponding master equation for a colloid on site 1, i.e. $n = 1$, from Eq. (1.29) we obtain

$$\frac{\partial}{\partial t}p_1(t) = \frac{1}{2\tau}p_2(t) + \frac{1}{2\tau}p_0(t) - \frac{1}{2\tau}p_1(t). \tag{C.12}$$

Alternatively, it is possible to derive the master equation directly for this particular site of the system. As shown in Fig. (C.1), for the case of the left island of the gap the transition rate between sites 1 and 2 is given by $1/(2\tau)$, as previously explained. The transition from 1 to 0 has a similar form, but the hopping rate is not necessarily the same, so it is written $1/(2\tau')$. Therefore, the master equation can be written as follows

$$\begin{aligned}\frac{\partial}{\partial t}P_1(t) &= \frac{1}{2\tau}P_2(t) - \left(\frac{1}{2\tau} + \frac{1}{2\tau'}\right)P_1(t), \\ &= \frac{1}{2\tau}P_2(t) - \left(\frac{1}{2\tau} + \frac{1}{2\tau'}\right)P_1(t) - \frac{1}{2\tau}p_1(t) + \frac{1}{2\tau}p_1(t) + \frac{1}{2\tau}p_0(t) - \frac{1}{2\tau}p_0(t),\end{aligned} \tag{C.13}$$

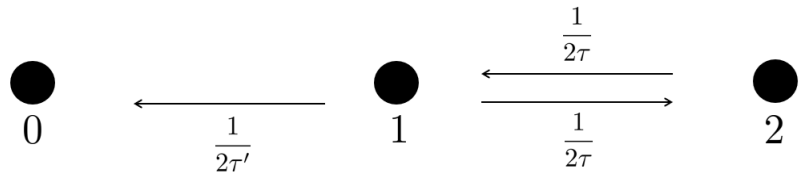

Figure C.1: Diagrammatic representation of the incoming and outcoming flux to/from site 1. The transition probability from 1 to 0 is define as $1/(2\tau')$ in order to study the effect of the boundary.

where the last step made to obtain Eq. (C.13) is necessary to make the comparison easier with Eq. (C.12). It is not difficult to see that, in order for both equations to be equal, it is necessary that the following condition be satisfied

$$\left(\frac{1}{2\tau} - \frac{1}{2\tau'}\right) p_1(t) - \frac{1}{2\tau} p_0(t) = 0. \tag{C.14}$$

Finally, from Eq. (C.14) we can derive the left boundary condition. We find

$$p_0(t) = \left(1 - \frac{\tau}{\tau'}\right) p_1(t) \equiv \epsilon P_1(t), \tag{C.15}$$

where the parameter $0 \leq \epsilon \leq 1$ characterizes the interaction between the islands and the free colloids. Analogously, we can derive the boundary condition for the right island of the gap, that is, for a particle at the site N. As shown in Fig. C.2, the transition rate between sites $N-1$ and N is given by $1/(2\tau)$, while the transition from N to $N+1$ is $1/(2\tau')$. Then, after similar calculations as the one presented for the left island, the boundary condition for the right border is

$$P_{N+1}(t) = \left(1 - \frac{\tau}{\tau'}\right) P_N(t) \equiv \epsilon P_N(t). \tag{C.16}$$

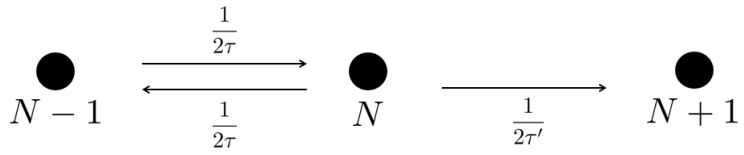

Figure C.2: Diagrammatic representation of the incoming and outcoming flux to/from site N. The transition probability from N to $N+1$ is define as $1/(2\tau')$ in order to study the effect of the boundary.

C.4 Solution of the master equation

A solution of the master equation can be found using the finite-difference method. In the discrete-time limit, Eq. (C.9) can be written as

$$\frac{p_n(t+1)-p_n(t)}{\tau} = \frac{1}{2\tau}\left(p_{n+1}(t)+p_{n-1}(t)\right)-\frac{p_n(t)}{\tau}. \tag{C.17}$$

Some terms of Eq. (C.17) can be simplified, obtaining

$$p_n(t+1)=\frac{1}{2}\left(p_{n+1}(t)+p_{n-1}(t)\right), \tag{C.18}$$

with boundary conditions $p_0(t)=\epsilon\, p_1(t)$ and $p_{N+1}(t)=\epsilon\, p_N(t)$.

In order to solve the difference equation we make use of the well-known anzats of separation of variables, where it is assumed that the solution of Eq. (C.18), $p_n(t)$, can be written as the product of independent functions of its variables, as follows

$$p_n(t)=X(n)F(t). \tag{C.19}$$

Using the anzats, Eq. (C.19), in the difference equation, Eq. (C.18), we obtain the following.

$$X(n)F(t+1)=\frac{1}{2}\left(X(n+1)F(t)+X(n-1)F(t)\right). \tag{C.20}$$

Note that Eq. (C.20) can be rearranged in such a way that the left side only depends on t while the right side only depends on n

$$\frac{F(t+1)}{F(t)} = \frac{X(n+1)+X(n-1)}{2X(n)} \equiv \lambda, \tag{C.21}$$

where $0<\lambda<1$ is a constant, which corresponds to the only solution of Eq. (C.21) besides the trivial one. In order to determine the solutions of Eq. (C.21), the following ansatz can be used [**?**, 63]

$$F(t) = \lambda^t\, F(0), \tag{C.22}$$
$$X(n) = A\,\sin(n\phi)+B\,\cos(n\phi), \tag{C.23}$$

where $F(t)$ is written in terms of its eigenvalues, λ, and $X(n)$ is written as a general harmonic superposition such as Eq. (C.19) have periodicity properties. The eigenvalue λ can be determined from Eq. (C.23) and Eq. (C.21), according to

$$\frac{X(n+1)+X(n-1)}{2X(n)} = \cos(\phi), \tag{C.24}$$

where we have defined $\lambda = \cos(\phi)$. The constants A, B, and ϕ can be determined using of the boundary conditions. Using the left boundary condition, we obtain

$$\begin{aligned} p_0(t) &= \epsilon\, p_1(t), \\ X(0)F(t) &= \epsilon\, X(1)F(t), \\ B\,\lambda^t F(0) &= \epsilon\,(A\sin(\phi) + B\cos(\phi))\,\lambda^t F(0). \end{aligned} \tag{C.25}$$

Rearranging the terms of Eq. (C.25), it is possible to find a relation for A and B in terms of ϕ and ϵ. We find

$$\frac{B}{A} = \frac{a\sin(\phi)}{1 - a\sin(\phi)} \tag{C.26}$$

Using the right boundary condition we can find the following relation for ϕ

$$\begin{aligned} p_{N+1}(t) &= \epsilon\, p_N(t) \\ X(N+1)F(t) &= \epsilon\, X(N)F(t) \\ (A\sin(N+1)\phi + B\cos(N+1)\phi)\,F(t) &= \epsilon\,(A\sin(N\phi) + B\cos(N\phi))\,F(t) - \end{aligned} \tag{C.27}$$

Through the use of trigonometric identities and some algebra we found a transcendental equation for ϕ, as follows

$$\tan(N\phi_k) = \frac{(\epsilon^2-1)\sin(\phi_k)}{(\epsilon^2+1)\cos(\phi_k) - 2\epsilon}, \quad \text{for } k = 0, 1, 2, \ldots. \tag{C.28}$$

Finally, the solution of the master equation, Eq. (C.17), can be written as follows

$$p_n(t) = \sum_{k=1}^{N} A_k F(0)\cos^t(\phi_k)\left[sin(n\phi_k) + \frac{B_k}{A_k}\cos(n\phi_k)\right]. \tag{C.29}$$

C.4.1 Solution of the Master Equation for Perfect Traps

Note that the parameters of the solution of the master equation, Eq. (C.29), λ, B/A, ϕ, depends either implicitly or explicitly on the interaction colloid-island, given by ϵ. Due to the set of parameters considered in the simulations, the islands can be considered as perfect traps, i.e., $\epsilon = 0$. Consequently, Eq. (C.28) reduces to

$$\tan(N\phi_k) = -\tan(\phi_k) \longrightarrow \phi_k = \frac{k\pi}{N+1}, \quad \text{for } k = 0, 1, 2, \ldots . \tag{C.30}$$

Also, from Eq. (C.26) we obtain,

$$\frac{B}{A} = 0 \longrightarrow X_k(n) = A_k \sin\left(\frac{nk\pi}{N+1}\right). \tag{C.31}$$

The constants A_k can be calculated as follows. Let us consider Eq. (C.29) at initial time $t = 0$,

$$p_n(0) \;\; = \;\; \sum_{k=1}^{N} A_k \sin\left(\frac{nk\pi}{N+1}\right). \tag{C.32}$$

In order to calculate the coefficients A_k, we start from Eq. (C.32) and then multiply by an orthogonal sine function, as follows

$$\sum_{n=1}^{N} p_n(0)\, \sin\left(\frac{nk'\pi}{N+1}\right) = \sum_{k=1}^{N} A_k \left[\sum_{n=1}^{N} \sin\left(\frac{nk\pi}{N+1}\right) \sin\left(\frac{mk'\pi}{N+1}\right)\right]. \tag{C.33}$$

Using the orthogonality relation of the sine functions in Eq. (C.33) we find

$$\sum_{n=1}^{N} p_n(0)\, \sin\left(\frac{nk'\pi}{N+1}\right) = \frac{(N+1)}{2} \sum_{k=1}^{N} A_k\, \delta_{kk'}\, \delta_{mn}. \tag{C.34}$$

Taking $n = m$ and simplifying terms in Eq. (C.34) we obtain

$$A_k = \frac{2}{L+1} \sum_{n=1}^{N} p_n(0) \sin\left(\frac{n\,k\,\pi}{N+1}\right). \tag{C.35}$$

Now, the complete solution of the master equation for the case of perfect traps, $\epsilon = 0$, is given by

$$p_n(t) = \sum_{k=1}^{N} A_k \cos^t\left(\frac{k\pi}{N+1}\right) \sin\left(\frac{nk\pi}{N+1}\right). \tag{C.36}$$

Eq. (C.36) can be found in the works of Castellano and Politi.

C.5 Two-Dimensional Master Equation

The evolution of two free colloids on the substrate is required to describe the nucleation. The associated master equation is given by

$$\frac{dp_{m,n}(t)}{dt} = \frac{1}{4\tau}\left[p_{m+1,n}(t) + p_{m-1,n}(t) + p_{m,n+1}(t) + p_{m,n-1}(t) - 4p_{m,n}\right], \tag{C.37}$$

with the conditions $p_{0,n}(t) = p_{N+1,n}(t) = p_{m,0}(t) = p_{m,N+1}(t) = 0$ and $p_{n,n}(t) = 0$, where the first set of restrictions is simply an extension of the boundary conditions for two-dimensions and the last one takes account for the impossibility of two particles to be on the same site.

The solution of Eq. (C.37) can be found in a similar way that in the one-dimensional case using the finite difference method, as follows

$$\begin{aligned} \frac{1}{\tau}\left(p_{m+1,n}(t) - p_{m,n}(t)\right) &= \frac{1}{4\tau}\left[p_{m+1,n}(t) + p_{m-1,n}(t) + p_{m,n+1}(t) + p_{m,n-1}(t) - 4p_{m,n}\right], \\ p_{m,n}(t) &= \frac{1}{4}\left[p_{m+1,n}(t) + p_{m-1,n}(t) + p_{m,n+1}(t) + p_{m,n-1}(t)\right]. \end{aligned} \tag{C.38}$$

The anzats of separation of variables in this case have the form

$$p_{m,n}(t) = Y(m,n)G(t). \tag{C.39}$$

Replacing Eq. (C.39) in Eq. (C.38) we obtain

$$\frac{G(t+1)}{G(t)} = \frac{1}{4}\left[\frac{Y(m+1,n) + Y(m-1,n) + Y(m,n+1) + Y(m,n-1)}{Y(m,n)}\right] \equiv \gamma, \tag{C.40}$$

where, $0 < \gamma < 1$ corresponds to the an eigenvalue of $G(t)$ and $Y(m,n)$ is chosen such as the $p_{m,n}(t)$ have periodicity properties, as follows

$$G(t) = \lambda^t G(0), \tag{C.41}$$

$$Y(m,n) = C\,\sin(m\varphi)\sin(n\varphi) + E\,\cos(m\varphi)\cos(n\varphi). \tag{C.42}$$

As in the one-dimensional case, it is necessary to determine the values of γ, C, E and φ. Using Eq. (C.40) we can determine φ is similar way as in the one-dimensional case, obtaining

$$\varphi = \frac{1}{2}\left(\cos(m\varphi) + \cos(n\varphi)\right). \tag{C.43}$$

Analogously as in the one-dimensional case, for $\epsilon = 0$, we obtain $\varphi = \pi/(N+1)$ and $E/C = 0$, obtaining a solution of for the master equation of the form

$$p_{m,n}(t) = \frac{1}{2^t}\sum_{k,j=1}^{N} B_{kj}\left[\cos\left(\frac{k\pi}{N+1}\right) + \cos\left(\frac{j\pi}{N+1}\right)\right]^t Y_k(m)Y_j(n), \tag{C.44}$$

where $Y_k(m) = \sin\left(\frac{mk\pi}{N+1}\right)$, and B_{kj}, again, corresponds to the Fourier coefficient of the harmonic expansion of Eq. (C.44), and the its explicit form is given by

$$B_{kj} = \left(\frac{2}{N+1}\right)^2 \sum_{m,n=1}^{N} p_{m,n}(0)Y_k(m)Y_j(n). \tag{C.45}$$

Appendix D

Publications

The main findings of this thesis can be found in Ref. [2]. A comprehensive review of one-dimensional epitaxial growth, authored by us, is available in Ref. [48]. Both references have been included in this appendix to provide a thorough overview and to reinforce the context of the research presented in this thesis. These manuscripts serve as key sources of this thesis, not only summarizing the main results but also offering a broader perspective on the current advancements in the one-dimensional EG.

Colloidal model for nucleation and aggregation in one dimension: Accessing the interaction parameters

Juan David Álvarez-Cuartas [1,*] Manuel Camargo [2,†] and Diego Luis González-Cabrera [1,‡]
[1]*Departamento de Física, Universidad del Valle, Apartado Aéreo 25360, Cali, Colombia*
[2]*DCA and CICBA, Universidad Antonio Nariño–Campus Farallones, Km 18 Vía Cali-Jamundí, Cali 760030, Colombia*

(Received 13 February 2024; accepted 2 May 2024; published 6 June 2024)

Through a one-dimensional colloidal model for epitaxial growth, we characterize the nucleation and aggregation processes occurring in a gap between adjacent islands. The timescales associated with deposition, diffusion, aggregation, and nucleation inside the gap are studied in terms of the parameters defining the interaction between colloidal particles. Numerical results from molecular-dynamics (MD) simulations are compared with analytical models and good agreement is found between both data sets. The results for the timescales are used to calculate the associated rates to generate kinetic Monte Carlo (KMC) simulations, which allow exploring larger systems and longer timescales in comparison with MD simulations. The KMC simulations reproduce the global behavior of the densities of islands and monomers as well as the gap length distribution between adjacent islands.

DOI: 10.1103/PhysRevE.109.064604

I. INTRODUCTION

Epitaxy involves the growth of crystalline layers on a substrate, allowing precise control over the arrangement and properties of the deposited material. This process has contributed significantly to modern technology as it is indispensable in the fabrication of advanced electronic and optoelectronic devices. In standard epitaxial growth, atoms are deposited on a substrate at a controlled rate. After deposition, these adatoms or monomers diffuse on the substrate until they cluster with other monomers forming stable islands or until they aggregate to preexisting ones. These two processes are called nucleation and aggregation, respectively, and these are of great interest since their characteristic parameters ultimately determine the properties of the epitaxially grown structures [1–3].

Despite the conceptual simplicity of the fundamental processes involved in epitaxial growth, the theoretical models proposed so far to describe them are not able to completely predict various magnitudes of interest for controlling the layer growth, for example, the critical size of islands, the time evolution of the density of islands, the size distribution of islands, and the distribution of the so-called capture zones [4–18].

The knowledge of many phenomena in condensed-matter physics has been improved in recent decades due to using colloidal systems as models for mimicking their atomic counterparts [19]. Due to the tunability of both the extent and the intensity of the interactions between colloidal particles, these are convenient systems for studying fundamental phenomena such as crystallization, gelation and vitrification, and formation of crystal defects [20–22]. In particular, sedimentation of particles from a dilute colloidal suspension on a flat or patterned surface is a common method to form colloidal crystals [23–25]. These studies have led to the conclusion that the nature of colloidal epitaxy is, in many aspects, similar to that found in atomic epitaxy. Closely related, the drop-drying method is also of interest for the formation of highly ordered monolayers; as the droplet evaporates, the suspended colloidal particles are swept away and adsorbed at the interface, where they diffuse and aggregate on the gas-liquid surface of the droplet [26,27].

In addition to the possibility of tuning the interactions between colloidal particles, the length and timescales involved in colloidal systems allow the experimental observation of nucleation and growth dynamics of self-assembled colloidal monolayers with a resolution equivalent to the particle size [28–30]. For instance, the mechanisms leading to the creation of Ehrlich-Schwoebel barriers, which determine the interlayer transport of monomers, were found to have a kinetic origin in colloidal systems [28,29]. It was also demonstrated that the surface energy landscape can help precisely control nucleation and consequently the size and symmetry of the growing islands [31]. These studies have also considered heteroepitaxy, where, for example, parallel mechanisms between colloidal and atomic systems were found for strain relief for lattice misfit between the growing film and the substrate [32,33].

On the other hand, simulation-based studies of colloidal systems have given results on the role of different physical parameters, such as the effect of the stress field of the substrate in the dynamics of island formation and the morphology of the resulting islands [34]. Empirical interaction potentials have also been considered to understand the dependence on the colloidal size of the critical island size and the energy barriers for both island relaxation and interlayer diffusion [35]. In practice, the results obtained through simulations of colloidal epitaxy can be experimentally replicated. Considering that these observables are to some degree scalable between the

*juan.david.alvarez@correounivalle.edu.co
†manuel.camargo@uan.edu.co
‡diego.luis.gonzalez@correounivalle.edu.co

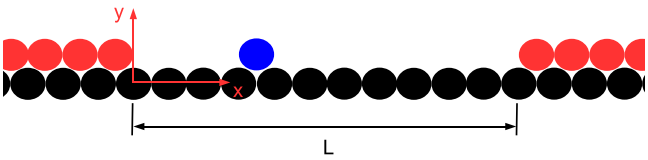

FIG. 1. One free monomer (blue circle) inside a gap of length L between two fixed islands (red circles). Both red and blue are A-type particles, while the substrate is formed by B-type particles (black circles).

molecular and atomic, mostly for submonolayer growth [36], they provide a better understanding of the interactions and processes related to island formation and monolayer growth.

Recently, a two-dimensional colloidal model was introduced to explore the time evolution of both monomer and island densities when a two-step protocol is used for epitaxial growth. Such a protocol has the major advantage that nucleation and aggregation processes take place at different timescales [37]. The main assumption of this model is that the interactions between the colloidal particles are known quantities; therefore, molecular-dynamics (MD) simulations can be employed to follow the deposition of colloids on a one-dimensional substrate due to the slow sedimentation from a two-dimensional dilute suspension. By comparing the simulation results with analytical considerations based on rate equations, it was concluded that the analysis of both monomer and island densities, which are experimentally accessible, can indeed help gain information about the system's microscopic dynamics as well as the validity range of the point-island assumption.

It is important to note that a distinctive feature of a one-dimensional substrate is that islands divide it into independent segments called gaps (see Fig. 1). It turns out that the information gathered for nucleation and aggregation processes occurring inside a single gap can be exploited to recover the time evolution of the whole system in the submonolayer regime [14,17,38–40]. More specifically, the capture kernels associated with nucleation and aggregation in a gap are directly related to the time evolution of the densities of islands and monomers. Furthermore, the knowledge of the nucleation and aggregation rates, in conjunction with the appropriate fragmentation equation, makes it possible to evaluate the gap length distribution between adjacent islands. Experimental and numerical methods can be employed to measure all of these quantities, providing valuable insights to test the validity of the proposed theoretical model.

In this work, molecular dynamics is employed to analyze deposition, nucleation, and aggregation events occurring inside a single gap for a one-dimensional substrate. The simulations allow us to calculate the transition rates associated with deposition, nucleation, aggregation, and diffusion as a function of the interaction parameters between colloidal particles. To explore the evolution of the densities of islands and monomers, the evaluated transition rates are used as input for kinetic Monte Carlo (KMC) simulations. Both MD and KMC results are compared with those from a fragmentation equation based on the description of aggregation and nucleation inside a single gap. In particular, a comparison is made for the gap length distribution between adjacent islands.

This paper is structured as follows. Section II describes the single-gap model employed. In Sec. III the relevant timescales are calculated both numerically and analytically for several interaction parameters. The distribution of nucleation sites is also discussed there. In Sec. IV we provide an analytical expression for the distribution of the nucleation sites for gaps having different lengths. The comparison between the results of KMC simulations and those from MD is presented in Sec. V. In Sec. VI we show how our results for a single gap can be used to describe the gap length distribution. In Sec. VII we draw some conclusions.

II. MODEL DESCRIPTION

Consider a single mobile colloidal particle (monomer) confined inside the gap between two adjacent islands deposited on a substrate, as depicted in Fig. 1. The islands are considered immobile, stable, and formed by monomers of type A, while immobile particles of type B form the substrate. All monomers have diameter σ and mass m and are influenced by an external constant sedimentation field $\vec{F}$. The absolute temperature of the suspension above the substrate is T, and D_0 denotes the diffusion coefficient of a particle in the suspension. In the following σ, m, k_BT, and $\tau_{\rm MD}$ are taken as length, mass, energy, and time units, respectively, with $\tau_{\rm MD} = \sqrt{m\sigma^2/k_BT}$ and k_B the Boltzmann constant.

The particle-particle interaction is modeled by the Morse potential

$$V_{ij}(r) = \begin{cases} \mathcal{A}_{ij}(e^{-2\alpha(r-\sigma)} - 2e^{-\alpha(r-\sigma)}), & r \leqslant r_{\rm cut} \\ 0, & r > r_{\rm cut}, \end{cases} \tag{1}$$

where r is the center-to-center distance between two colloidal particles. The parameters $\mathcal{A}_{ij}$ $(i, j = A, B)$, α, and $r_{\rm cut}$ determine the strength, range, and cutoff distance of the interaction potential, respectively. While the selection of the potential may seem arbitrary, it maintains two primary characteristics: a hard-core interaction and a short-range attractive contribution. These features are exemplified, for instance, by the Asakura-Oosawa potential, which effectively describes the depletion potential resulting from adding small polymers into the colloidal suspension [36,37].

The colloids evolve according to Langevin dynamics in such a way that the position of the ith colloid, $\vec{r}_i$, changes according to

$$m\frac{d^2\vec{r}_i}{dt^2} = -\zeta_0\frac{d\vec{r}_i}{dt} + \nu\vec{\eta}(t) + \vec{F}_i(t), \tag{2}$$

where $\vec{F}_i(t)$ is the total force on the ith colloid due to the external field and all the other colloidal particles [41]. The solvent is taken into account implicitly through the parameters ζ_0 and ν, which give the intensity of the viscous and stochastic forces [first and second terms of Eq. (2)], respectively. As usual, the stochastic variable $\vec{\eta}(t)$ is defined according to

$$\langle\vec{\eta}(t)\rangle_\eta = 0, \quad \langle\vec{\eta}(t)\vec{\eta}(t')\rangle_\eta = \mathbf{I}\delta(t-t'), \tag{3}$$

where $\langle\cdot\rangle_\eta$ indicates the ensemble average, $\delta(t)$ is the Dirac delta function, $\mathbf{I}$ is the 2×2 identity matrix, and the intensity of the random force, ν, is chosen to satisfy the fluctuation-dissipation theorem.

The deposition of colloids inside the gap proceeds as follows. A colloid is introduced in the simulation box at random x, height $y_{\rm ins} = 1.02\sigma$, and with a vertical velocity equal to $-F/m\zeta_0$, which corresponds to the monomer's steady-state velocity in the suspension. Inserting the colloid with these initial conditions helps shorten the simulation time since these implicitly assume that the monomers are deposited at a height high enough to reach the substrate with a velocity equal to that of the steady state. The sedimentation field ensures that the colloid moves toward the substrate and is eventually incorporated into the gap. The substrate generates a periodic potential with well-defined minima, each comprising a metastable site for the deposited mobile monomer. After thermalization, the free monomer moves on the substrate by hopping between consecutive sites, with τ the average hopping time. Therefore, the (lateral) diffusion constant of the monomer on the substrate is given by $D = \sigma^2/2\tau$.

For the numerical description of nucleation, configurations involving only two free monomers within the gap are required, so we proceed as follows. The average time elapsed between the deposition of these two colloids is $\tau_{\rm dep}$. To improve the computational efficiency of the MD simulation, we deposit both colloids simultaneously. However, one of them was deposited at random x having a uniform distribution, while the other one was deposited at random x following the distribution of free colloids of the steady state [see Eq. (20)]. This way, it is implicitly assumed that the first monomer has enough time to reach the steady-state regime before the arrival of the second one.

III. TIMESCALES

A. Diffusion constant

From Eq. (2), the Fokker-Planck equation associated with the distribution $P(x, y, t)$ of finding a particle at position (x, y) at time t is given by [41]

$$\zeta_0 \frac{\partial P(x,y,t)}{\partial t} - \left[\frac{\partial}{\partial x}\left(\frac{\partial \mathcal{V}(x,y)}{\partial x} + \frac{v^2}{2\zeta_0}\frac{\partial}{\partial x}\right) + \frac{\partial}{\partial y}\left(\frac{\partial \mathcal{V}(x,y)}{\partial y} + \frac{v^2}{2\zeta_0}\frac{\partial}{\partial y}\right)\right] P(x,y,t) = 0. \quad (4)$$

Equation (4) is not separable due to the presence of the term associated with the interaction potential $\mathcal{V}(x, y)$, preventing one from finding an exact solution for $P(x, y, t)$ with the Morse potential. However, for a suitable choice of the system parameters, the free colloids will move on the substrate by infrequent events. Therefore, the distribution probability of finding a monomer close to a potential minimum, i.e., once it has been adsorbed by the substrate, can be approximated by the equilibrium distribution

$$P(x, y, t) \approx C \exp[-\beta \mathcal{V}(x, y)], \quad (5)$$

where C is the normalization constant of the distribution. Figure 2 shows the marginal probabilities

$$p_x(x) = \int_0^{r_{\rm cut}} dy\, P(x, y, t) \quad (6)$$

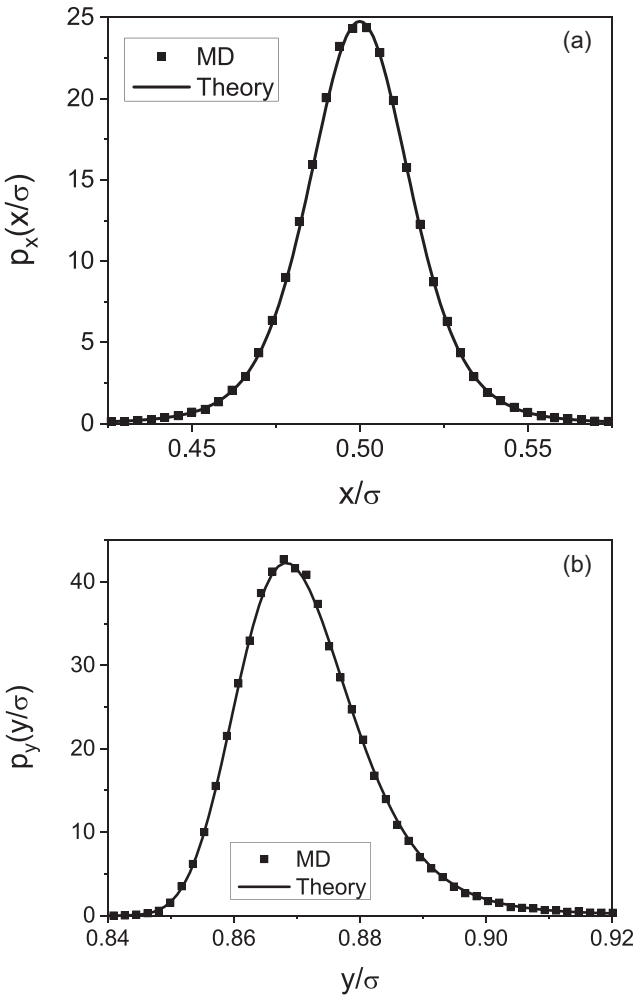

FIG. 2. Marginal distributions (a) $p_x(x)$ and (b) $p_y(y)$ given by Eqs. (6) and (7). As expected, $p_y(y)$ has a well-defined peak at $y \simeq (\sqrt{3}/2)\sigma$, while $p_x(x)$ has its maximum at the midpoint between the center of two consecutive colloids of the substrate.

and

$$p_y(y) = \int_{-\sigma/2}^{\sigma/2} dx\, P(x, y, t), \quad (7)$$

which were evaluated using MD simulations for the parameters $\mathcal{A}_{AA} = 8.8k_BT$, $\mathcal{A}_{AB} = 8.0k_BT$, $\alpha = 25/\sigma$, $\zeta_0 = m/\tau_{\rm MD}$, $F = k_BT/\sigma$, and $r_{\rm cut} = 1.6\sigma$. As shown in Ref. [37], this set of parameters allows the stable growth of islands in the submonolayer regime with a negligible detachment of monomers from the substrate. However, in the case of eventual evaporation, we impose a reflective boundary condition at $y = r_{\rm cut} = 1.6\sigma$, which corresponds to the interaction cutoff distance. In Fig. 2, squares and lines correspond to MD and theoretical results, respectively, the latter being obtained using Eqs. (1) and (5)–(7); as can be seen there, the agreement between numerical and analytical results is excellent.

Using Eq. (4) and the periodicity of the potential energy on the substrate, in Ref. [41] it is demonstrated that, in the high-friction limit, the diffusion coefficient for a horizontal

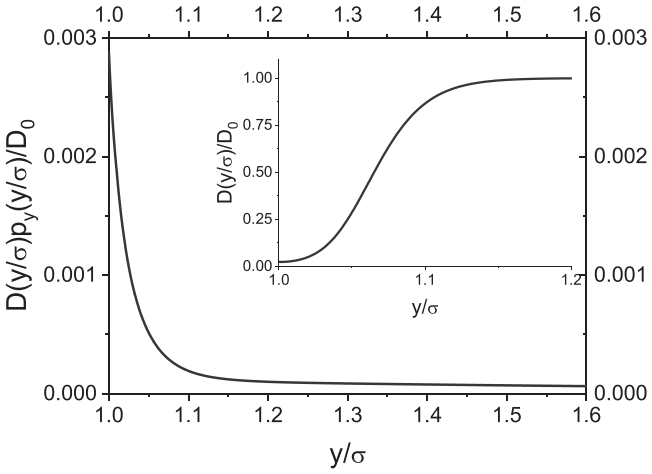

FIG. 3. Behavior of the distribution $D(y)p_y(y)$ as a function of y. The inset shows how $D(y)$ increases with y until it equals the value of the diffusion constant in the suspension. The $D(y)$ is given by Eq. (8) with system parameters taken from Ref. [37].

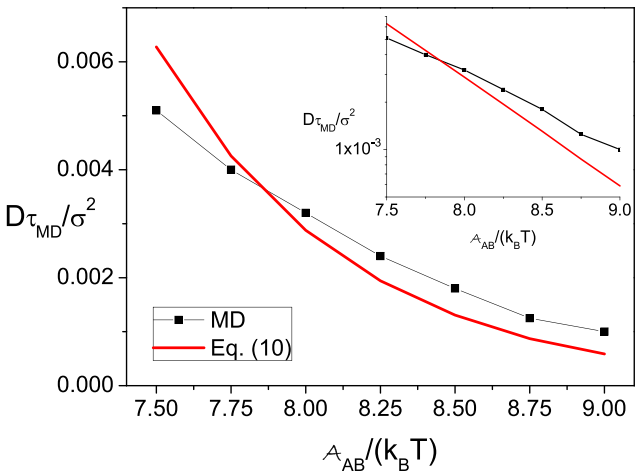

FIG. 4. Diffusion coefficient for different values of the interaction parameter $\mathcal{A}_{AB}$. The results are evaluated from Eq. (10) and molecular-dynamics simulations.

trajectory at a given y can be expressed as

$$D(y) = D_0\sigma^2 I_2^{-1}(y), \tag{8}$$

where D_0 is the diffusion coefficient in the suspension and $I_2(y)$ corresponds to the Lifson-Jackson formula [42]

$$I_2(y) = \int_0^\sigma dx\, \mathrm{e}^{\mathcal{V}(x,y)/k_BT} \int_0^\sigma dx\, \mathrm{e}^{-\mathcal{V}(x,y)/k_BT}. \tag{9}$$

Equation (8) cannot be directly applied to our system because free monomers do not move along a horizontal line due to the fluctuations of the y coordinate. Additionally, the result of the integral in Eq. (9) strongly depends on y, as shown in the inset of Fig. 3. Note that in the region $y > \sigma$, $D(y)$ equals the diffusion constant at the suspension. However, we can estimate the diffusion constant using Eq. (8) as follows. Due to the finite size of the colloids, the transitions between metastable states only occur for $y \gtrsim \sigma$. As shown in Fig. 2 for $p_y(y)$, the probability of finding the particle in this region is quite small. Consequently, the distribution $D(y)p_y(y)$ decays rapidly as y becomes greater than σ, as can be seen in Fig. 3. Then the effective (lateral) diffusion coefficient D can be estimated as

$$D = D(\sigma)p_y(\sigma). \tag{10}$$

Figure 4 displays the results for the diffusion coefficient D obtained by numerically evaluating Eqs. (8) and (10) at $y = \sigma$ for different values of $\mathcal{A}_{AB}$. The theoretical results are compared to those from MD simulations estimated from the long-time behavior of the mean-square displacement. The diffusion constant $D = D(\sigma)p_y(\sigma)$ strongly depends on $\mathcal{A}_{AB}$ as it decreases two orders of magnitude as $\mathcal{A}_{AB}$ increases from $7.0k_BT$ to $9.0k_BT$. The inset shows that our approximation reproduces the exponential decay of D as a function of $\mathcal{A}_{AB}$ but overestimates the decay rate. As mentioned in Ref. [37], taking $A_{AB} = 8.0k_BT$ guarantees the mobility of the free colloids on the substrate but makes unlikely their detachment from the substrate.

B. Deposition rate

The deposition rate due to the slow sedimentation of colloids from the suspension on the substrate can be calculated as follows. Let ρ be the density of colloids in the suspension. For $y > 1.6\sigma$ the colloids do not interact with the substrate, and for small densities ρ, the interaction between mobile colloids can be ignored. Under these conditions, $\mathcal{V}(x, y) \simeq 0$ and in Eq. (4) can be analytically solved. The probability of finding a colloid between y and $y + dy$ in the steady state is given by

$$P(y, t) = \frac{\zeta_0 J}{F}(1 - \mathrm{e}^{-2\zeta_0 Fy/v^2}), \tag{11}$$

where J is the probability current for a single colloid. The deposition rate $\mathcal{F}$ (number of particles deposited per unit length per time) is given by

$$\mathcal{F} = \frac{2\rho F^2 L_y}{v^2(\mathrm{e}^{-2\zeta_0 FL_y/v^2} - 1) + 2\zeta_0 FL_y}, \tag{12}$$

with L_y the height of the suspension. For $k_BT \ll FL_y$, Eq. (12) reduces to the simple linear form $\mathcal{F} = \rho F/\zeta_0$. The average time between consecutive depositions in a gap of length L is given by $\tau_{\mathrm{dep}} = (\mathcal{F}L)^{-1}$. Figures 5 and 6 show the behavior of τ_{dep} and $\mathcal{F}$ as a function of F, respectively. In both cases, good agreement is found between MD results and those from the analytical model. As expected, the linear approximation for the deposition rate gives good results for large values of F.

C. Aggregation time

The traversal time τ_{tr} is defined as the average time after deposition required for a monomer to reach one of the gap edges, while the residence time τ_{res} measures the survival time of a monomer before it aggregates to one of the islands of the gap. Both quantities can be estimated using a simple random-walk model for a colloid confined inside a gap. Let $p_n(t)$ be the probability of finding a single monomer at time t in the nth site of the gap, which can be calculated from the master

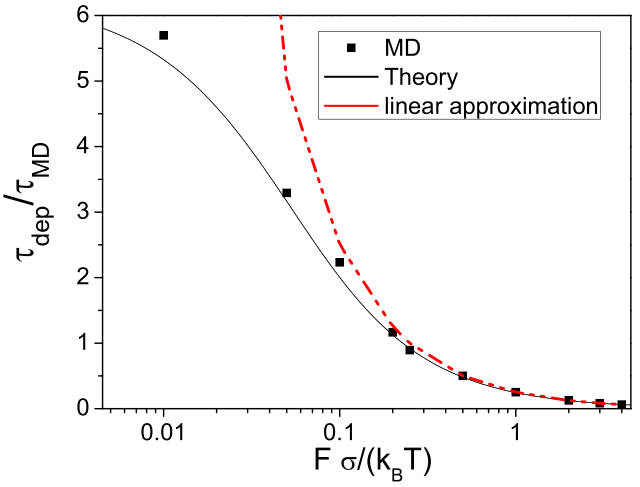

FIG. 5. Deposition time as a function of F evaluated from MD simulations and from the analytical result [Eq. (12)].

equation

$$\frac{dp_n(t)}{dt} = \frac{1}{2\tau}[p_{n+1}(t) + p_{n-1}(t) - 2p_n(t)], \tag{13}$$

where $\tau = \sigma/2D$ is the average hopping time. The boundary conditions are $p_0(t) = \epsilon p_1(t)$ and $p_{N+1}(t) = \epsilon p_N(t)$, where N is the number of lattice sites (potential minima in the gap) and $L = N\sigma$. The parameter $0 \leqslant \epsilon \leqslant 1$ characterizes the interaction between the islands and free colloids. For $\epsilon = 0$ the islands behave as perfect traps, i.e., once a monomer reaches the interaction range of an island, it is instantly captured by the island. Then $\tau_{res} = \tau_{tr}$ since aggregation takes place instantaneously. On the other hand, for $\epsilon = 1$ we have perfect reflecting boundary conditions and aggregation is impossible in this case.

From $p_n(t)$, the survival probability $P_s(t)$, defined as the probability of finding the monomer inside the gap at time t, can be evaluated as

$$P_s(t) = \sum_{n=1}^{N} p_n(t). \tag{14}$$

Then the probability for a monomer to be captured in the time interval $[t, t + \Delta t]$ determines the residence probability distribution $P_{res}(t)$ as

$$P_{res}(t)\Delta t = -P_s(t + \Delta t) + P_s(t), \tag{15}$$

which in the limit $\Delta t \to 0$ takes the form

$$P_{res}(t) = -\frac{dP_s(t)}{dt}. \tag{16}$$

The residence time τ_{res} is the average time a monomer spends inside the gap before being captured by an island. Therefore, using Eq. (16), τ_{res} can be calculated from

$$\begin{aligned}\tau_{res} &= \int_0^\infty dt\, tP_{res}(t) \\ &= \int_0^\infty dt\, P_s(t) \\ &= \sum_{n=1}^{N} \rho_n,\end{aligned} \tag{17}$$

where the density at site n, ρ_n, is defined as

$$\rho_n = \int_0^\infty dt\, p_n(t), \tag{18}$$

where the integration domain was extended up to infinity as $p_n(t)$ is a rapidly decreasing function of t for the parameters used.

Using the definition given by Eq. (18) in Eq. (13), it is found that ρ_n satisfies the recurrence relation

$$-2\tau p_n(0) = \rho_{n+1} + \rho_{n-1} - 2\rho_n, \tag{19}$$

with boundary conditions $\rho_0 = \epsilon\rho_1$ and $\rho_{N+1} = \epsilon\rho_N$. The linear nonhomogeneous recurrence relation given by Eq. (19) can be solved using standard procedures [43]. The solution can be written as $\rho_n = \sum_{j=0}^{2} c_j n^j$, where the coefficients c_j are calculated by replacing the proposed solution in Eq. (19) and using the boundary conditions mentioned above. The explicit form of ρ_n is given by

$$\rho_n = \frac{\tau}{N}\left(\frac{\epsilon N}{1-\epsilon} + (N+1)n - n^2\right). \tag{20}$$

From Eqs. (17) and (20), the residence time is

$$\tau_{res} = \tau\left(\frac{\epsilon N}{1-\epsilon} + \frac{(N+1)(N+2)}{6}\right). \tag{21}$$

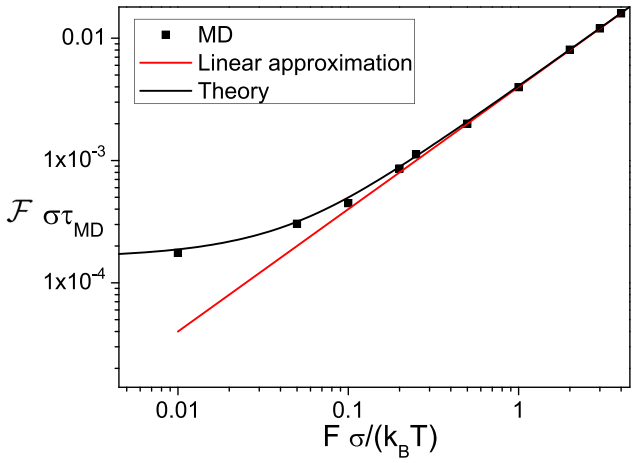

FIG. 6. Deposition rate as a function of F. As predicted, the deposition rate increases linearly for large values of F.

Figure 7 shows the behavior of the parameter ϵ for different values of $\mathcal{A}_{AB}$, which was calculated using Eq. (20) and the MD results for ρ_n. Large values of $\mathcal{A}_{AB}$ ensure that islands behave like perfect traps, i.e., $\mathcal{A}_{AB} \to \infty$ and $\epsilon \to 0$. For small values of the interaction parameter, the detachment of colloids from the islands is very likely and the density of free colloids inside the gap turns out to be homogeneous, as shown in the inset of Fig. 7. For the three values of $\mathcal{A}_{AB}$ considered, Eq. (20) gives an excellent description of the normalized density.

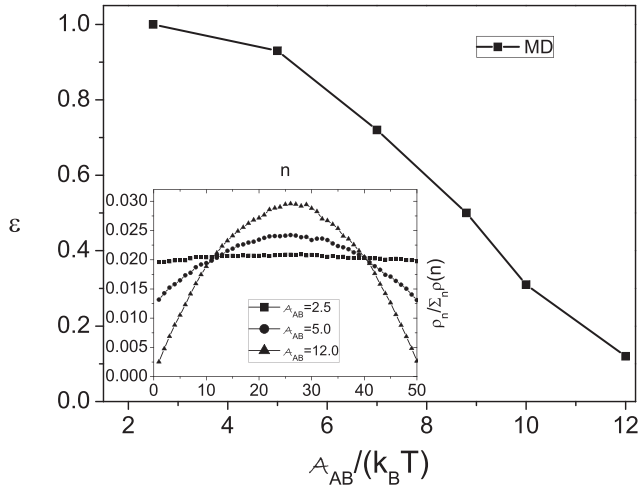

FIG. 7. Molecular-dynamics results for the parameter ϵ as a function of the interaction strength $\mathcal{A}_{AB}$. The inset shows the normalized density $\rho_n/\sum_n \rho_n$ for three different values of $\mathcal{A}_{AB}$. Symbols correspond to MD results and lines to Eq. (20).

However, for large values of $\mathcal{A}_{AB}$ the diffusion coefficient D becomes comparable to the deposition rate $\mathcal{F}$. This is not a desired situation since it leads to an evolution in which nucleation and aggregation occur simultaneously, decreasing the chance of controlling the formed structure. To avoid this issue, from now on we take $\mathcal{A}_{AB} = 8.0k_BT$ and set the density in the suspension in such a way that $\mathcal{F} \simeq 2 \times 10^{-6}$, which gives $\mathcal{R} = D/\mathcal{F} \approx 1.6 \times 10^3$. Despite ϵ being finite for this interaction strength, taking $\epsilon = 0$ in Eqs. (20) and (21) gives an excellent approximation for evaluating both ρ_n and $\tau_{\rm res}$. Figure 8 shows the density for gaps with different lengths ($N = 10$, 20, 30, 40, and 50). The numerical evidence suggests that the islands can be considered perfect traps for the employed parameters and then the system is limited by diffusion. Similarly, the behavior of $\tau_{\rm res}$ as a function of N with $\epsilon = 0$ is shown in Fig. 9. The agreement with Eq. (21) is excellent, especially for large gaps where $\tau_{\rm res} \approx \tau N^2/6$.

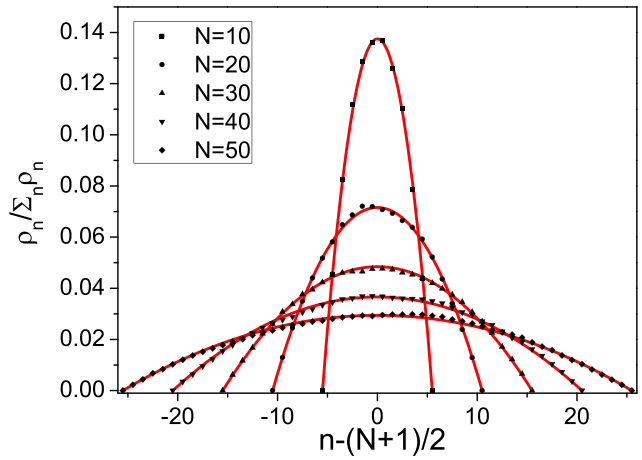

FIG. 8. Density ρ_n for five different gap lengths. Symbols correspond to MD results and lines to analytical results from Eq. (20) with $\epsilon = 0$.

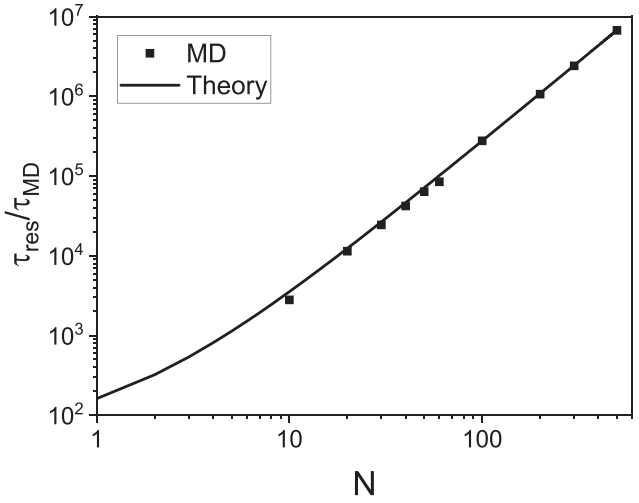

FIG. 9. Behavior of $\tau_{\rm res}$ as a function of N. Symbols correspond to MD results and the line to Eq. (21). The inaccuracy induced by taking $\epsilon = 0$ becomes negligible for large gaps ($N > 20$).

IV. SPATIAL DESCRIPTION OF NUCLEATION

For small densities of colloidal particles in the suspension, the deposition rate of monomers satisfies $\mathcal{F} \ll D$. Therefore, $\tau_{\rm res} \ll \tau_{\rm dep} = \mathcal{F}L$ for a gap of length L and the probability of simultaneously finding more than one colloid inside a gap is small. In this limit, the probability of finding i monomers in the gap at the moment of the $(i+1)$th deposition, q_{i+1}, is given by [44]

$$q_{i+1} = \frac{1}{i!}\left(\frac{\tau_{\rm res}}{\tau_{\rm dep}}\right)^i = \frac{1}{i!}\left[\frac{L^2}{12\mathcal{R}}\left(L + \frac{6\epsilon\sigma}{1-\epsilon}\right)\right]^i. \tag{22}$$

As expected, q_{i+1} strongly depends on ϵ, L, and $\mathcal{R}$. For the parameters used in the simulations $\tau_{\rm dep} \gg \tau_{\rm res} \approx \tau_{\rm tr}$ and $q_{i+1} \approx (L^3/12\mathcal{R})^i/i!$. In epitaxial growth, the critical size is the maximum size of an unstable island. In our MD simulations we set $\mathcal{A}_{AA} = 8.8k_BT$, which makes dimers stable, i.e., clusters of two monomers can be considered as immobile and stable islands.

On the other hand, given that $\tau_{\rm res} \ll \tau_{\rm dep}$, if two monomers coincide in the gap, whenever the second monomer arrives, it is very likely that the first one has already reached the steady state. This situation is equivalent to having a gap where both monomers are deposited simultaneously at random sites; the first one is deposited at site n with uniform probability $1/N$ and the second with a probability given by $\rho_n/\sum_n \rho_n$. The time evolution of two free colloids is given by the master equation

$$\frac{dp_{m,n}(t)}{dt} = \frac{1}{4\tau}[p_{m+1,n}(t) + p_{m-1,n}(t) + p_{m,n+1}(t) + p_{m,n-1}(t) - 4p_{m,n}], \tag{23}$$

where $p_{0,n}(t) = p_{N+1,n}(t) = p_{m,0}(t) = p_{m,N+1}(t) = 0$ and $p_{n,n} = 0$. In the following, we assume that nucleation occurs once the colloids are separated by a distance smaller than the interaction range, which is a reasonable assumption as the set $\mathcal{A}_{AB}$ makes detachment negligible. The solution of Eq. (23)

can be found using the auxiliary initial condition [45–47]

$$\tilde{p}_{m,n}(0) = \begin{cases} -p_{n,m}(0) & \text{for } m > n \\ 0 & \text{for } m = n \\ p_{m,n}(0) & \text{for } m < n, \end{cases} \tag{24}$$

where the symmetrized $p_{m,n}(0)$ can be written as

$$p_{m,n}(0) = \frac{\rho_n + \rho_m}{2L\sum_n \rho_n}. \tag{25}$$

In this way, the probability of having two colloids in sites m and n in the gap has the form

$$p_{m,n}(t) = \sum_{k,j=1}^{N} B_{k,j} e^{c_{kj}t/4\tau} X_{m,n}, \tag{26}$$

where

$$X_{m,n} = \sin\left(\frac{\pi km}{N+1}\right)\sin\left(\frac{\pi jn}{N+1}\right). \tag{27}$$

The constants c_{kj} and B_{kj} are given by

$$c_{kj} = 2\left[\cos\left(\frac{\pi k}{N+1}\right) + \cos\left(\frac{\pi j}{N+1}\right) - 2\right] \tag{28}$$

and

$$B_{kj} = \left(\frac{2}{N+1}\right)^2 \sum_{m<n} \tilde{p}_{m,n}(0) X_{m,n}, \tag{29}$$

respectively. The probability that nucleation occurs at site n, $\mathcal{P}(n)$, is given by

$$\mathcal{P}(n) = \frac{1}{4\tau}\int_0^\infty dt[p_{n+1,n}(t) + p_{n-1,n}(t) + p_{n,n+1}(t) + p_{n,n-1}(t)]. \tag{30}$$

Using Eqs. (26)–(30), the probability of nucleation can be written as

$$\mathcal{P}(n) = \frac{1}{2}\sum_{k,j=1}^{N} \frac{B_{kj}(X_{n,n+1} + X_{n,n-1})}{1 - \frac{1}{2}\left[\cos\left(\frac{k\pi}{N+1}\right) + \cos\left(\frac{j\pi}{N+1}\right)\right]}. \tag{31}$$

Note that we do not consider the direct deposition of one colloid on top of another at $t = 0$. Numerical evidence from KMC simulations has shown that an excellent mean-field approximation for Eq. (31) is given by the Walton relation, i.e., it is assumed that $\mathcal{P}(n)$ is proportional to the squared density [14,38,48]

$$\mathcal{P}_{\mathrm{MF}}(n) \approx \frac{30n^2(N-n+1)^2}{(N+1)^5}. \tag{32}$$

This distribution can be scaled using the transformation $\lambda = n/N$ and $p(\lambda) = N\mathcal{P}(\lambda)$ so that Eq. (32) can be rewritten as

$$p_{\mathrm{MF}}(\lambda) \approx 30\lambda^2(1-\lambda)^2. \tag{33}$$

Figure 10 shows the scaled distribution of the nucleation sites for gaps having different lengths ($N = 20$, 40, and 60). Both $\mathcal{P}(n)$ and $\mathcal{P}_{MF}(n)$ provide an adequate description of the simulation results. These results also support the approximation $\epsilon = 0$, since $\mathcal{P}(n)$ should be flatter and $\mathcal{P}(0) > 0$ otherwise. The main differences between the analytical and numerical results are due to the assumption that a nucleation occurs when a colloid hops on top of the other used in the former, while in the simulations a nucleation occurs when the centers of two colloids are closer than the interaction cutoff distance, which leads to a more pronounced distribution peak. The initial condition given by Eq. (24) is formally fulfilled in the limit $\mathcal{R} \to \infty$, which cannot be easily achieved for colloids; as mentioned previously, in this work $\mathcal{R} \approx 1.6 \times 10^3$ is far from the desired limit.

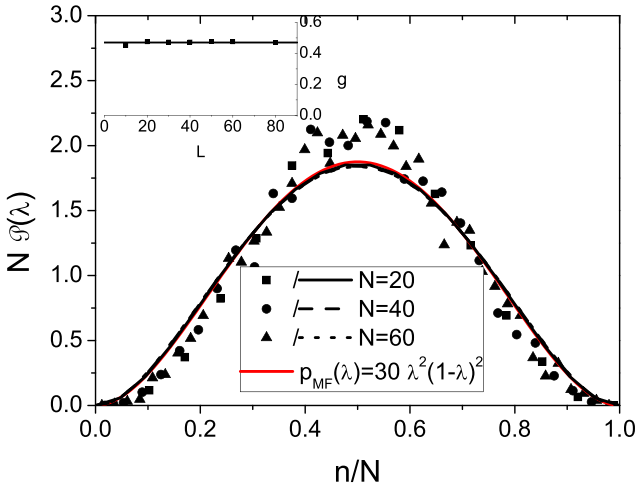

FIG. 10. Probability distribution for nucleation taking place at site n. Symbols correspond to MD simulation results, black lines to theoretical results from Eq. (31), and the red line to the mean-field approximation given by Eq. (33). The inset shows that the nucleation rate inside the gap ($g \simeq 0.47$) is found to be independent of the gap length.

The nucleation rate inside the gap, ω, indicates the number of nucleation events per time unit. Let g be the conditional probability for a nucleation inside a gap given that two monomers are inside the gap at the time of the second deposition. Consequently, ω can be written as

$$\omega = gq_2\mathcal{F}L, \tag{34}$$

where q_2 is given by Eq. (22) and g can be evaluated from $\mathcal{P}(n)$ according to

$$g = \sum_{n=1}^{N} \mathcal{P}(n). \tag{35}$$

The numerical evaluation of Eq. (35) using the result of Eq. (31) leads to $g \approx 0.47$ regardless of the gap length, as shown in the inset of Fig. 10. This is a consequence of the chosen interaction parameters, which make dimers stable. For a different set of interaction parameters, the critical nucleus size can be larger than $i = 1$ and g would depend on L [17].

V. KMC SIMULATION FROM MD RESULTS

Two typical quantities used in epitaxial growth to describe the time evolution of the growing monolayer are the monomer ($\mathcal{N}_1$) and island ($\mathcal{N}$) densities. Starting from the results described in the preceding section, we implement kinetic Monte Carlo simulations for monolayer growth using the same interaction parameters and the ratio $\mathcal{R} = D/\mathcal{F} \simeq 1.6 \times 10^3$. In

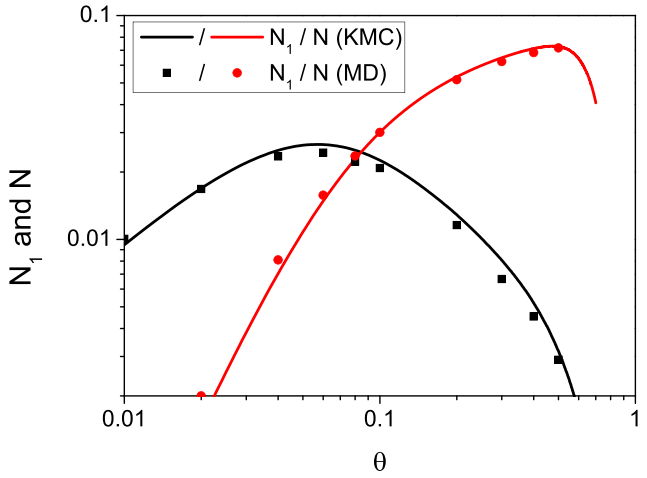

FIG. 11. Evolution of monomer $\mathcal{N}_1$ and island $\mathcal{N}$ densities as a function of the coverage $\theta = \mathcal{F}t$. Symbols correspond to MD simulations and lines to the KMC results.

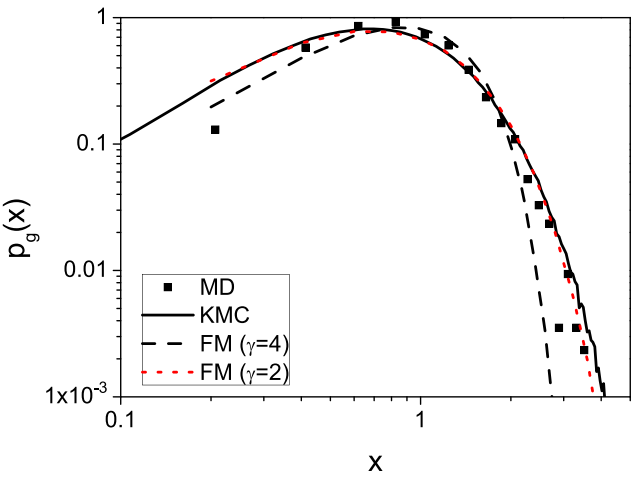

FIG. 12. Gap length distribution for adjacent islands for a coverage $\theta = 0.25$. Symbols and the solid line correspond to MD and KMC results, respectively. Dashed and dotted lines are obtained from the solution of the fragmentation model given by Eq. (36) with different values of γ.

these simulations, we consider a one-dimensional lattice (substrate) with $N = 1000$ sites on which colloids are deposited at random. On average, $2\mathcal{R}\mathcal{N}_1$ random moves are made by the free colloids on the lattice between two consecutive depositions. In this way, the hopping time is guaranteed to be $\tau = \sigma^2/2D$ and the time between consecutive depositions is $(\mathcal{F}L)^{-1}$. Note that the interaction parameters determine not only the diffusion coefficient of the colloids on the substrate but also the critical nucleus size i. For the set of parameters used in the MD simulations, once two colloids are in consecutive lattice sites they form a stable island. Therefore, we implement the extended island model in the KMC simulations, i.e., if a free colloid moves onto a site that is adjacent to one already occupied by another colloid, then either an aggregation or a nucleation event is considered to occur.

VI. FROM LOCAL TO GLOBAL BEHAVIOR

Evolution of densities

Figure 11 shows the evolution of $\mathcal{N}$ and $\mathcal{N}_1$ as a function of the coverage $\theta = \mathcal{F}t$, where t is the physical time and θ is the total density of deposited particles. As can be seen there, the agreement between the two simulation methods is excellent. A major advantage of the KMC over the MD simulations is that the KMC simulation allows one to simulate much larger systems and longer timescales with less computational effort.

Another quantity that is also useful for studying epitaxial growth is the gap length distribution for gaps of length l between neighboring islands. This distribution provides information about the effective interaction between islands as well as about the capture zone distribution [14,38,39]. The gap length distribution can be recovered using a fragmentation model which uses as input the results of Sec. III. Following Ref. [38], we define the scaled gap length distribution $p_g(x)$, which satisfy the fragmentation equation

$$x\frac{dp_g(x)}{dx} + 2p_g(x) = -Q^g(x) + 2Q^x(x), \tag{36}$$

with $Q^g(x)$ the probability density of nucleation inside a gap with scaled length $x = L/\langle L\rangle$ and $Q^x(x)$ the probability that, given a gap with length y, nucleation occurs at a position x inside the gap [39], i.e.,

$$Q^x(x) = \int_x^\infty dy \frac{1}{y} p_g(y)\mathcal{P}(x/y). \tag{37}$$

In particular, $Q^g(x)$ can be written as

$$Q^g(x) \propto \omega p_g(x), \tag{38}$$

where ω is the nucleation rate inside a gap with scaled length x. Evaluating Eq. (34) for the parameters considered, it is found that $\omega \simeq 0.04\mathcal{F}^2L^4/D$ and consequently

$$Q^g(x) = \frac{x^4}{\mu_4} p_g(x), \tag{39}$$

with μ_4 the fourth moment of $p_g(x)$.

The resulting integro-differential equation for $p_g(x)$ given by Eqs. (36), (37), and (39) cannot be analytically solved. However, it can be solved numerically as shown in Ref. [39]. For large values of x, $p_g(x) \propto x^{-2}\exp(-x^\gamma/\gamma\mu_\gamma)$, with γ the exponent of L in the nucleation rate ω and therefore its behavior is completely determined by $Q^g(x)$. Furthermore, in the limit $x \ll 1$ we have $p(\lambda) \sim \lambda^2$, which in turn implies $p_g(x) \sim x^2$ and $Q^x(x) \sim x^2$. Figure 12 displays the behavior of $p_g(x)$ evaluated for coverage $\theta = 0.25$. As expected, the KMC results coincide with those from MD simulations, especially for large values of x. However, the fragmentation model [Eqs. (36) and (39)] fails to describe the simulation results for $p_g(x)$ at large x. This discrepancy can be understood considering that Eq. (36) implicitly assumes that the system has reached a quasisteady state, in which nucleation and aggregation balance each other; this assumption is reasonable for $\mathcal{R} \to \infty$. In this limit $p_g(x)$ reaches a scaling regime, but for the set of parameters used in our simulations, $\mathcal{R}$ is not large enough to meet this requirement. Additionally, the fragmentation approach assumes that the colloidal density of

the gaps reaches the long-time behavior, which is true for small gaps but not necessarily for large gaps if $\mathcal{R}$ is not large enough. The statistical behavior of the system for large values of x is dominated by the breakup of the largest gaps, and under the steady-state assumption, Eq. (39) predicts $\gamma = 4$. However, for small values of $\mathcal{R}$, we can expect a smaller γ. The numerical evidence suggests that this issue can be overcome by proposing

$$Q^g(x) \propto x^\gamma p_g(x), \tag{40}$$

with $\gamma = 2$. For this empirical value, the fragmentation approach gives excellent results for describing $p_g(x)$ when compared to simulations, as can be seen in Fig. 12.

VII. CONCLUSION

Utilizing established analytical and numerical tools for investigating the colloid dynamics within a single gap, relevant timescales related to nucleation and aggregation can be accurately estimated from the interaction parameters between particles. This allows one to gain valuable insights into the time evolution of monomer and island densities by examining the local behavior of monomers within a gap, which in turn contributes to understanding the global behavior of the epitaxial monolayer growth. Furthermore, the results for the timescales can be used as input for a fragmentation model [Eq. (36)] to calculate the gap length distribution $p_g(x)$ and consequently the capture zone distribution and the effective interaction between islands [14,39]. For $p_g(x)$, our results suggest an exponent $\gamma = 2$, i.e., $p_g(x) \sim x^{-2}\exp(-x^2)$, which differs from the analytical result of $\gamma = 4$. This is not an unexpected result because the exponent γ determines the right tail of the gap length distribution; in other words, it determines the behavior for large gaps. However, for small values of $\mathcal{R}$ the steady-state assumption used for the nucleation description does not apply to large gaps. Additionally, the simultaneous presence of more than two monomers inside a gap is not negligible for large gaps, which is one of the assumptions used to formulate Eq. (22). In our case, the deposition rate is not small enough ($\mathcal{R} \approx 1.6 \times 10^3$) and therefore nucleation in large gaps can occur before the monomer density reaches the steady-state regime. In principle, $\mathcal{R}$ can be arbitrarily large, implying a very long time between depositions and therefore deposition times that in practice cannot be achieved by MD simulations due the long associated simulation times. Consequently, for colloidal epitaxial growth, the typical values of $\mathcal{R}$ are much smaller than those found for molecular beam epitaxy. It is possible to extrapolate the procedure discussed in this paper to higher dimensions. However, for $d > 1$ space is not divided into gaps, and it is necessary to consider the concept of a capture zone (CZ) and the fragmentation equation is written to describe the effect of a single nucleation in the CZ distribution. Finally, we highlight that linking the interaction parameters between colloids with the relevant timescales of the system allows more control of the size and form of the structure formed, which is one of the main goals in epitaxial growth.

ACKNOWLEDGMENTS

D.L.G.-C. is grateful for support from Vicerrectoría de Investigaciones, Universidad del Valle (Colombia) C.I. 71369. M.C. thanks Universidad Antonio Nariño (VCTI-UAN) for financial support through Project No. 2023202.

[1] J. W. Evans, P. A. Thiel, and M. C. Bartelt, Surf. Sci. Rep. **61**, 1 (2006).
[2] H. Ibach, *Physics of Surfaces and Interfaces* (Springer, Berlin, 2006), Vol. 12.
[3] T. Michely and J. Krug, *Islands, Mounds and Atoms* (Springer Science + Business Media, New York, 2012), Vol. 42.
[4] J. W. Evans and M. C. Bartelt, Phys. Rev. B **63**, 235408 (2001).
[5] J. G. Amar, M. N. Popescu, and F. Family, Surf. Sci. **491**, 239 (2001).
[6] M. N. Popescu, J. G. Amar, and F. Family, Phys. Rev. B **64**, 205404 (2001).
[7] J. G. Amar and M. N. Popescu, Phys. Rev. B **69**, 033401 (2004).
[8] A. Pimpinelli and T. L. Einstein, Phys. Rev. Lett. **99**, 226102 (2007).
[9] V. I. Tokar and H. Dreyssé, Phys. Rev. B **80**, 161403(R) (2009).
[10] M. Li, Y. Han, and J. W. Evans, Phys. Rev. Lett. **104**, 149601 (2010).
[11] A. Pimpinelli and T. L. Einstein, Phys. Rev. Lett. **104**, 149602 (2010).
[12] M. Grinfeld, W. Lamb, K. P. O'Neill, and P. A. Mulheran, J. Phys. A: Math. Theor. **45**, 015002 (2012).
[13] T. J. Oliveira and F. D. A. A. Reis, Phys. Rev. B **83**, 201405(R) (2011).
[14] D. L. González, A. Pimpinelli, and T. L. Einstein, Phys. Rev. E **84**, 011601 (2011).
[15] K. P. O'Neill, M. Grinfeld, W. Lamb, and P. A. Mulheran, Phys. Rev. E **85**, 021601 (2012).
[16] P. A. Mulheran, K. P. O'Neill, M. Grinfeld, and W. Lamb, Phys. Rev. E **86**, 051606 (2012).
[17] D. L. González, A. Pimpinelli, and T. L. Einstein, Phys. Rev. E **96**, 012804 (2017).
[18] J. A. Sánchez, D. L. González, and T. L. Einstein, Phys. Rev. E **100**, 052805 (2019).
[19] W. C. Poon, J. Phys. A: Math. Theor. **49**, 401001 (2016).
[20] V. N. Manoharan, Science **349**, 1253751 (2015).
[21] C. P. Royall, S. R. Williams, and H. Tanaka, J. Chem. Phys. **148**, 044501 (2018).
[22] A. Jangizehi, F. Schmid, P. Besenius, K. Kremer, and S. Seiffert, Soft Matter **16**, 10809 (2020).
[23] A. Van Blaaderen, R. Ruel, and P. Wiltzius, Nature (London) **385**, 321 (1997).

[24] A. Van Blaaderen, J. P. Hoogenboom, D. L. Vossen, A. Yethiraj, A. van der Horst, K. Visscher, and M. Dogterom, Faraday Discuss. **123**, 107 (2003).
[25] N. Nakamura, Y. Sakamoto, and H. Ogi, Sci. Rep. **11**, 8929 (2021).
[26] C. P. Joshi, Y. Shim, T. P. Bigioni, and J. G. Amar, Phys. Rev. E **90**, 032406 (2014).
[27] S. P. Thampi and M. G. Basavaraj, Ann. Rev. Chem. Biomol. Eng. **14**, 53 (2023).
[28] R. Ganapathy, M. R. Buckley, S. J. Gerbode, and I. Cohen, Science **327**, 445 (2010).
[29] M. Einax, W. Dieterich, and P. Maass, Rev. Mod. Phys. **85**, 921 (2013).
[30] S. M. Rupich, F. C. Castro, W. T. Irvine, and D. V. Talapin, Nat. Commun. **5**, 5045 (2014).
[31] C. K. Mishra, A. Sood, and R. Ganapathy, Proc. Natl. Acad. Sci. USA **113**, 12094 (2016).
[32] J. Nozawa, S. Uda, A. Toyotama, J. Yamanaka, H. Niinomi, and J. Okada, J. Colloid Interface Sci. **608**, 873 (2022).
[33] M. Mondal and R. Ganapathy, Phys. Rev. Lett. **129**, 088003 (2022).
[34] D. Deb and H. H. von Gruenberg, J. Phys.: Condens. Matter **21**, 245102 (2009).
[35] B. C. Hubartt and J. G. Amar, J. Chem. Phys. **142**, 024709 (2015).
[36] N. Kleppmann, F. Schreiber, and S. H. L. Klapp, Phys. Rev. E **95**, 020801(R) (2017).
[37] M. Camargo and D. L. González, J. Phys.: Condens. Matter **34**, 144006 (2022).
[38] J. A. Blackman and P. A. Mulheran, Phys. Rev. B **54**, 11681 (1996).
[39] D. L. González and T. L. Einstein, Phys. Rev. E **84**, 051135 (2011).
[40] H. Krcelic, M. Grinfeld, and P. A. Mulheran, Phys. Rev. E **98**, 052801 (2018).
[41] H. Risken and T. Frank, *The Fokker-Planck Equation* (Springer, Berlin, 1996).
[42] S. Lifson and J. L. Jackson, J. Chem. Phys. **36**, 2410 (1962).
[43] S. B. Maurer and A. Ralston, *Discrete Algorithmic Mathematics* (CRC, Boca Raton, 2005).
[44] J. Krug, P. Politi, and T. Michely, Phys. Rev. B **61**, 14037 (2000).
[45] P. Politi and J. Villain, Phys. Rev. B **54**, 5114 (1996).
[46] C. Castellano and P. Politi, Phys. Rev. Lett. **87**, 056102 (2001).
[47] P. Politi and C. Castellano, Phys. Rev. E **66**, 031605 (2002).
[48] D. Walton, J. Chem. Phys. **37**, 2182 (1962).

IOP Publishing Journal of Physics: Condensed Matter
J. Phys.: Condens. Matter **36** (2024) 463001 (19pp) https://doi.org/10.1088/1361-648X/ad6c98

Topical Review

Epitaxial growth in one dimension

Juan David Álvarez-Cuartas[1], Diego Luis González-Cabrera[1,*] and Manuel Camargo[2]

[1] Departamento de Física, Universidad del Valle, A.A. 25360 Cali, Colombia
[2] DCA & CICBA, Universidad Antonio Nariño—Campus Farallones, Km 18 vía Cali-Jamundí, 760030 Cali, Colombia

E-mail: diego.luis.gonzalez@correounivalle.edu.co

Received 31 March 2024, revised 20 July 2024
Accepted for publication 7 August 2024
Published 23 August 2024

Abstract

The final structure and properties of layers grown by epitaxy techniques are determined in the very early stage of the process. This review describes one-dimensional models for epitaxial growth, emphasizing the basic theoretical concepts employed to analyze nucleation and aggregation phenomena in the submonolayer regime. The main findings regarding the evolution of quantities that define the properties of the system, such as monomer and island densities, and the associated island size, gap length, and capture zone distributions are discussed, as well as the analytical tools used to evaluate them. This review provides a concise overview of the most widely used algorithms for simulating growth processes, discusses relevant experimental results, and establishes connections with existing theoretical studies.

Keywords: epitaxial growth, 1D models, reaction-diffusion systems, nucleation, aggregation

1. Introduction

The study of epitaxial growth (EG) has a long history due to its relevance in solid-state physics, materials science, and semiconductor technology. Understanding the microscopic mechanisms related to the deposition and growth processes is required to enable precise control of the material properties for a wide range of applications such as micro- and optoelectronics, life sciences, and fuel cells [1–3]. Indeed, the significant progress of nanoscience and nanotechnology has been partially achieved thanks to the advancements of epitaxial deposition [4], as unprecedented developments of diverse nanostructures are currently available, including nanodots [5], nanowires [6, 7], and thin films [8–10] with enhanced electronic, magnetic, optical, or mechanical features.

For instance, in [5], highly ordered arrays of GaAs-based dots of nanoscale size were successfully prepared on GaAs (001) substrates by molecular beam epitaxy (MBE). The average length of the dots is adjustable from 45 to 85 nm. On the other hand, [6] reports the construction of the well-defined (La, Pr, Ca)MnO_3 epitaxial oxide nanowall wire. The structure is built by a combination of nanolithography and subsequent thin-film growth. This growth technique allows the direct investigation of its insulator-metal transition at the single-domain scale. Another example is found in [7], where three-dimensional (3D) Fe_3O_4 epitaxial nanowires at a 10 nm length scale on a 3D MgO nanotemplate were built using nanoimprint lithography and inclined thin-film deposition. The ultrasmall Fe_3O_4 nanowires exhibit a prominent Verwey transition at a temperature close to 112 K with a relative change in resistance six times larger than that found by the standard thin-film configuration.

In [8, 9] the properties of some structures constructed by pulsed laser deposition (PLD) were studied; particularly, $(AlGa)_2O_3$ films were deposited on sapphire substrates which exhibit high transmittance and a tunable bandgap with the Al content. Similarly, Ga_2O_3 films were deposited on (0001) sapphire substrates by PLD and the dependence of crystal quality, surface morphology, and transmittance on the substrate temperature was investigated. Those results suggest that PLD allows the growth of high-quality films at low temperatures.

* Author to whom any correspondence should be addressed.

On the other hand, the deposition of $NdNiO_3$ on different substrates has been carried out to analyze the role of lattice strain on proton diffusion in the film. It shows that tensile/compressive strain strongly suppresses/enhances proton diffusion and demonstrates the potential applications of this intrinsic factor in designing multifunctional materials for electronics [10].

In EG, the basic units of growth, called monomers, are deposited onto a (crystalline) substrate at a controlled rate. Then, each monomer diffuses on the surface until it gets captured by other diffusive monomers or an island, the latter being a stable cluster of immobile monomers. From a fundamental point of view, EG involves many out-of-equilibrium processes leading to rich and complex behaviors due to the number of timescales implicated, which have been studied theoretically, numerically, and experimentally. The first theoretical studies on the subject were based on rate equations (RE) and aimed to determine the island growth exponents [11, 12]. Later, key quantities of the growing layer dynamics, such as island size and capture zone distributions, were employed to include information about the spatial fluctuations of monomer and island densities [11, 13, 14]. At the same time, several numerical studies founded on kinetic Monte Carlo (kMC) simulations were performed providing important insights into the most relevant microscopical mechanism determining the system evolution in EG [11–13]. Some experimental results for island size distribution and growth exponents are found in [15–19]. Most experimental works focus on finding optimal conditions for controlling the island growth and, by contrasting their results with theoretical models, on extracting microscopical parameters from experimentally measurable quantities.

Although EG is inherently a three-dimensional process involving the slow deposition of atoms, molecules, or colloidal particles on a substrate surface, one-dimensional (1D) models have been amply used to simplify the analysis and gain insights into magnitudes describing the growing dynamics [20–23]. These magnitudes include, among others, the time evolution and scaling of island size, the capture zone distribution, and the gap length distribution [24–29]. Even if one-dimensional substrates are geometrically simpler than two-dimensional ones, the spatial density fluctuations of the growing layer generally play a more relevant role than those in higher dimensions. Consequently, understanding the microscopic processes involved in 1D EG requires a more precise description of monomers and islands' spatial fluctuations. In this sense, analyzing 1D EG is more challenging than its two-dimensional counterpart. From the theoretical perspective, the strong correlations render useless mean-field-like approaches, and from the practical point of view, having enough control over the deposition and diffusion of monomers to form ordered one-dimensional structures is not an easy task.

Moreover, practical realizations of 1D models are related to the formation of atomic chains in nanoscale devices (nanowires) by using stepped surfaces [22, 30–32] or anisotropic diffusion on two-dimensional substrates [33–36]. For example, [37] discusses the advantages and challenges of using self-assembled, one-dimensional semiconductor nanowires, which offer a coaxial gate-dielectric-channel geometry for the downscaling of electronic devices. The application of such devices as a powerful and general platform for direct electrical detection of biological and chemical species is reviewed in [38]. Similarly, tunned 1D nanostructured Pt-based, Pd-based, or 1D metal-free nanomaterials can be employed in advanced electrocatalysis for boosting fuel-cell reactions with high activity and stability [39]. Additionally, the physics and technology of nanowire photodetectors offer several potential applications in different areas such as nanoscale optoelectronics, photovoltaics, plasmonics, and emerging negative indexes metamaterials-based devices [40].

This review presents the most relevant analytical, numerical, and experimental results regarding the unique features of 1D EG. Since submonolayer film growth determines most of the physical properties of the surface, most experimental and analytical results discussed are limited to this regime. The paper is divided as follows: section 2 introduces the basic definitions necessary to study EG, while section 3 describes the relevant time scales associated with the fundamental processes. In section 4 the standard RE for EG are presented including the information that can be gained from them. Section 5 presents a brief discussion about the gap length and capture zone distributions. The most important results related to the island size distribution are presented in section 6. A description of the numerical methods used to model EG is summarized in sections 7 and 8 is devoted to a relatively novel two-step protocol for EG. Finally, in section 9, some related experimental results are presented.

2. Basic definitions

As mentioned above, in EG the basic growth units, called monomers, are deposited onto a substrate. Depending on the specific characteristics of the deposited particles, the deposition process can be achieved using MBE, vapor phase epitaxy (VPE), chemical beam epitaxy (CBE), atomic layer epitaxy (ALE), or liquid phase epitaxy (LPE) [41, 42]. For example, in the case of MBE atomic or molecular beams are directed onto a heated substrate surface under high vacuum conditions. By controlling the flux and energy of the beams, MBE enables the sequential deposition of monomers and therefore the precise control of the deposition rate $\mathcal{F}$, i.e. the number of deposited monomers per time and length units[3]. The time evolution is usually parameterized in terms of the coverage defined as $\theta = \mathcal{F}t$, where t is the physical time; if re-evaporation is negligible, θL_s is equivalent to the total number of monomers on the substrate of length L_s. It is also convenient to define the density of free monomers N_1, i.e. the number of diffusing monomers per length unit. In general, $N_1 \neq \theta$ due to the existence of islands, detachment processes, re-evaporation, etc.

After the arrival of monomers at the surface, their fundamental transport mechanism on the substrate is *diffusion*. Eventually, free monomers meet on the substrate and form

[3] This definition applies to 1D substrates; for the two-dimensional case, the deposition rate corresponds to the number of deposited monomers per time and area units.

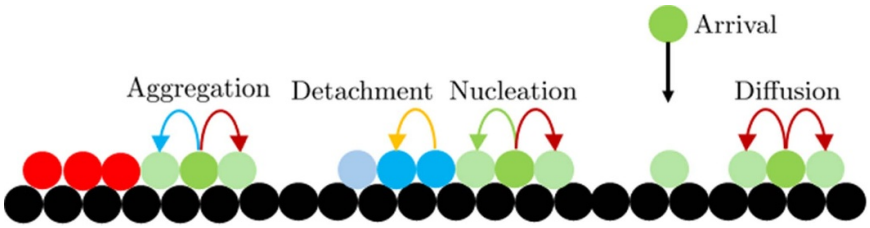

Figure 1. Representation of the fundamental processes for $i = 2$. Red and blue circles represent an island and an unstable cluster, respectively. The substrate is formed by black circles. Black, red, green, and blue arrows represent deposition, diffusion, nucleation, and aggregation events. The orange arrow illustrates the detachment of a monomer from an unstable cluster.

clusters until they become stable. The size of the largest unstable cluster is called critical size, i, which depends on the strength of the interaction between monomers and temperature. Once a free monomer is captured by an unstable cluster with size i, a *nucleation* process takes place, and a stable cluster forms, which is commonly called an island. In the context of reaction-diffusion systems, the critical dimension (d_c) is defined as the spatial dimension at which the nature of nucleation and cluster formation undergoes a significant change. Above d_c, the RE description leads to asymptotically correct behavior; on the contrary, below d_c, this approach does not provide satisfactory results. Finally, at d_c, the RE approach is almost correct except for logarithmic corrections. In the diffusion-limited regime, the many-particle nucleation process of $i+1$ monomers has an upper critical dimension $d_c = 2/i$, meaning that for higher dimensions, nucleation is expected to be described using a mean-field approach [43–45]. Consequently, d_c decreases as the critical nucleus size increases. This result can be understood by considering that many-particle encounters rarely occur, favoring the mixing of the system. For a 1D system, we can expect mean-field approaches to be successful for critical sizes $i > 2$. Similarly, when an island captures a free monomer, its size increases, and an *aggregation* occurs. In this way, the basic 'microscopic' events involved in EG are arrival, diffusion, aggregation, and nucleation, as illustrated in figure 1 for a critical nucleus size $i = 2$. Other processes, such as detachment and re-evaporation, are possible but undesirable since they reduce the control over the layer growth.

Diffusion happens by monomer hopping between neighboring lattice sites on the substrate. The average time between two consecutive hops is given by $\tau_{\rm dif} = 1/(2D)$ where D is the (lateral) diffusion coefficient of a free monomer on the substrate. This parameter depends on the temperature and is usually taken as a known quantity as it can be determined experimentally. The dependence $D(T)$ is usually assumed to be given by an Arrhenius form $D = D_0 \exp(-E_D/k_B T)$, where E_D is the activation energy of diffusion and D_0 a preexponential factor. For the case of Pt adatoms on a Pt(111) surface, it was found $E_D \approx 0.26$ eV [46]; similarly, for a closed-packed [110]-step on Cu(100), it is found $E_D \approx 0.30 \pm 0.04$ eV [47].

Starting from the Fokker-Planck equation for the diffusion of a monomer on a periodic potential $\mathcal{V}(x)$, which represents the monomer-substrate interaction, it can be shown that the diffusion coefficient can be expressed as [48]

$$D = D_0 \sigma^2 I_2^{-1}, \tag{1}$$

with D_0 the diffusion coefficient for $\mathcal{V}(x) = 0$ and $I_2(y)$ given by

$$I_2(y) = \int_0^\sigma {\rm d}x {\rm e}^{\mathcal{V}(x)/k_{\rm B}T} \cdot \int_0^\sigma {\rm d}x {\rm e}^{-\mathcal{V}(x)/k_{\rm B}T}, \tag{2}$$

where σ measures the size of the monomer. As expected, the diffusion coefficient depends on the interplay between the strength of the monomer-substrate interaction and the typical thermal energy. In the limits $\mathcal{V}(x) \gg k_{\rm B}T$ and $\mathcal{V}(x) \ll k_{\rm B}T$, it results $D \to 0$ and $D \to D_0$, respectively. In [49–51] the applicability of equation (1) is discussed for a simple colloidal model of EG. The typical time between two consecutive monomer arrivals on the substrate with length L_s, hereinafter referred to as deposition time[4], is given by $\tau_{\rm dep} = (\mathcal{F} L_s)^{-1}$. The monolayer evolution can be fully described by two independent variables, coverage and the diffusion-to-deposition ratio. The latter is defined as $\Re = D/\mathcal{F}$ so that when it is large, monomers have enough time to diffuse across the surface between consecutive depositions, which typically renders in more uniform layers; for atomic and molecular epitaxy $\Re > 10^6$, so in practice $\tau_{\rm dep} \gg \tau_{\rm dif}$.

In [49, 50], the deposition rate due to the slow sedimentation of colloidal particles from a diluted suspension on a one-dimensional substrate is discussed. It is found that the deposition rate is given by

$$\mathcal{F} = \frac{2\rho F^2 L_y}{g_n^2 \left[\exp\left(-2\zeta_0 F L_y / g_n^2\right) - 1\right] + 2\zeta_0 F L_y}, \tag{3}$$

with L_y being the height of the suspension, F the sedimentation field, ρ the density of colloids in the suspension, ζ_0 is intensity of the viscous force and $g_n = \sqrt{2\zeta_0 k_{\rm B} T}$. If the thermal energy is much smaller than the work done by F, $k_{\rm B}T \ll F L_y$, equation (3) takes the simple linear form $\mathcal{F} = \rho F/\zeta_0$ and the deposition rates becomes a linear function of the sedimentation field. In the opposite case, the deposition is driven by thermal fluctuation $\mathcal{F} = 2k_{\rm B}\rho T/(L_y \zeta_0)$. Equation (3) assumes that the deposition is instantaneous, i.e. the substrate captures the monomers at the first encounter. If the thermal energy is

[4] Note that in an experimental context, deposition time usually refers to the entire interval during which monomers are being deposited on the substrate.

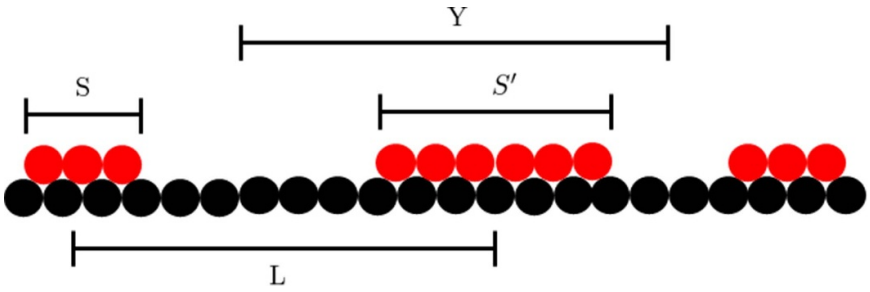

Figure 2. Representation of two adjacent islands (black segments) and the gap between them (white segment) in the extended island model (EIM). The gap length, L, between the islands and the capture zone length Y of the island with size S' are indicated.

larger than the typical monomer-substrate interaction energy, the monomer can escape from the substrate and require many attempts before being incorporated into it.

The role of the substrate is quite important in the case of heteroepitaxial growth, in which the thin film is deposited on top of a dissimilar material. In that case, it is usual that the lattice constants of the growing layer and the substrate are different. It generates lattice strain in the growing layer, and high strain levels produce defect formation [3, 52]. In colloidal heteroepitaxy, experimental studies have shown that the growth process is influenced by particle interactions and the lattice-misfit ratio [53, 54], and the properties of the film are strongly related to the interfacial energy between it and the substrate. Including the effect of lattice mismatch in theoretical models is challenging. However, molecular dynamics (MD) simulations, as proposed in [55], offer a direct and practical approach to studying it. These simulations have shown that different structures can grow depending on the size ratio between the layer and substrate particles.

Two island models can be employed to describe the structure of the growing layer theoretically. The point island model (PIM) considers each island to occupy only one lattice site on the substrate, and the island size corresponds to the number of monomers that belong to it. On the other hand, in the extended island model (EIM), the island grows laterally and its length is proportional to its size (i.e. the number of monomers in it), as shown in figure 2. A distinctive feature of 1D systems is that the islands divide the substrate into disjoint segments called gaps, which can mostly be considered independent. Figure 2 shows a gap between two consecutive islands with its associated length L. Within a gap, the aggregation process can be characterized by two different time scales: the transversal time, $\tau_{\rm tr}$, which is the average time that a monomer initially in the gap requires to reach one of the islands at the gap ends, and the aggregation time, $\tau_{\rm agg}$, which is the typical time after deposition that a monomer requires to be captured by an island. If $\tau_{\rm tr} = \tau_{\rm agg}$, the aggregation is instantaneous, and the system is limited by diffusion. On the other hand, if $\tau_{\rm tr} \ll \tau_{\rm agg}$, aggregation is limited by reaction due to the presence of an additional energy barrier hindering the aggregation of the monomer to the island.

The density of free monomers, N_1, was already mentioned as a key quantity to describe the growth process. Two other are the density of islands of size S, N_S, and the total island density, $N = \sum_{S>i} N_S$. The former is defined as $N_S = \mathcal{N}_S/L_s$, with $\mathcal{N}_S$ the number of islands containing $S > i$ monomers. The time evolution of N_1 and N_S sheds light on the microscopic processes associated with the layer growth; for instance, N_1 and N_S are related to the global rates of nucleation and aggregation and provide information about i. Closely related, the island size distribution $P_S = N_S/N$ is also a fundamental quantity. For the extended islands model, the island length is proportional to S and the island size distribution is equivalent to the island length distribution.

For both PIM and EIM, the spatial structure formed by the island centers can be characterized by the gap length (GL) and capture zone (CZ) distributions, $\tilde{p}(L)$ and $\tilde{P}(Y)$, respectively. By definition, $\tilde{p}(L)$ is the distribution of lengths between the centers of adjacent islands, which is closely related to the monomer and island density distributions around a given island. On the other hand, the capture zone of an island is given by the lattice sites that are closer to it than to any other island. Figure 2 indicates the GL between the islands of size S and S', as well as the CZ associated with the S' island; the length of this CZ is represented by Y. For extended islands, the effective CZ and GL are given by $Y - S'$ and $L - (S + S')/2$, respectively. The predictions of both island models generally coincide when the average distance between islands is much larger than the typical island length.

It is a usual practice to employ the scaled quantities $s = S/\bar{S}$, $\ell = L/\bar{L}$, and $y = Y/\bar{Y}$, with the corresponding distributions P_s, $p(\ell)$, and $P(y)$, where the bar represents the average of the given quantity. These distributions provide complementary but not necessarily equivalent information about the microscopic details of the processes involved in the layer growth. Therefore, analyzing experimental and theoretical results requires the simultaneous examination of all of them [21, 28, 32, 51, 56, 57].

3. Time scales in a single gap

The nucleation and aggregation processes can be characterized by studying them within a single gap. Aggregation inside a single gap with length L was extensively studied in [58–63] by exactly solving the master equation for a single monomer. These works consider the existence of an energy barrier E_a that hinders the aggregation. As expected, for zero

and weak barriers $\tau_{\rm agg} = L^2/(12D)$ coincides with the transversal time. In contrast, for strong barrier $\tau_{\rm agg} = Ll_a/(2D)$ with $l_a = b\left[\exp\left(E_a/k_{\rm B}T\right) - 1\right]$ a length associated to the barrier E_a and b the lattice parameter. The presence of E_a implies the existence of the three following regimes:

- Regime I: the system is diffusion-limited with $\tau_{\rm dep} \gg \tau_{\rm agg} \approx \tau_{\rm tr}$ and $\Re \gg L^3/12$.
- Regime II: the system has strong but finite barriers with $\tau_{\rm dep} \gg \tau_{\rm agg} \gg \tau_{\rm tr}$, $l_a \gg L/6$, and $\Re \gg L^2 l_a/2$.
- Regime III: the system is reaction-limited with $l_a \to \infty$ and $\tau_{\rm agg} \gg \tau_{\rm dep} \gg \tau_{\rm tr}$.

Generally, the values of the activation energy of the microscopical process strongly depend on the material and external conditions. Unfortunately, apart from the case of a single monomer moving on a flat surface, the activation energies are rarely accessible by direct measurement; mainly because following the time evolution of individual monomers is a quite difficult task in atomic and molecular systems. In most cases, it is necessary to rely on measurements of mesoscopic quantities, such as the island density, and compare these with analytical models to estimate the value of microscopic parameters. For instance, [62] reports $E_a \approx 0.36$ eV for Pt homoepitaxy on Pt(111) at a CO pressure of 1.85×10^9 mbar and $b \simeq 2.83$ Å.

On the other hand, the time scale associated with nucleation denoted by $\tau_{\rm nuc}$ can be studied by solving the exact diffusion equation for $i+1$ monomers inside a gap. This way, it is possible to express analytically the probability $p_{n,m}(t)$ of finding two monomers at positions n and m in the gap at time t. This probability was calculated for the case $i = 1$ in [58–61], where the master equation for two monomers inside a gap was solved. This approach referred to from now on as the Castellano-Politi (CP) method, assumes as the initial condition that the first monomer has already reached the steady state at the arrival time of the second one. In [63], the CP method was generalized for $i > 1$ leading to the extended Castellano-Politi (eCP) method. Naturally, for a nucleation to occur inside a gap of length L, it is necessary to have more than i monomers inside the gap. The events related to the existence of more than $i+1$ monomers are much more unlikely than those with $i+1$ monomers and, therefore, these can be neglected. For finite and zero barriers the probability to find i monomers in the gap at the moment of the $(i+1)$th deposition is given by [62]

$$p_{i+1} = \frac{1}{i!}\left(\frac{\tau_{\rm agg}}{\tau_{\rm dep}}\right)^i = \frac{1}{i!}\left[\frac{L^2}{12\Re}\left(L + 6l_a\right)\right]^i. \qquad (4)$$

For Regimes I and II, $p_{i+1} \ll 1$ while for Regime III aggregation is not possible as $l_a \to \infty$ and then $p_{i+1} = 1$.

The distribution of nucleation sites, $\mathcal{P}_n(m,L)$, which gives the probability of having nucleation at position m ($0 \leqslant m \leqslant L$) regardless of time, has also been calculated numerically and analytically [58–63]. The mean-field (MF) approximation assumes that $\mathcal{P}_n(m,L)$ is proportional to $n_1^{i+1}(m,L)$ with $n_1(m,L)$, the density of monomers inside large gaps at the steady-state

$$n_1\left(m,L\right) = \left[l_a L + Lm - m^2\right]. \qquad (5)$$

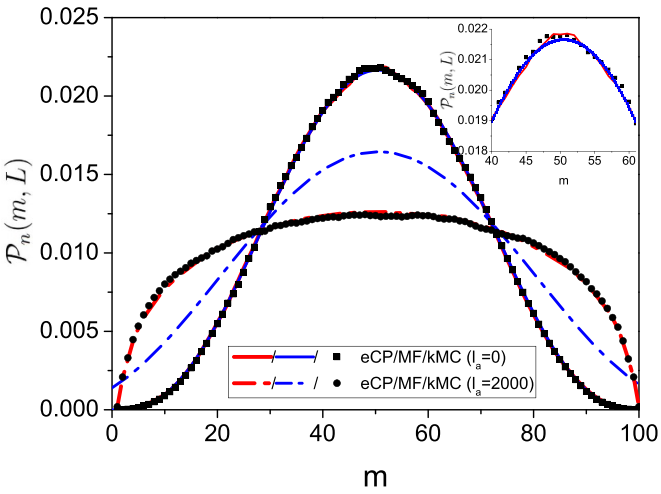

Figure 3. Distribution of the nucleation sites, $\mathcal{P}_n(m,L)$, for a gap with $i = 2$, $L = 100$, $l_a = 0$ (continuous lines) and $l_a = 2000$ (dashed lines). Red lines correspond to results from the eCP approach [58–61], blue lines to that of the MF approximation, and dots to kMC simulations.

Remarkably, for zero barriers and $i = 1$, the MF approach provides an excellent approximation for $\mathcal{P}_n(m,L)$. The MF approximation becomes exact as i increases [63]. However, the MF approximation fails to describe $\mathcal{P}_n(m,L)$ for non-zero barriers. In that case, the exact $\mathcal{P}_n(m,L)$ is flatter close to the center of the gap than that given by the MF. Furthermore, the MF predicts $\mathcal{P}_n(0,L) = \mathcal{P}_n(L,L) > 0$ while the exact results give $\mathcal{P}_n(0,L) = \mathcal{P}_n(L,L) = 0$, as shown in figure 3. The inset highlights the subtle difference between the three data sets near the maximum of the distribution for $i = 2$ and $l_a = 0$. In cases like this, it is more convenient to use the expression given by the MF approach than that from the eCP method. Additionally, some discrepancies have been found between the analytical model used in [58–61] and kMC results for large gaps [63, 64]. In particular, the eCP method predicts sharper distributions than those found by numerical simulations, strongly suggesting that the assumed initial condition for the CP and eCP approaches does not apply to large gaps, i.e. the deposition of the second monomer usually occurs before the first monomer reaches the steady state. As mentioned previously, density fluctuations are relevant in one-dimensional systems. Note that for strong barriers, the density of monomers, N_1, and $\mathcal{P}(m,L)$ become nearly uniform close to the center of the gap, but they strongly depend on the position near the islands at the gap edges. This is an important detail because the aggregation of monomers to the islands depends on the density behavior in this region. As a result, mean-field approximations are not appropriate for describing the aggregation process for strong barriers.

The nucleation rate, ω, defined as the number of nucleation events inside the gap per time unit, is given by [62, 63]

$$\omega = g_i p_{i+1} \mathcal{F} L, \qquad (6)$$

with g_i the nucleation (conditional) probability given that there are i monomers at the time of the $(i+1)$th deposition. For the

CP approach with irreversible attachment, $g_{i=1} \approx 0.47$ is independent of the gap length and $\omega \propto L^4$.

The results from the eCP method suggest that $g_{i>3} \sim L^{-(i-2)}$ and $g_{i=2} \sim (\log L)^{-0.875}$ when zero barriers are considered. In general, it can be shown that the nucleation rate behaves as $\omega \sim L^{\gamma} l_a^{\delta}$. Again, in the case of zero barriers, $\delta = 0$ and $\gamma = 4$ for $i = 1$, $\gamma \approx 6.785$ (large gaps) and $\gamma \approx 6.75$ (intermediate gaps) for $i = 2$ and $\gamma = 2i + 3$ for $i \geqslant 3$. The non-integer value of γ for $i = 2$ is related to the typical logarithmic corrections that appear when the dimension of the system is equal to the critical dimension d_c. On the other hand, in Regime II the presence of $i + 1$ monomers ensures nucleation, i.e. $g_i \approx 1$. Additionally, both eCP and MF results coincide $\gamma = 2i + 1$ and $\delta = i$ for all values of i. For the case $l_a \to \infty$, $\delta = 1$ and $\gamma = 2i + 3$.

Finally, both ω and $\mathcal{P}_n(m, L)$ strongly depend on the attachment barrier making it possible to use experimental data together with the eCP model to estimate the value of these barriers.

4. RE

One of the most extended methods for evaluating the time evolution of epitaxially growing layers is RE. However, these have a mean-field nature that ignores fluctuations of the island and monomer densities on the substrate, i.e. the local densities of monomers and islands are assumed to be well-described by their average values N_1 and N, respectively. This issue can be overcome by considering time-dependent capture kernels, which derive from the spatial fluctuations of the monomer density around a given island or monomer. It is customary to propose the following set of RE [20, 21, 56]:

$$\frac{dN_1}{d\theta} = \gamma - (i+1)\,\sigma_u \Re N_1\,\eta_i - \Re N_1 \sum_{S \geqslant i+1} \sigma_S N_S, \qquad (7)$$

$$\frac{dN_S}{d\theta} = \Re N_1\,(\sigma_{S-1} N_{S-1} - \sigma_S N_S), \qquad (8)$$

where η_S is the density of unstable clusters with size $1 \leqslant S \leqslant i$, $N_1 = \sum_{S=1}^{i} \eta_S$, and γ denotes the substrate fraction uncovered by islands, i.e. $\gamma = 1 - \theta + N_1$ for the EIM and $\gamma = 1 - N$ for the PIM, with $N = \sum_{S \geqslant i+1} N_S$ the total island density. Note that in equations (7) and (8) the nucleation term is proportional to $N_1\,\eta_{S=i}$, $\sigma_u = \sigma_{S=i}$, and $N_i = \eta_i$.

The evolution of the densities in terms of N can be reformulated by summing equation (8) over $s > i$, using the approximation $\eta_i \approx N_1^i$ [65] and defining the average aggregation kernel

$$\bar{\sigma} = \frac{1}{N} \sum_{S \geqslant i+1} \sigma_S N_S. \qquad (9)$$

In this way, equations (7) and (8) take the simpler form [20, 21, 56]:

$$\frac{dN_1}{d\theta} = \gamma - (i+1)\,\Re \sigma_u N_1^{i+1} - \bar{\sigma}\,\Re N_1 N, \qquad (10)$$

$$\frac{dN}{d\theta} = \Re \sigma_u N_1^{i+1}. \qquad (11)$$

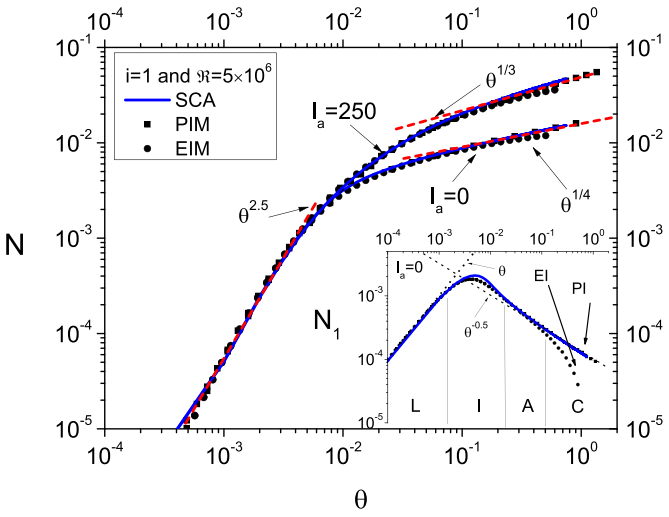

Figure 4. Island and monomer densities as a function of coverage for $i = 1$ and two different energy barriers $l_a = 0$ and $l_a = 250$; both the point (PIM) and extended (EIM) island models are considered. Dots correspond to the kMC results while the blue line corresponds to the self-consistent approach (SCA) presented in [21]. The inset shows the different evolution regimes: low-coverage (L), intermediate (I), aggregation (A), and coalescence (C) regimes.

This equation system is easier to analyze than the original one and provides the growth exponents for N_1 and N, which can be directly compared to experimental measurements. In EG standard protocol the monomers are deposited sequentially such that for early times (low-coverage or L regime) $N_1 = \theta$ and $N \approx 0$, as shown in figure 4. Once some islands are formed, a competition arises between nucleation and aggregation characterized by $N \approx N_1$ (intermediate or I regime). For later times, the system reaches a quasi-steady state (aggregation or A regime), in which the monomer deposition balances the monomer aggregation to preexisting islands, $N \gg N_1, dN_1/d\theta \ll 1$, and aggregation is the dominant process. The last regime is found at large coverage and is characterized by the coalescence of islands (C regime). Figure 4 displays the evolution of the monomer and island densities for irreversible attachment and $i = 1$ obtained by the self-consistent approach discussed in section 6. The inset there shows the behavior of N_1; as expected, the coalescence regime is reached at a lower coverage for the EIM than for the PIM. As can be seen, the intermediate regime starts approximately at $\theta \sim 10^{-3}$ and lasts until $\theta \sim 10^{-2}$. In this regime, N and N_1 do not have an algebraic dependence on the coverage and, since a competition between nucleation and aggregation takes place, both densities are comparable. In particular, the maximum value of N_1 is found when the deposition of monomers equals the monomers loss due to aggregation and nucleation.

For the aggregation regime it is expected [20] that the densities dependency on θ and $\Re$ follows

$$N_1 \sim \theta^{-\beta_1} \Re^{-\tilde{\omega}} \text{ and } N \sim \theta^{1-z} \Re^{-\chi}, \qquad (12)$$

where the exponents β_1, $\tilde{\omega}$, z and χ have been assessed using both experiments and kMC simulations [20, 21, 66]. The resulting data contradict the assumption of constant capture

kernels and therefore, the spatial fluctuations of the monomer density must be considered to evaluate the coverage dependence of σ_u and σ_S. In [20], the exponents were calculated analytically in the A regime for the point-island model with $i=1$. By taking into account the fluctuations of the monomer density around a given island, it results in $\tilde{\omega}=1/2$, $\beta_1=1/2$, $z=3/4$, and $\chi=1/4$; in contrast, $N=2\Re\theta^4$ for the L regime. These results were obtained assuming that the capture kernels follow $\sigma_1\sim\bar{\sigma}\sim N$ for the A regime and $\sigma_1\sim\bar{\sigma}\sim N_1$ for the L regime.

More refined analytical and numerical calculations were performed by Amar *et al* [21], where $N\approx(4/5)\,\Re^{1/2}\,\theta^{5/2}$ was found for the L regime, which is different from that reported in [20] but consistent with the kMC results, as can be seen in figure 4. According to Amar's approach, the capture kernel σ_1 is given by [21]

$$\sigma_1=\left(\frac{4}{\Re N_1\gamma}\right)^{1/2}. \tag{13}$$

The functional form of the capture kernel given by equation (13) describes well the numerical results for the whole pre-coalescence regime for both point and EIMs (see figure 4). In contrast, the MF approximation of [20] uses a two-regime model for σ_1. On the other hand, a crossover between L and A regimes is found, i.e. $N\approx N_1\approx\theta_c$, which is explicitly given by $\theta_c=(5/4)^{2/3}\,\Re^{-1/3}$ for $i=1$ [21]. For the parameters employed in figure 4, $\theta_c\approx0.007$ agrees with the numerical results. As shown in figure 4, the PIM and EIM only have differences in the coalescence regime, in the previous regimes both models give similar results.

The growth exponents depend on the critical size i but can also be affected by barriers hindering aggregation or nucleation. Based on previous works [58–62], a model with hindered aggregation was proposed in [66]. According to this model, monomers must hop onto an occupied site to be incorporated; if the occupied site is a stable island, the diffusion process is hindered by an additional attachment barrier E_a reducing the hopping rate to that site. The associated characteristic length $l_a=b\,[\exp(E_a/k_{\mathrm{B}}T)-1]$ measures the asymmetry between the hopping rates, so that the ratio between the probability P_{st} to move the monomer to a stable island and the probability P_{un} to move it to a site with fewer than $i+1$ monomers is given by $P_{\mathrm{un}}/P_{\mathrm{st}}=\exp(E_a/k_{\mathrm{B}}T)$. In this model, nucleation is independent of l_a.

Under this hypothesis, equation (13) applies for $i=1$ but σ_u can be assumed time-independent for $i>1$, which agrees with the well-known critical dimension for nucleation. This implies that in the L regime, the island density for $i>1$ behaves according to

$$N\sim\Re\theta^{i+2}. \tag{14}$$

On the other hand, in the aggregation regime, the densities and their associate growth exponents strongly depend on l_a. For $i=1$ and $l_a\ll1$ it is found

$$N_1(\theta)\sim\left(\frac{1}{\Re\theta}\right)^{\frac{1}{2}}\text{ and }N(\theta)\sim\left(\frac{\theta}{\Re}\right)^{\frac{1}{4}}, \tag{15}$$

Table 1. Growth exponents in the aggregation regime are defined according to $N\propto\Re^{-\chi}\theta^{\beta}$ and $N_1\propto\Re^{-\chi_1}\theta^{\beta_1}$. $^{(*)}$For $l_a\ll\bar{L}$, the entries for general i do not apply for $i=1$.

	i		$i=1$		$i=2$		$i=3$	
$l_a/\bar{L}$	$\ll1^{(*)}$	$\gg1$	$\ll1$	$\gg1$	$\ll1$	$\gg1$	$\ll1$	$\gg1$
χ	$\frac{i}{2i+3}$	$\frac{i}{i+2}$	1/4	1/3	2/7	1/2	1/3	3/5
χ_1	$\frac{2}{2i+3}$	$\frac{2}{i+2}$	1/2	2/3	3/7	1/2	1/3	2/5
β	$\frac{1}{2i+3}$	$\frac{1}{i+2}$	1/4	1/3	1/7	1/4	1/9	1/5
β_1	$-\frac{2}{2i+3}$	$-\frac{1}{i+2}$	−1/2	−1/3	−2/7	−1/4	−2/9	−1/5

while for $i=1$ and $l_a\gg1$

$$N_1(\theta)\sim\left(\frac{l_a}{\Re^2\theta}\right)^{\frac{1}{3}}\text{ and }N(\theta)\sim\left[\frac{\theta\,l_a^2}{\Re}\right]^{\frac{1}{3}}. \tag{16}$$

Analytical predictions and numerical results for $i=1$ are compared in figure 4. It is worth noting that the scaling behavior predicted by the RE agrees with the PIM but some discrepancies are present in the case of the EIM. For example, the aggregation regime lasts longer in the PIM than in the EIM since in the latter, regime A is interrupted by the appearance of the coalescence regime. For $i\geqslant2$ and zero barriers, σ_u is time independent and $\bar{\sigma}\sim N$. Therefore, the densities behave as

$$N_1(\theta)\sim\left(\frac{1}{\Re^{3/2}\theta}\right)^{\frac{2}{2i+3}}\text{ and }N(\theta)\sim\left(\frac{\theta}{\Re^i}\right)^{\frac{1}{2i+3}}, \tag{17}$$

In contrast, for $i\geqslant2$ and large barriers, $\bar{\sigma}\sim l_a^{-1}$ attains a constant value, and the densities follow

$$N_1(\theta)\sim\left(\frac{l_a}{\Re^2\theta}\right)^{\frac{1}{i+2}}\text{ and }N(\theta)\sim\left(\frac{\theta\,l_a^{i+1}}{\Re^i}\right)^{\frac{1}{i+2}}. \tag{18}$$

Assuming the general forms $N\propto\Re^{-\chi}\theta^{\beta}$ and $N_1\propto\Re^{-\chi_1}\theta^{\beta_1}$, the growth exponents for the A regime are summarized in table 1. In principle, the growth exponents can be used to determine the existence of aggregation or nucleation barriers, the diffusion coefficient, and the critical nucleus size i. Note that in the case of weak and large barriers, the quantities $N^2\cdot N_1$ and $N\cdot N_1$ are independent of the coverage, respectively. As discussed later, this is related to the behavior of $p(\ell)$ for large ℓ values. For arbitrary i, the crossover coverage θ_c between L and A regimes can be determined by equating the expressions for $N(\theta)$ for both regimes [66]. The crossover coverage found through this method and equations (15) and (18) is shown in table 2. We can conclude that, the crossover coverage and the corresponding island density increase with l_a. In fact, for $l_a\to\infty$ attachment is completely suppressed, and the aggregation regime disappears altogether. For instance, for $i=1$ and $\Re\approx10^6$, one would need $l_a\approx10^8$ in order to have $\theta_c=1$.

In the case of strong barriers, an aggregation occurs after many attempts of a monomer to be incorporated into a stable island. Therefore, for small coverage, aggregation is negligible and deposition is balanced by nucleation. This implies that, in

Table 2. Crossover coverage θ_c between the L and A regimes for arbitrary i in the cases of weak and strong barriers. In all cases, there are numerical factors of order unity.

θ_c	$l_a/\bar{L} \ll 1$	$l_a/\bar{L} \gg 1$
$i=1$	$\Re^{-1/3}$	$\left(l_a^4 \Re^{-5}\right)^{1/13}$
$i \geqslant 2$	$\Re^{-3/(2i+5)}$	$\left(l_a \Re^{-2}\right)^{1/(i+3)}$

contrast with the zero barrier case, there is an additional region in the crossover where the island density is proportional to the coverage $N \approx \theta/(i+1)$. This regime lasts until the critical coverage $\tilde{\theta}_c$ is reached. According to [66], the latter follows

$$\tilde{\theta}_c \approx (l_a+1)\,(i+1)^{(i+2)/(i+1)}\,\Re^{-i/(i+1)}. \tag{19}$$

In [67], a second quantization formalism is used to find analytical expressions for the RE governing the local density of monomers $n_1(x)$ at position x. This approach provides a more formal framework for deriving the RE and generalizes previous works where the local density around a given monomer or islands for irreversible attachment is calculated. The most remarkable difference between the expression given by the formal method of [67, 68] and previous approaches [12, 21] is that nucleation is described by the square of the local density of monomers $n_1^2(x)$ instead of the standard approximation $N_1 \cdot n_1(x)$. In the formal approach, the monomers form islands meeting at one spatial point. In contrast, in the approximation used in [12, 21], a monomer at position x nucleates an island with any other monomer in the system regardless of its position, which is unphysical. A detailed comparison of these approaches with kMC simulations is required to determine the impact of the formal approaches on the growth exponents.

Finally, motivated by experimental results [69–72] suggesting anomalously large values of the exponent χ, the effects of long-range Lévy diffusion in submonolayer EG were studied using kMC simulations [73] and RE [74]. The diffusion exponent μ defined as $\langle x^2(t)\rangle \sim t^{\mu}$ satisfies $\mu<1$ for subdiffusion and $\mu>1$ for superdiffusion. In particular, the effect of Lévy walks and flights on the exponent χ is calculated. The relation between the diffusion (μ) and Lévy (β_L) exponents is given by $\mu=1$ for $\beta_L \geqslant 2$, $\mu=3-\beta_L$ for $1 \leqslant \beta_L \leqslant 2$ and, $\mu=2$ for $\beta_L \leqslant 1$. For the case of one-dimensional Lévy walk, i.e. finite hopping velocity, the exponent χ is given by

$$\chi = \begin{cases} \frac{1}{4} & \beta_L \geqslant 2, \\ \frac{(3-\beta_L)}{2+(6-2\beta_L)} & 1 \leqslant \beta_L \leqslant 2, \\ \frac{1}{3} & \beta_L \leqslant 1. \end{cases}$$

In contrast, for Lévy flights, i.e. instantaneous hopping, the exponent behaves as

$$\chi = \begin{cases} \frac{1}{4} & \beta_L \geqslant 2, \\ \frac{1}{\beta+2} & \beta_L \leqslant 2, \end{cases}$$

The analytical results for χ agree with those from kMC simulations. However, P_s is almost the same for the case of long-range diffusion as for short-range diffusion suggesting that the main effect of long-range diffusion is to increase the scaling exponent χ rather than to alter the island-size distribution.

5. Gap length and capture zone distributions

As mentioned above, the spatial structure formed by the islands is crucial to describe the spatial fluctuations of the monomer density. To determine a discrete version of the gap length distribution for islands formed at step edges, an equilibrium model based on free energy minimization was proposed in [32]. Let $E_{\rm b}$ and $E_{\rm ad}$ be the island boundary energy and the adsorption energy at steps, respectively. For a substrate at temperature T, the free energy of a monomer is given by

$$F = 2KE_{\rm b} + (E_{\rm ad}-\mu)\,M_m - TS, \tag{20}$$

where μ is the chemical potential of the adsorbed atoms (monomers), S is the entropy term, K is the total number of islands, and M_m is the total number of monomers. Parameters K and M_m can be related to the energy barriers $E_{\rm ad}$ and $E_{\rm b}$ [32]. The entropy is given by

$$S_{\rm ent} \approx J\ln J - (J-K)\ln(J-K) - \sum_{i=1}^{\infty} K_i \ln K_i, \tag{21}$$

with $J = M_s - M_m$, M_s the number of lattice sites, and K_i the number of islands of size i. Equation (20) assumes that interactions between island boundaries are negligible. Moreover, its first term considers that monomers belonging to islands have lower free energy than monomers. The minimization of the free energy leads to the following discrete gap length distribution

$$p_j = K^2\,(M_s - M_m - K)^{j-1}\,(M_s - M_m)^{-j}, \tag{22}$$

where p_j is the probability of finding a gap of length equal to j lattice sites. The applicability of this model is discussed in section 9.

In [29] a fragmentation equation is proposed to describe the impact of nucleation on the gap length distribution for the aggregation regime in the case $i=1$. The probability density of finding a gap with scaled length $\ell = L/\bar{L}$, $p(\ell)$, satisfies the integro-differential equation

$$\ell\,\frac{{\rm d}p(\ell)}{{\rm d}\ell} + 2p(\ell) = -q_L(\ell) + 2q_x(\ell), \tag{23}$$

where $q_x(\ell)$ is the probability density that a given nucleation occurs at scaled position ℓ inside a gap of any size, and $q_L(\ell)$ is the probability density that a given nucleation occurs anywhere inside a gap of scaled length ℓ. Equation (23) has been corroborated by a rigorous derivation using the second quantization formalism in the continuum approximation [67].

In Blackman's original paper [20], $q_L(\ell)$ and $q_x(\ell)$ were estimated by using the (local) monomer density $n_1(x,L)$ inside a gap of length L in the aggregation regime. Assuming that in

this regime the monomer density inside a gap reaches a steady state, for which

$$\frac{\mathrm{d}^2 n_1(x,L)}{\mathrm{d}x^2} + \Re^{-1} \approx 0, \tag{24}$$

then $n_1(x,L) \approx \Re^{-1} x(L-x)/2$ [20]. Within this approximation, the distribution of nucleation sites for arbitrary i is given by

$$\mathcal{P}_n(x,L) = \frac{n_1^{i+1}(x,L)}{\int_0^L n_1^{i+1}(x,L)\,\mathrm{d}x}, \tag{25}$$

which helps define the fragmentation kernel $\psi(\lambda)$ as shown below. According to the MF approximation for $i=1$,

$$q_L(\ell) \propto p(\ell) \int_0^\ell n_1^2(x)\,\mathrm{d}x \quad \text{and}$$
$$q_x(\ell) \propto \int_\ell^\infty x^4 p(x)\,\psi(\ell/x)\,\mathrm{d}x,$$

with $\psi(\lambda) = L\int_0^L \mathrm{d}x\,\mathcal{P}_n(x,L)\,\delta(\lambda - x/L) = 30\lambda^2(1-\lambda)^2$ [20]. This implies $\omega \propto \ell^5$ for the nucleation rate inside a gap. As mentioned in section 3, later works [58–62] used kMC simulation to demonstrate that the MF approximation provides an excellent approximation for $\psi(\lambda)$ in the case of irreversible attachment. However, the 'exact' nucleation rate calculated in [58–62] is proportional to ℓ^4 instead of ℓ^5, so that MF approximation overestimates ω and leads to a distribution $p(\ell)$ that decays faster than that found by kMC simulations.

The asymptotic behavior of equation (23) was evaluated in [64] for different values of i, resulting

$$p(\ell) \sim \begin{cases} \ell^\alpha & \ell \to 0 \\ \ell^{-2}\exp(-c\,\ell^\gamma) & \ell \to \infty, \end{cases} \tag{26}$$

with c a constant, and the exponents α and γ determining the distribution behavior for small and large values of ℓ, respectively. The MF approach leads to $\alpha = i+1$ and $\gamma = 2i+3$ by assuming that nucleation is a rare event solely driven by monomer diffusion, i.e. $i+1$ monomers are necessary to create a stable island and the probability of nucleation is proportional to $n_1^{i+1}(x,L)$ (see equation (25)) [29, 64].

For the PIM and $i=1$, [23, 64, 75, 76] present extensive numerical simulations devoted to analyzing the $p(\ell)$ tails. The behavior $p(\ell) \sim \ell^2$ for $\ell \ll 1$ and $p(\ell) \sim \ell^{-2}\exp(-C\ell^3)$ for $\ell \gg 1$ was found in [23], where it is suggested that the large gap behavior is a manifestation of the conserved quantity $12N^2N_1\Re \approx 1.6$, which corresponds to the third moment of $p(\ell)$. Similarly, simulation results of the gap length distribution for irreversible attachment were explored in [64] for different values of i. The numerical results (α_{num} y γ_{num}) obtained from kMC simulation [67] for the exponents defined in equation (26) are summarized in table 3 and compared to results from the MF approximation and the eCP method. It must be noted that the exponents (α_{num} y γ_{num}) are effective exponent; for instance, in the CP approach for $i=1$ and $l_a=0$, $\omega \sim L^4$ implying $\gamma = 4$ while the 'average' value of the gap ensemble is $\gamma_{\text{num}} \approx 3.1$, suggesting the existence of gaps for which the nucleation rate is lower than that predicted by the CP approach.

Table 3. Exponents α and γ defining the asymptotic behavior of the gap length distribution in equation (26). Results from the mean-field approximation (MF), kMC simulations (num), and the extended Castellano-Politi method (eCP) are included.

i	$\alpha_{\text{MF}} = i+1$	α_{num}	$\gamma_{\text{MF}} = 2i+3$	γ_{num}	γ_{eCP}
0	1	0.88	3	2.5	N/A
1	2	1.7	5	3.1	4
2	3	2.8	7	4.4	6.875
3	4	2.7	9	5.1	9

Both, the MF approximation and the eCP overestimate the exponent of the nucleation rate. In the case of the MF approach, the discrepancies originate from the complete disregard of the correlations between the $i+1$ monomers. In turn, the failure of the eCP method is rooted in the assumption that the monomer density profile has already reached its steady-state value in larger gaps at the time of nucleation.

The effect of an aggregation barrier on the gap length distribution was considered in [66]. For finite barriers, both eCP and MF approximations fail to describe nucleation inside a gap, leading to distributions that decay faster than these found by kMC simulations. As expected, the distribution $p(\ell)$ for finite barrier decays slower than the case with zero barrier. The presence of large gaps in which the monomer density cannot reach its steady state before fragmentation leads to the formulation of a two-regime fragmentation kernel [66]. In this way, the following empirical nucleation rate was suggested

$$\omega(\ell) \propto \ell^\gamma \text{ with } \gamma = \begin{cases} \gamma_{\text{ex}} - 1 & \text{if } \ell > \ell_c \\ \gamma_{\text{ex}} & \text{if } \ell \leqslant \ell_c, \end{cases} \tag{27}$$

where ℓ_c is an unknown fit parameter determining the scaled gap length below which the monomer density reaches the steady state before nucleation occurs. On the other hand, γ_{ex} is an integer exponent depending on l_a and i. For $l_a = 0$, γ_{ex} is given by the exponents shown in table 3 [64]. For the strong barrier case, $\gamma_{\text{ex}} = 3$ for $i=1$ and $\gamma_{\text{ex}} = 4$ for $i=2$. As natural, the presence of an aggregation barrier decreases the exponent of the nucleation rate. Additionally, the results presented in [66] suggest that $p(\ell) \sim \ell^\alpha$ for strong barriers with $0 < \alpha < 1$. This is a consequence of the fact that, even for strong barriers, the density of monomers is equal to zero in the vicinity of a given island.

Mulheran *et al* [76] presented a more recent approach than Blackman's [20] for the description of $p(\ell)$, which applies the distributional fixed-point equation (DFPE) for island nucleation to both point and extended islands. DFPE is expressed by

$$\ell \triangleq \lambda(1+\ell), \tag{28}$$

where ℓ is the normalized gap length, $\psi(\lambda)$ is the probability density of fragmenting such gap into sections with lengths λ and $1-\lambda$, and a is an independent random variable with such

probability density. The symbol $\triangleq$ implies that the quantities on the left and the right sides of the DFPE share the same distribution. Then, the main assumption of this approach is that the functional form of $p(\ell)$ does not change by nucleation except for a scale factor. The latter leads to the integral equation

$$p(\ell) = \int_0^{\min(x,1)} p\left(\frac{\ell}{\lambda} - 1\right) \frac{\psi(\lambda)}{\lambda} \mathrm{d}\lambda, \tag{29}$$

which assumes that the distribution of the gap lengths is unchanged by fragmentation.

According to the MF approach the function $\psi(\lambda)$ can be approximated by using equation (25). DFPE relates the fragmentation probability distribution within the gaps with the consequent gap size distribution $p(\ell)$. DFPE and the fragmentation approach lead to the same asymptotic behavior for $p(\ell)$ in the limit $\ell \to 0$. However, although the analytical behavior given by the solution of equation (29) for $\ell \to \infty$ is unknown, numerical evidence shows different asymptotic behaviors in this limit for DFPE and fragmentation approach. Indeed, DFPE predicts a distribution that decays slower than the kMC result. These discrepancies are attributed to using an MF approach for the nearest-neighbor gap sizes and neglecting longer-range correlations. The latter are expected to be more relevant for larger gaps created early in the growth process when the functional form of $p(\ell)$ strongly depends on the coverage θ. Nonetheless, the numerical solution of equation (28) describes properly the simulation results.

The gap length distribution relates directly to the average island concentration at a distance x around a given island, $c(x)$. It has been shown that [56, 77, 78]

$$p(\ell) = c(\ell) \exp\left(-\int_0^{\ell} \mathrm{d}x\, c(x)\right). \tag{30}$$

with the concentration related to the probability of nucleation. In the MF approach, the latter is written as the square of the density of monomers and therefore $c(x) \sim \tilde{n}_1^2(x)$ where $\tilde{n}_1(x)$ is the density of monomers around an island.

On the other hand, the capture zone (CZ) of an island is defined as the distance between the midpoints of its adjacent gaps (see figure 3). The CZ distribution is related to the gap length distribution between next-nearest neighbor islands [23]. To explore the possibility of finding a universal distribution for arbitrary i and dimension d, the ansatz

$$P_w(y) = a_w y^w \exp\left(-b_w y^2\right), \tag{31}$$

was proposed, i.e. that $P(y)$ followed the Wigner distribution, with a_w and b_w normalization constants, and $w = (2/d)(i+1)$ [24]. This result is the focus of some controversy leading to a broad discussion on the shape of the gap length and capture zone distributions [23, 64, 75, 76]. Extensive numerical simulations suggest that this ansatz can be used to describe those distributions around the maxima but fails to describe their tails.

As a first approximation, the CZ distribution can be estimated by the convolution of two gap length distributions [20, 23]

Table 4. kMC results for the exponent γ for the gap length and capture zone distribution, γ_g and γ_c, respectively [64]. Equation (32) only provides satisfactory results for $i = 0$. However, the functional form provided by equation (33) is satisfied by the kMC results for all the considered i values [64].

i	γ_g	γ_c
0	2.51	2.73
1	3.13	4.18
2	4.36	5.88
3	5.09	7.20

$$P(y) = \int \mathrm{d}x\, p(x)\, p(2y - x), \tag{32}$$

which intrinsically assumes that the lengths of two consecutive gaps are uncorrelated. Using the asymptotic ($\ell \to \infty$) form of the gap length distribution given by equation (26) into equation (32), it can be shown that [29]

$$P(y) \sim \begin{cases} y^{2\delta+1} & y \ll 1 \\ y^{2\delta+1-\gamma/2} \exp\left(-2cy^{\gamma}\right) & y \gg 1. \end{cases} \tag{33}$$

For the particular case of the MF approximation, $P(y) \sim y^{-9/2-i} \exp\left(-2cy^{2i+3}\right)$ for large y and $P(y) \sim y^{2i+3}$ for small y. Note that equation (32) implies that both $p(\ell)$ and $P(y)$ decay with the same exponent γ for large ℓ. However, simulation results in [64] show that this is not the case with $P(y)$ decaying faster than $p(\ell)$. Table 4 displays the results found in [64] for the γ exponents of GL and CZ distributions; both exponents coincide only when $i = 0$ and their difference increases with i. This suggests that the correlations between adjacent gaps cannot be neglected and equation (32) overestimates the exponent γ. O'Neill *et al* [64] explains this result by realizing that the nucleation rate decreases significantly over time for larger critical island sizes, hinting at less well-mixed systems. Additionally, for $i = 0$ the island nucleation is driven by monomer deposition while for $i > 0$, it is driven by monomer diffusion and deposition.

The CZ distribution also provides information about the aggregation capture kernel of an island. The capture kernel of a given island, σ_s, can be calculated using the local density of monomers inside a gap with length L, $n_1(x, L)$ and equating the global capture rate of a monomer $D\sigma_s N_1$ to the local rate $2D\left[\mathrm{d}n_1(x, L)/\mathrm{d}x\right]_{x=0}$. The case of irreversible attachment was considered [21] and later generalized for finite aggregation barriers l_a [56]. According to these studies, the capture kernel of an island having a CZ of length y is

$$\tilde{\sigma}_s(y) = \frac{2\xi_u}{\gamma \xi_1^2} \frac{\tanh(\tilde{y}/2)}{1 + l_a \xi_u^{-1} \tanh(\tilde{y}/2)}, \tag{34}$$

where ξ_u and ξ_1 are the nucleation and monomer capture lengths, respectively, and $\tilde{y} = y/\xi_1$ [21, 56]. The capture

lengths are completely defined by the capture kernels according to

$$\frac{1}{\xi^2} = \frac{1}{\xi_u^2} + \sum_{s \geqslant i+1} \sigma_s N_s \tag{35}$$

and

$$\frac{1}{\xi_u^2} = (i+1)\,\sigma_u N_i^i . \tag{36}$$

For zero and small barriers, $\tilde{\sigma}_s(y)$ is proportional to the hyperbolic tangent of the CZ length. In contrast, for strong barriers, $\tilde{\sigma}_s \approx 2/(\gamma l_a)$ implies that the local capture kernel becomes independent of the CZ length. Hence, the CZ offers insight into the spatial structure formed by the islands and also sheds light on the aggregation rate. It should be noted that $P(y)$ and $p(\ell)$ provide mutually complementary information. Several systems are recognized to exhibit the same gap length distribution, yet they display different capture zone distributions [79].

On the other hand, the notion of gap length distribution and the approach of the fragmentation equation have been discussed in different contexts [78, 80–82]. Therefore, the methods used for EG can be applied to other one-dimensional systems described by an array of points. For instance, [83, 84] report the distribution of distances (gaps) between adjacent parked cars in London, which is modeled using equation (23) in [78, 81]. In the car parking context, $q_L(\ell)$ is the probability that a driver chooses a gap with scaled length ℓ to park, while $\mathcal{P}_n(x,L)$ is the probability to park at a position x inside a gap with length L. It is reasonable to assume that the driver should avoid parking too close to the cars on the borders of the gap to guarantee enough space to leave the gap when necessary. This ansatz implies that $\mathcal{P}_n(x=0,L) = \mathcal{P}_n(x=L,L) = 0$, similar to what happens in the case of one-dimensional EG. Furthermore, [78] shows that the results $\psi(\lambda) = 2\sin^2(\pi\lambda)$ and $\gamma = 4$ give an excellent fit to the empirical data presented in [83, 84]. The value of γ shows the natural strong preference of drivers to park in large gaps rather than in small ones.

6. Island size distribution

The island size distribution $P_s = N_s/N$ is one of the most extensively measured quantities in EG experiments. Several empirical models have been proposed to explain the experimental findings. For instance, Amar and Family [85] suggested a coverage-independent distribution in the aggregation regime given by

$$P_s = A_i\, s^i \, \exp\left(-\mathrm{i}\, B_i\, s^{1/B_i}\right), \tag{37}$$

where C_i and a_i are fitting parameters that depend on the critical nucleus size i.

Based on the results of many extensive MC simulations, Bartelt and Evans demonstrated that the island density takes the form [11, 86, 87]

$$N_s \sim \theta \bar{S}^{-2} f(s), \tag{38}$$

with $f(s)$ a universal scaling function of i, independent of coverage and deposition rate and $s = S/\bar{S}$. From the continuum limit of the RE, it can be shown that $f(s)$ is related to the scaled capture number distribution, $C(s) = \sigma_s/\bar{\sigma}$, according to

$$f(s) = f(0)\exp\left[\int_0^s \mathrm{d}x\, \frac{2z - 1 - C'(x)}{C(x) - zx}\right], \tag{39}$$

where the parameter z is the dynamical exponent related to the time evolution of the average island size $\bar{S} \sim \theta^z$, and the constant $f(0)$ is determined by the normalization condition $\int_0^\infty \mathrm{d}s f(s) = 1$.

Perhaps the most common approach to theoretically estimate P_s is based on the solution of RE. The time evolution of the island size distribution for a given set of capture kernels (σ_u and σ_s) can be evaluated from the solution of equations (7) and (8). Unfortunately, analytical solutions are available for a few specific kernel cases. One example is the simple case of size and coverage independent kernels, i.e. constant kernels $\sigma_s = \bar{\sigma}$. For large coverage, it can be shown that [56]

$$N_{s+i+1} \approx \frac{\sigma_u}{\sqrt{\pi}\,\bar{\sigma}} \int_z^\infty \mathrm{d}v \exp\left(-v^2\right) \left[\sqrt{2\tau}\,(v-z)\right]^{-i\chi(1+\chi)}, \tag{40}$$

where χ is the growth exponent defined by $N_1 \sim \theta^{\beta_1}$, $z = (s-\tau)/\sqrt{2\tau}$ and $\tau = \bar{\sigma}\,\Re\int_0^\theta N_1\,\mathrm{d}\theta'$.

Whenever the aggregation barrier can be considered infinite, the formation of islands with a size larger than $i+1$ is very unlikely. Consequently, the aggregation capture kernel can be taken as constant. In most cases, the capture kernel of an island (σ_s) strongly depends on both the coverage and the island size, and equation (40) does not apply. A second case in which analytical solutions can be found is presented [88], where the RE are solved in the continuum limit for a kernel given by the power-law $\sigma_s/\sigma_1 = m s^{(m-1)/m}$, with m a constant depending on the growth model. This assumption gives rise to universal, time-invariant size distributions that depend only on m.

Another example of an analytical expression for P_s is given in [32], in which a 1D lattice gas at thermodynamic equilibrium was introduced to model the size distribution of monoatomic wires formed at step edges. As described in section 5, starting from an analytic expression for the system free energy, the minimization procedure leads to a (unscaled) size distribution that depends only on the island density and coverage, given by

$$P_S = \frac{K_S}{K} = K\,(M_m - K)^{S-1}\, M_m^S, \tag{41}$$

where K and M_m denote the total number of islands and monomers, respectively.

For most realistic cases it is necessary to resort to numerical schemes to solve the RE. For example, [89] presents a method to evaluate the island size distribution for the EIM with

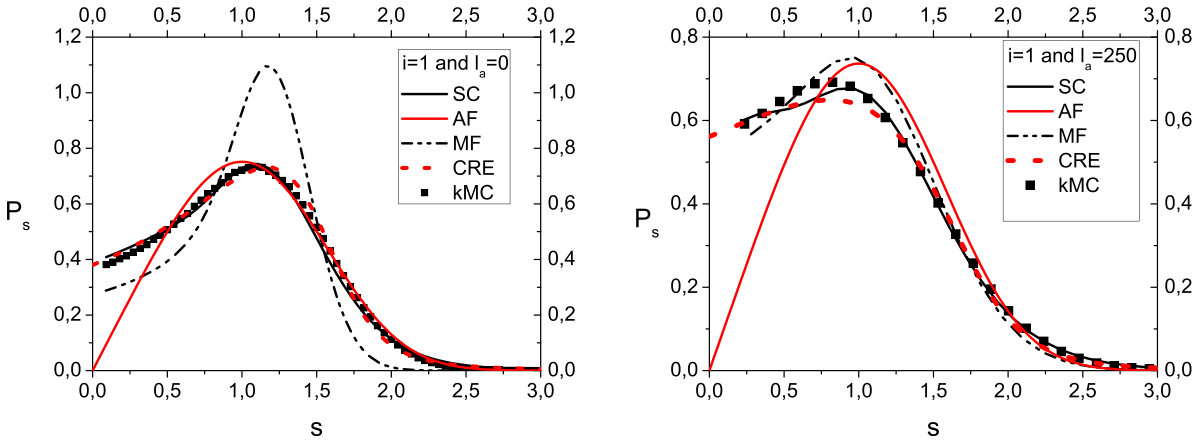

Figure 5. Island size distribution for point islands with $i = 1$ and attachment barriers $l_a = 0$ (left) and $l_a = 250$ (right) at coverage $\theta = 0.25$ and $\Re = 5 \times 10^6$ [56]. Symbols correspond to kMC simulations, while continuous and dotted lines correspond to the self-consistent (SC) and mean-field (MF) approaches. The red line corresponds to the Amar and Family equation (AF, equation (38)). As usual, P_s is normalized according to $\sum_s P_s = 1$ and $\bar{s} = \sum_s s P_s = 1$.

$i = 1$. This approach is based on the solution of difference-differential RE assuming that the unscaled island size distribution can be written as

$$P_S = \theta^S (1-\theta)^2 \sum_{n=0}^{\infty} \varphi_{n,S}(\theta) \frac{\Re^n}{n!}, \tag{42}$$

where $\varphi_{n,S}(\theta)$ represent the coefficients of the Taylor expansion, which must be calculated numerically. In contrast with the other approaches, this method does not assume that $\Re$ tends to infinity nor a scaled form for P_S. In this way, its main advantage is that it allows the evaluation of P_S with high precision for finite values of $\Re$.

As previously shown, the capture kernels and the distributions $p(\ell)$, P_{cz}, and P_s are related quantities that provide complementary details about the microscopic process associated with EG and allow the analysis and interpretation of experimental results. In fact, the connection between $P(y)$ and P_s is indirect; as shown in [90], P_s displays a mean-field behavior in $d = 4$ whereas $P(y)$ does not exhibit such behavior. The explicit relation between $p(\ell)$, P_{cz} and P_s remains unknown.

In an attempt to mutually relate these quantities, a self-consistent (SC) rate-equation approach to irreversible submonolayer growth with $i = 1$ was developed in [21, 91, 92]. This approach considers the correlations between the island size and the corresponding average capture zone. The method requires the numerical integration of the RE for the island size distribution and the analytical solution of a set of approximate equations for the evolution of the average CZ surrounding an island of size s. As the main assumption, the average capture size per freshly nucleated dimer is considered proportional to the average length per island. Moreover, by uniformly rescaling the average CZ of each island, the combined effect of both the preferred nucleation of dimers in large capture zones and the preferred 'breakup' of large capture zones due to nucleation is approximated. This self-consistent scheme was generalized to incorporate the effect of hindered aggregation on the island formation processes for arbitrary nucleus size i [56]. A major advantage of the SC approach is the possibility of calculating P_s for arbitrary coverage values in excellent agreement with results from kMC simulations, as shown in figures 4 and 5.

In the regime of zero and weak barriers, P_s is a monomodal distribution with a well-defined maximum. On the contrary, this distribution becomes a monotonically decreasing function for large enough barriers. In fact, theory predicts $P_s \to \delta_{s,i+1}$ as $l_a \to \infty$, and therefore islands with size $i+1$ are the only ones formed. This result can be explained as follows. The formation of large islands requires the aggregation of several monomers into smaller islands. However, the typical time of aggregation for a gap of length L increases for large l_a values by a factor $6l_a/L$ compared to the case of zero barriers. For strong barriers, the formation of large islands requires a significantly longer time than in the case of zero and weak barriers. Additionally, nucleation events occur more frequently than aggregation ones for large l_a values; at a given coverage, this leads to a decrease in the average island size for large barriers measured against the case of weak barriers.When no barrier is present, the most probable island size is larger than the average $\bar{s}$; in contrast, the aggregation is hindered for large barriers, the distribution becomes monomodal, and it is more likely to find islands with size $i+1$.

On the other hand, an explanation for experimental results [93–95] showing mono- and bimodal P_s distributions has been provided in [96, 97]. In these works, a 1D model including diffusion, aggregation, and detachment of particles from islands in the post-deposition regime, i.e. without flux, was studied using computer simulations. For completely reversible attachment, the system lacks an equilibrium or steady state. Moreover, the average island size has three different regimes from which the long-time one corresponds to an exponential decay of P_s. Nevertheless, for partially reversible attachment, a sequence of four aggregation regimes is found with P_s featuring a pronounced peak for small i. This result is explained

in terms of the stability of small islands, which stops giving monomers away to the largest ones at earlier times.

A related study focuses on the effects of lattice mismatch and long-range repulsive interactions that prevent the formation of large islands [98]. This work proposed a model including diffusion, attachment, and detachment, where the detachment rate of particles at the (stable or unstable) cluster edges increases with the cluster size. Depending on the temperature and the coverage, the functional form of the island size distribution changes from monomodal to monotonically decreasing. This is a remarkable result because both types of distribution have been reported for island growth near step edges of vicinal surfaces [32, 35]. Indeed, the distribution shape is quite sensitive to the detachment rate; for instance, rapidly increasing detachment rates preventing the formation of large islands lead to peaks very close to the average size and to rapidly decreasing tails. Conversely, slowly decreasing rates provide peaks close to half the average size and fat right tails. These results can be used to interpret experimental data in real systems and differentiate the mechanisms that work against large island formation.

7. Numerical simulation

Most of the simulation studies designed to describe the time evolution of monomer and island densities in EG are based on the kMC algorithms using solid-on-solid models [15, 20, 23, 66]. Growth is initiated by the random deposition of monomers at a rate $\mathcal{F}$ per site onto an empty one-dimensional lattice (substrate) with length L. Usually, re-evaporation is forbidden implying that coverage $\theta = \mathcal{F}t$. This condition can be reached experimentally by setting the appropriate temperature. The hopping rate at which any monomers hops to a neighbor site is determined by the configuration-dependent Arrhenius-type expression $r(T) = D\exp(-nE_N/k_{\rm B}T)$ with $D = (2k_{\rm B}T/h)\exp(-E_S/k_{\rm B}T)$ the free atom migration rate, and $n = 0, 1, 2$ the number of lateral nearest-neighbors before the hop occurs. The parameter E_N defines a pair bond energy, k_B is the Boltzmann constant, and T is the temperature. The original kMC algorithm considers a one-dimensional array with $N_1L + 1$ cells. The first N_1L cells have length $r(T)$ and correspond to diffusion events. The last cell has a length $\mathcal{F}L$ associated with deposition. A random number between 0 and $N_1L + \mathcal{F}L$ allows the selection of a cell and the specific process of the system evolution. If the kth cell ($1 \leqslant k \leqslant N_1L$) is chosen, the kth monomer is selected to hop to one of its nearest neighbors. If the last cell is selected, a new monomer is deposited at a random site on the lattice. The physical time is updated by $\Delta t = -\log r_a/(r(T)N_1L + \mathcal{F}L)$ where $0 \leqslant r_a \leqslant 1$ is a uniformly distributed random number.

In practice, it is more convenient to implement an equivalent algorithm [15] in which the total rate associated with hops and depositions are given by $R_h = rN_1L$ and $R_d = \mathcal{F}L$, respectively. At each simulation step, one process between hop and deposition is selected with probabilities [15, 20]

$$p_h = \frac{2\Re N_1}{1 + 2\Re N_1} \quad \text{and} \quad p_d = \frac{1}{1 + 2\Re N_1}, \tag{43}$$

and a new monomer is randomly deposited on the substrate if deposition occurs. The algorithm described before can be simplified considering that $2\Re N_1$ hops of the monomers happen on average between consecutive depositions. Therefore, each time a monomer is deposited, $2\Re N_1$ diffusive moves of monomers are made and the physical time is tracked using the coverage θ.

In most simple EG models, deposition on occupied sites is forbidden. If a hop is selected, a free monomer is randomly chosen and displaced to one of its nearest neighbors. For unbiased diffusion, the hop probability to the left or right is 1/2. However, barriers hindering aggregation or nucleation can be included by decreasing the probability of hopping into occupied sites [56, 63, 66].

The described algorithms can be applied for both extended or PIMs. Furthermore, nucleation and aggregation can be treated in different ways. For instance, when an irreversible attachment is considered, a monomer is irreversibly captured if it is deposited on or hops onto an occupied site. Similarly, nucleation or aggregation occurs when the site is occupied by either a monomer or an island [90].

Evans and Bartelt introduced monomer-monomer and monomer-island short-range interactions in simulation procedures [11, 14]. In these works, nucleation or aggregation occurs when a monomer is deposited on or diffuses to the nearest neighbor site of an occupied site. For point islands, irreversible attachment ($i = 1$), and finite $\Re$, simulation results show that $P(y)$'s peak increases with $\Re$ for $d = 1$, in contrast to higher dimensions behavior. The dependence of the peak height on $\Re$ is more relevant for the model without short-range interactions than for Evans and Bartelt's model. However, the asymptotic functional form of $P(y)$ is almost independent of model details such as the short-range interaction.

Although the algorithms described before are quite simple, the simulation of EG is challenging as it must be implemented in the $\Re \to \infty$ limit. To improve the efficiency of the simulations, [99] proposes an alternative method to simulate one-dimensional EG. The method is based on the idea that given a stochastic system whose evolution can be divided into non-interacting parts for some periods, then the kinetics of each part can be simulated independently. In this way, a 1D lattice with L sites and periodic boundary conditions is considered, in which monomers can be classified according to the monomer-monomer and monomer-island separation lengths. At the time t a configuration consists of $n_{\rm A}$ active monomers, $n_{\rm B}$ boxed (passive) monomers, and n islands, where passive monomers are those located too far away from islands or other monomers, and evolve according to an analytical approach instead of kMC rules. Therefore, the box of a given passive monomer is an imaginary region of the space where its evolution can be calculated analytically due to the absence of other islands or monomers. The gain in the speed of the simulation is achieved because as long as passive monomers stay within the boxes, it is unnecessary to employ computational resources in their evolution. The original algorithm allows simulating EG for $i = 1$ and large values $\Re \sim 10^{12}$ and $L \sim 10^7$, while its generalization to higher i allows the numerical evaluation of $p(\ell)$ and $P(y)$ asymptotic behaviors [64].

8. Two-Step growth protocol

A novel EG protocol based on two different steps was proposed in [28]. In the first step, a small quantity of monomers is deposited simultaneously on the substrate at random positions. This step finishes when the last monomer nucleates forming a new island or aggregates to a previously formed one. However, the predominant reaction during this step is nucleation, and then $N_1 + 2N \approx \theta_0$, with θ_0 the density of monomers at the beginning of the first step. During the second step, additional monomers are sequentially deposited on the substrate at a controlled rate $\mathcal{F}$. These additional monomers are more likely to attach to the islands formed during the first step than to nucleate new ones. Therefore, aggregation is the predominant reaction in the second step. A major advantage of the two-step growth (2SG) protocol is that nucleation and aggregation occur in different time regimes. Then the two processes are well separated by design, allowing a better control and understanding of the island formation mechanism. Another advantage is that both $p(\ell)$ and $P(y)$ can be accurately approximated with the Gamma probability distribution [100, 101]

$$P(y) = \frac{\beta^\beta}{\Gamma(\beta)} y^{\beta-1} \exp(-\beta y). \tag{44}$$

Assuming that the gaps between neighbor islands are not correlated, $P(y)$ can be calculated from the convolution of two gap length distributions (see equation (32)). This implies that the shape/scale parameter β for $P(y)$ is twice the corresponding one to $p(\ell)$. In [101] it was shown that

$$\begin{aligned} p(\ell) &= a\theta_0^2 \ell \exp(-a\theta_0 \ell) \quad \text{and} \\ P(y) &= \frac{8}{3} a^4 \theta_0^4 y^3 \exp(-2a\theta_0 y), \end{aligned} \tag{45}$$

where a is the fraction of nucleated monomers, with $a = 0$ at $t = 0$ and $a = 2N/\theta_0$ at the end of the first step. For large $\Re$ values, nucleation is negligible, and equation (45) remain valid during the second step. In contrast, the gap length distribution remains unknown for the standard protocol based on the sequential deposition of monomers during the whole process.

Moreover, in the first step of the 2GS protocol, the gap length distribution is related to the monomer density according to

$$N_1 \approx N \int_0^\infty \mathrm{d}\ell \bar{n}_1 \ell p(\ell), \tag{46}$$

where $\bar{n}_1$ is the average local density of monomer inside a gap of length ℓ.

Since nucleation is negligible during the second step, the RE can be simplified. For the case $i = 1$, equation (8) can be rewritten as

$$\frac{\mathrm{d}N_S}{\mathrm{d}\tau} = \begin{cases} -\sigma_2 N_2 & S = 2 \\ \sigma_{S-1} N_{S-1} - \sigma_s N_S & S > 2, \end{cases} \tag{47}$$

where the transformation $\tau = D\int_0^t N_1(t)\mathrm{d}t$ has been considered. Assuming that coverage is θ_0 at the beginning of the second step and that the island distribution satisfies the initial condition $N_{S=2}(t=0) = \theta_0/2$ and $N_{S>2}(t=0) = 0$, the solution of equation (47) in the Laplace space results [100]

$$\tilde{N}_S(z) = \frac{\theta_0}{\bar{S}} \sigma_S \prod_{k=2}^{S} \frac{\sigma_k}{z + \sigma_k}, \tag{48}$$

with $\bar{S} = \sum_{S=2}^\infty S P_S$. This result can be numerically inverted for a given set of capture kernels. In the simplest case of constant kernels, $\sigma_k = \sigma$, the island size distribution is given by

$$N_S(\tau) = \frac{N}{(S-2)!} \tau^{S-2} \exp(-\tau), \tag{49}$$

with $\bar{S} = \tau + 2$ [56].

The effect of hindered reactions in the 2SG protocol was studied in [101]. As natural, the nucleation barrier affects the evolution during the first step only, while the aggregation barrier appears exclusively in the second step. The simulation results suggest that the time evolution of the monomer density strongly depends on the values of the barriers. Concurrently, different barrier values could lead to the same island size distribution even if $p(\ell)$ and $P(y)$ are different. This hints that $p(\ell)$ and $P(y)$ are more sensitive to the energy barriers than P_s, showing that these distributions provide complementary information. Then, none of them alone completely describes the statistical behavior of the system.

A summary of the most important results of [101] for the gap length distributions and monomer density is shown in table 5. It is important to highlight that equations (32) and (49) remain valid for all barrier limits shown in table 5. For all the regimes considered, $p(\ell)$ decays exponentially, implying that the island nucleation probability for points far away from the islands edges can be taken as constant. In contrast, for $\ell \ll 1$, both the monomer density and the nucleation probability strongly depend on the distance from the island, especially for strong nucleation and aggregation barriers where $\vartheta \to \infty$. On the other hand, the long time behavior for N_1 can be calculated using equation (46), which relates the global density N_1 to the local density inside a gap with a given length. In all cases, it results found $N_1 \sim t^{-\xi} \exp\left[-(t/\bar{\tau}_a)^\zeta\right]$ with ξ and ζ exponents depending on the barrier strength, and $\bar{\tau}_a$ is the global aggregation time. Moreover, equation (46) predicts an exponential factor that is not present in the results given by the RE.

Table 5. Key results from [101] for the gap length distribution evaluated for different nucleation (l_n) and aggregation (l_a) barriers.

Nucleation length Aggregation length	$l_a = 0$ $l_n = 0$	$l_a \gg 1$ $l_n = 0$	$l_a = 0$ $l_n \gg 1$	$l_a \gg 1$ $l_n \gg 1$
$p(\ell) \sim \ell^\vartheta$ $(\ell \ll 1)$	$\vartheta = 1$	$\vartheta = 1$	$\vartheta = 1$	$\vartheta \to \infty$
$p(\ell) \sim \exp(-\mathrm{C}\,\ell)$ $(\ell \gg 1)$	$\mathrm{C} = 2$	$\mathrm{C} = 2$	$\mathrm{C} = 3$	$\mathrm{C} = 2$
$N_1 \sim t^{-\xi}\exp(-t^\zeta)$	$\xi = 1/6$ $\zeta = 1/3$	$\xi = 3/8$ $\zeta = 0$	$\xi = 1/6$ $\zeta = 1/3$	$\xi = 3/8$ $\zeta = 1/2$

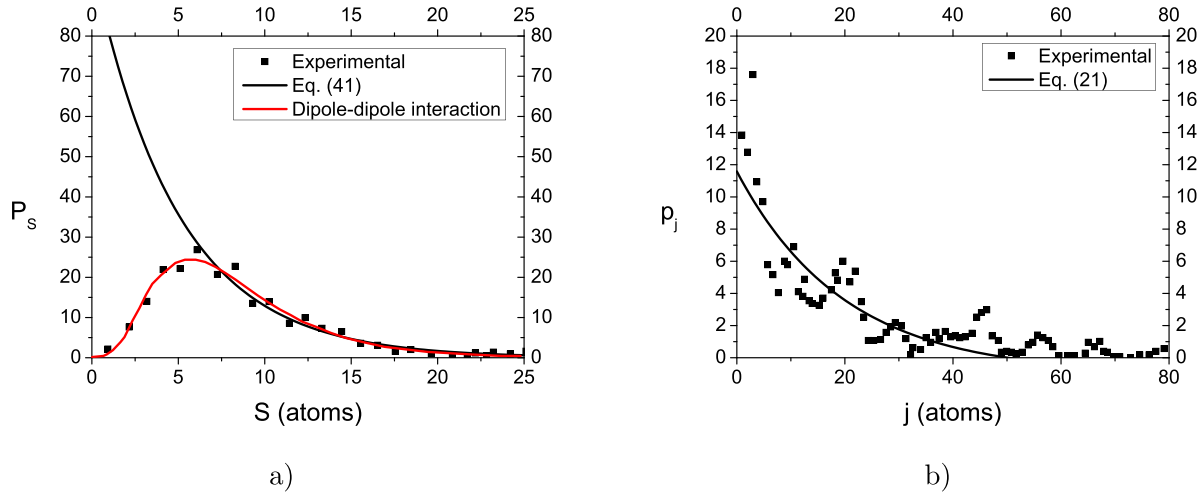

Figure 6. (a) Island size and (b) gap length distributions for Ag 1D wires grown at the step edges of a Pt(997) surface. Lines and dots correspond to analytical and experimental results, respectively. The data were taken from [32, 102].

9. Experimental results and applications

One of the most common methods for producing one-dimensional islands is the deposition on stepped surfaces. For example, the growth of Ag 1D wires at the step edges of a Pt(997) surface was analyzed in [32]. The P_s and $p(\ell)$ distributions were measured and compared to the equilibrium ones obtained from the discrete model given by equations (22) and (41), as shown in figure 6. Although the functional form of the gap length distribution is well described by the theoretical model (i.e. equation (22)), the island size distribution is predicted to be a monotonically decreasing function showing important differences with the experimental results in the case of small islands. The experimental P_S is well described by the analytical approach only for large islands sizes. Despite its simplicity and the absence of any fitting parameter, the proposed discrete model partially captures the physics determining P_s and $p(\ell)$.

To improve the comparison presented in [32], Tokar and Dreyssé considered additional interactions unaccounted for in the original model, which leads to length distributions fitting the experimental data with higher accuracy [102]. The inclusion of a dipole-dipole interaction proportional to r^{-3}, where r is the interatomic distance, modifies the energy of the islands giving origin to a non monotonic distribution which reproduces quite well the experimental results (see left panel of figure 6). Further, it is found that the chain energy as a function of its length exhibits a positive curvature attributable to repulsive forces.

Similarly, kMC simulations [95] describe well the monotonic decay of P_s for Co/Cu(775) and Ag/Pt(997) at temperatures of 160 and 190 K, respectively [32]. These results suggest that P_s depends not only on external parameters such as temperature and deposition rate but also on the duration of the experiment, since the lifetime of many one-dimensional structures at low temperatures can significantly exceed the duration of the experiment, these structures remain in a non-equilibrium state. Moreover, the simulation also revealed that a transition from one equilibrium state to another occurs at heating or cooling through a non-equilibrium state, which is observed in most experiments.

Another example of island formation on stepped surfaces is given in [93], and modeled in [22]. There, the self-assembly of uniform Co quantum wires on a vicinal Cu(111) surface was studied by scanning tunneling microscopy (STM). In contrast to other works, two phases of one- and two-atom-wide Co wires are found depending on coverage. Additionally, Co wires assemble only at the lower terrace of a step edge, unlike previous results where top-only or top-bottom step-edge Co island growth was observed. To explain these results, a simple model for reversible growth of 1D nanowires on the steps of vicinal surfaces has been proposed [22]. Using RE and kMC, the authors analyzed the fast qualitative change of the island size distribution as the system evolves from the low-temperature deposition to the high-temperature post-deposition annealing. This change occurs when the average size of the islands before the annealing is larger than that after the annealing. In the case of no deposition, the average island size decreases when monomers detach from large islands while small islands grow at their expense, which is called anti-ripening in [22]. The anti-ripening process produces in the course of its evolution bimodal and monotonous P_s distributions with functional forms distinct from those associated with equilibrium situations. This phenomenon offers a theoretical explanation of the island size distributions reported in [93].

In the same vein, a kMC simulation study of the formation of 1D cobalt chains on copper vicinal surfaces is presented in [94]. The growth process is determined exclusively by kinetic parameters such as the temperature, flux of deposited atoms, and degree of coating rather than by the binding energy or quantum effects. The binding energies obtained in this work were several times larger than the experimental ones found in [93]. This discrepancy arises because the islands are

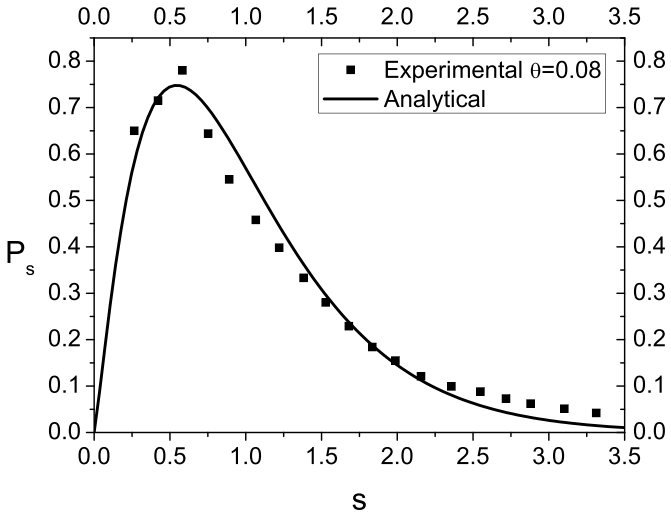

Figure 7. Island length distribution for monoatomic Ga chains grown on Si(100) surface at coverage $\theta = 0.08$. Dots corresponds to experimental data while the line corresponds to the solution of the RE with linear capture kernels $\sigma_S = a + S$. Data were taken from [103].

meta-stable structures, whose length is determined by diffusion barriers rather than by the binding energy, which in turn implies that the latter cannot be determined from P_s.

A second method to produce one-dimensional structures is based on the anisotropic diffusion of monomers across the substrate surface. For instance, single-atom-wide Ga rows were assembled by deposition of Ga on Si(100) surfaces at room temperature [35]. It was found that the experimental P_s is monotonically decreasing, which is an unexpected outcome for a system with homogeneous nucleation and no desorption. Results from kMC simulations suggest that this behavior arises from the significant capture inhibition of diffusing atoms occurring in Ga/Si(100).

Some experimental results of [35] were discussed in the light of the RE for irreversible heterogeneous growth at nucleation centers [103]. This theoretical approach assumes capture coefficients that depend linearly on size; then the RE solution for P_s can be written using the Polya distribution and satisfies the scaling hypothesis for large lengths. This approach farly fits the experimental length distributions of linear chains of indium and galium grown on Si(100) surfaces, as shown in figure 7. Dubrovskii *et al* [103] analyses different coverage values and, in all cases, P_s is well described for large s values with some discrepancies for small island sizes.

In a related study, one-dimensional chains of atomic indium were grown on a Si(100) surface at room temperature, and analyzed by STM and kMC simulations [34]. In particular, the island density and the island-size distribution were obtained for different coverages θ and deposition rates $\mathcal{F}$. As the main result, it was found that the monotonous decrease of P_s at low coverage is a consequence of the detachment of indium atoms from the islands, decreasing correlations between the positions of adjacent islands.

Finally, it is worth discussing briefly some works related to colloidal epitaxy. Due to the characteristic size and time scales of colloidal particles, both nucleation and aggregation in self-assembled colloidal monolayers can be experimentally observed with a resolution equivalent to the particle size [2, 104, 105]. Since both the range and strength of the monomer-monomer and monomer-substrate interactions can be easily tuned for colloidal particles, [50, 51] explores the application of colloidal systems to test generic theoretical models for EG. It is found that the established analytical tools used in MBE can describe the simulation results for a one-dimensional system under the two-step growth protocol. In these references, analytical results are compared with extensive simulations based on molecular dynamics (MD). A major advantage of MD simulations is that any assumptions about the relevant processes or their associated rates are required. Moreover, it is possible to study the interplay between the thermal energy and the energy associated with monomer-monomer, monomer-island, monomer-substrate, and islands-substrate interactions. Strong interactions favor nucleation and aggregation processes but decrease the mobility of monomers on the substrate. Similarly, it has been proposed that the self-assembly of colloidal structures can be explored experimentally using colloidal particles confined to microgrooved channels, on which the deposition can be controlled by phoretic flows [106]. Another possibility is the use of optical tweezers [107] which can be employed to manipulate the initial number of islands of the second step by configuring seed structures [108].

10. Conclusions and perspectives

One-dimensional structures can be fabricated using stepped surfaces or anisotropic diffusion. The nature and properties of the resulting structure depend on several parameters, such as temperature, pressure, deposition rate, lattice constants, etc. The growth protocol also plays a primordial role. In the standard protocol based on the sequential deposition of monomers, both nucleation and aggregation occur simultaneously; this leads to quite different gap length and capture zone distributions from those assembled using the two-step growth protocol. Despite advances in the individual description of each of the fundamental processes involved in EG, such as deposition, diffusion, nucleation, or aggregation, a complete understanding of the interplay among them remains unreachable.

Films grown by epitaxy techniques often evolve away from thermodynamic equilibrium, and their morphology is determined by kinetics. The out-of-equilibrium processes related to EG are complex; their understanding is crucial to improving the control over the final layer structure, which strongly depends on the phenomena occurring at the early stages of the process. Yet in the simplest models, several out-of-equilibrium processes are required to describe the system kinetics. Each of these processes has an associated time scale, and their relevance depends on the temperature as these are thermally activated. For instance, high temperatures activate the detachment of monomers from the substrate and the islands. So far, there is no unified analytical method to describe all physical phenomena involved in layer growth. None of the methods discussed

here offers a complete depiction of the complex phenomena associated with EG; for instance, despite the achievements facilitated by theoretical tools like fragmentation equations or RE, the role of nucleation and aggregation on the functional form of the island size, gap length, and capture zone distributions remains a topic of ongoing debate.

For one and two-dimensional systems it is possible to perform detailed kMC simulations for large values of $\Re$ and large evolution times. However, kMC simulations assume the knowledge of all the relevant processes and the associated characteristic times, which are not necessarily known. On the other hand, simulations based on MD require an approximation for the interaction potentials but implicitly consider all the processes. Unfortunately, performing MD simulations for long evolution times is computationally expensive.

It is worth emphasizing that the RE for EG has been extensively investigated for about forty years. Yet, controversial issues remain related to the functional forms of capture kernels and their dependence on the coverage. In addition, information about microscopical parameters such as typical nucleation and aggregation times, and critical nucleus size, encompassed in measurable quantities such as $N_1, N, P_s, p(\ell)$ or $P(y)$ requires further studies for a more complete understanding of the knowledge that can be acquired from experimental results. Moreover, the mutual relation between the main quantities used to describe the system such as P_s, $P(y)$, and $p(\ell)$ remains unknown.

Numerical evidence indicates that the nature of the nucleation depends on the length of the gap, as the monomer density seems to reach the steady state faster in small gaps than in large ones. This is evident in the behavior of $P(y)$ and $p(\ell)$, which can be described using a two-regime model based on two different nucleation mechanisms. Some efforts to clarify this relation include self-consistent expressions that require numerical solutions or approximations for the joint probability distribution to find an island with length S and capture zone y. The extraction of microscopical parameters from experimental results requires reliable expressions linking them to measurable quantities. Unfortunately, it is usual for different expressions to lead to different microscopic quantities. Similarly, the presence of energy barriers hindering nucleation and aggregation processes impacts the functional form of the island size distribution. For example, large aggregation barriers lead to a monomodal behavior for P_s while a bimodal behavior is found with zero barriers.

A major advantage of the 2SG protocol is that the nucleation and aggregation processes occur at different stages of film growth. This separation improves the understanding and control of the growth process; however, this protocol has not yet been explored experimentally. Similarly, experimental realizations of one-dimensional EG are not as well explored as their two-dimensional counterpart. However, efforts aimed at the EG of one-dimensional structures have been increasing in recent years, opening the door to the validation and refining of the theoretical frameworks proposed up to date.

Data availability statement

All data that support the findings of this study are included within the article (and any supplementary files).

Acknowledgments

DLG thanks support from Vicerrectoría de Investigaciones, Universidad del Valle (C.I. 71369). MC thanks Universidad Antonio Nariño (VCTI-UAN) for financial support through Project No 2023202.

ORCID iDs

Juan David Álvarez-Cuartas https://orcid.org/0009-0005-3884-1539
Diego Luis González-Cabrera https://orcid.org/0000-0002-1528-7345
Manuel Camargo https://orcid.org/0000-0003-0276-2650

References

[1] Evans J, Thiel P and Bartelt M C 2006 *Surf. Sci. Rep.* **61** 1–128
[2] Einax M, Dieterich W and Maass P 2013 *Rev. Mod. Phys.* **85** 921
[3] Tan C, Chen J, Wu X-J and Zhang H 2018 *Nat. Rev. Mater.* **3** 17089
[4] Zou J 2023 *Nanoscale Adv.* **5** 3129
[5] Mei X, Kim D, Ruda H and Guo Q 2002 *Appl. Phys. Lett.* **81** 361–3
[6] Hattori A N, Fujiwara Y, Fujiwara K, Nguyen T V A, Nakamura T, Ichimiya M, Ashida M and Tanaka H 2015 *Nano Lett.* **15** 4322–8
[7] Rakshit R, Hattori A N, Naitoh Y, Shima H, Akinaga H and Tanaka H 2019 *Nano Lett.* **19** 5003–10
[8] Zhang F, Saito K, Tanaka T, Nishio M, Arita M and Guo Q 2014 *Appl. Phys. Lett.* **105** 162107
[9] Zhang F, Saito K, Tanaka T, Nishio M and Guo Q 2014 *J. Cryst. Growth* **387** 96–100
[10] Sidik U, Hattori A N, Hattori K, Alaydrus M, Hamada I, Pamasi L N and Tanaka H 2022 *ACS Appl. Electron. Mater.* **4** 4849–56
[11] Bartelt M C and Evans J W 1992 *Phys. Rev.* B **46** 12675–87
[12] Bales G S and Chrzan D C 1994 *Phys. Rev.* B **50** 6057–67
[13] Mulheran P A and Blackman J A 1996 *Phys. Rev.* B **53** 10261–7
[14] Evans J W and Bartelt M C 2002 *Phys. Rev.* B **66** 235410
[15] Amar J G, Family F and Lam P-M 1994 *Phys. Rev.* B **50** 8781–97
[16] Cullen W and First P 1999 *Surf. Sci.* **420** 53–64
[17] Müller B, Nedelmann L, Fischer B, Brune H, Barth J V and Kern K 1998 *Phys. Rev. Lett.* **80** 2642–5
[18] Wasniowska M, Wulfhekel W, Przybylski M and Kirschner J 2008 *Phys. Rev.* B **78** 035405
[19] Cox E, Li M, Chung P W, Ghosh C, Rahman T S, Jenks C J, Evans J W and Thiel P A 2005 *Phys. Rev.* B **71** 115414
[20] Blackman J A and Mulheran P A 1996 *Phys. Rev.* B **54** 11681–92

[21] Amar J G, Popescu M N and Family F 2001 *Surf. Sci.* **491** 239–54
[22] Tokar V I and Dreyssé H 2011 *Phys. Rev.* B **84** 085456
[23] González D L, Pimpinelli A and Einstein T L 2011 *Phys. Rev.* E **84** 011601
[24] Pimpinelli A and Einstein T L 2007 *Phys. Rev. Lett.* **99** 226102
[25] Pimpinelli A and Einstein T 2010 *Phys. Rev. Lett.* **104** 149602
[26] Li M, Han Y and Evans J W 2010 *Phys. Rev. Lett.* **104** 149601
[27] Oliveira T J and Aar ao Reis F D A 2011 *Phys. Rev.* B **83** 201405
[28] Tokar V and Dreyssé H 2015 *Surf. Sci.* **637–638** 116–23
[29] Blackman J, Grinfeld M and Mulheran P 2015 *Phys. Lett.* A **379** 3146–8
[30] Morgenstern K, Kibsgaard J, Lauritsen J V, Lægsgaard E and Besenbacher F 2007 *Surf. Sci.* **601** 1967–72
[31] Repain V, Rohart S, Girard Y, Tejeda A and Rousset S 2006 *J. Phys.: Condens. Matter* **18** S17
[32] Gambardella P, Brune H, Kern K and Marchenko V I 2006 *Phys. Rev.* B **73** 245425
[33] Kučera M, Kocán P, Sobotík P, Majer K and Ošt'ádal I 2017 *Phys. Rev.* B **96** 045430
[34] Javorský J, Setvín M, Ošt'ádal I, Sobotík P and Kotrla M 2009 *Phys. Rev.* B **79** 165424
[35] Albao M A, Evans M M R, Nogami J, Zorn D, Gordon M S and Evans J W 2005 *Phys. Rev.* B **72** 035426
[36] Albia J R and Albao M A 2017 *Phys. Rev.* E **95** 042802
[37] Thelander C *et al* 2006 *Mater. Today* **9** 28–35
[38] Patolsky F, Zheng G and Lieber C M 2006 *Nanomedicine* **1** 51–65
[39] Wang W, Lv F, Lei B, Wan S, Luo M and Guo S 2016 *Adv. Mater.* **28** 10117–41
[40] Alhalaili B, Peksu E, Mcphillips L N, Ombaba M M, Islam M S and Karaagac H 2023 4 - nanowires for photodetection *Photodetectors* (*Woodhead Publishing Series in Electronic and Optical Materials*) 2nd edn, ed B Nabet (Woodhead Publishing) pp 139–97
[41] Capper P, Irvine S and Joyce T 2007 *Epitaxial Crystal Growth: Methods and Materials* (Springer) pp 271–301
[42] Herman M A, Richter W and Sitter H 2004 *Metal Organic Vapor Phase Epitaxy* (Springer) pp 171–200
[43] Krapivsky P L 1994 *Phys. Rev.* E **49** 3233–8
[44] Krapivsky P L 1991 *J. Phys. A: Math. Gen.* **24** 4697
[45] Kallabis H, Krapivsky P and Wolf D 1998 *Eur. Phys. J.* B **5** 801–4
[46] Kyuno K, Gölzhäuser A and Ehrlich G 1998 *Surf. Sci.* **397** 191–6
[47] Maroutian T, Douillard L and Ernst H-J 1999 *Phys. Rev. Lett.* **83** 4353–6
[48] Risken H and Risken H 1996 *Fokker-Planck Equation* (Springer)
[49] González D L, Camargo M and Sanchez J 2018 *Rev. Cienc.* **21** 37
[50] Álvarez-Cuartas J D, Camargo M and González-Cabrera D L 2024 *Phys. Rev.* E **109** 064604
[51] Camargo M and González D L 2022 *J. Phys.: Condens. Matter* **34** 144006
[52] Du Y, Xu B, Wang G, Miao Y, Li B, Kong Z, Dong Y, Wang W and Radamson H H 2022 *Nanomaterials* **12** 741
[53] Mondal M and Ganapathy R 2022 *Phys. Rev. Lett.* **129** 088003
[54] Nozawa J, Uda S, Niinomi H, Okada J and Fujiwara K 2022 *J. Phys. Chem. Lett.* **13** 6995–7000
[55] Sato M 2024 *Sci. Rep.* **14** 3245
[56] González D L, Camargo M and Sánchez J A 2018 *Phys. Rev.* E **97** 052802
[57] Popescu M N, Amar J G and Family F 2001 *Phys. Rev.* B **64** 205404
[58] Castellano C and Politi P 2001 *Phys. Rev. Lett.* **87** 056102
[59] Politi P and Castellano C 2002 *Phys. Rev.* E **66** 031605
[60] Politi P and Castellano C 2002 *Phys. Rev.* E **66** 031606
[61] Politi P and Villain J 1996 *Phys. Rev.* B **54** 5114–29
[62] Krug J, Politi P and Michely T 2000 *Phys. Rev.* B **61** 14037–46
[63] González D L 2016 *J. Phys. A: Math. Theor.* **50** 035001
[64] O'Neill K P, Grinfeld M, Lamb W and Mulheran P A 2012 *Phys. Rev.* E **85** 021601
[65] Walton D 1962 *J. Chem. Phys.* **37** 2182–8
[66] González D L, Pimpinelli A and Einstein T L 2017 *Phys. Rev.* E **96** 012804
[67] Tokar V I and Dreyssé H 2017 *J. Phys. A: Math. Theor.* **50** 375002
[68] Tokar V I and Dreyssé H 2013 *J. Stat. Mech.* **2013** 06001
[69] Winkler A and Tumbek L 2013 *J. Phys. Chem. Lett.* **4** 4080–4
[70] Morales-Cifuentes J R, Einstein T L and Pimpinelli A 2014 *Phys. Rev. Lett.* **113** 246101
[71] Tumbek L and Winkler A 2012 *Surf. Sci.* **606** L55–L58
[72] Pimpinelli A, Tumbek L and Winkler A 2014 *J. Phys. Chem. Lett.* **5** 995–8
[73] Amar J G and Semaan M 2016 *Phys. Rev.* E **93** 062805
[74] Amar J G, Family F and Hughes D C 1998 *Phys. Rev.* E **58** 7130–6
[75] Grinfeld M, Lamb W, O'Neill K P and Mulheran P A 2011 *J. Phys. A: Math. Theor.* **45** 015002
[76] Mulheran P A, O'Neill K P, Grinfeld M and Lamb W 2012 *Phys. Rev.* E **86** 051606
[77] Redner S and Ben Avraham D 1990 *J. Phys. A: Math. Gen.* **23** L1169
[78] González D L and Einstein T L 2011 *Phys. Rev.* E **84** 051135
[79] González D L and Téllez G 2007 *Phys. Rev.* E **76** 011126
[80] Olesen P, Ferkinghoff-Borg J, Jensen M H and Mathiesen J 2005 *Phys. Rev.* E **72** 031103
[81] Krapivsky P L 1992 *J. Stat. Phys.* **69** 135–50
[82] Ziff R M and McGrady E D 1985 *J. Phys. A: Math. Gen.* **18** 3027
[83] Rawal S and Rodgers G 2005 *Physica* A **346** 621–30
[84] Seba P 2008 *J. Phys. A: Math. Theor.* **41** 122003
[85] Amar J G and Family F 1995 *Phys. Rev. Lett.* **74** 2066–9
[86] Bartelt M C, Tringides M C and Evans J W 1993 *Phys. Rev.* B **47** 13891–4
[87] Bartelt M and Evans J 1993 *Surf. Sci.* **298** 421–31
[88] Dubrovskii V G and Sibirev N V 2014 *Phys. Rev.* B **89** 054305
[89] Petrov P, Miller W, Rehse U and Fornari R 2011 *Appl. Math. Modelling* **35** 1331–6
[90] Shi F, Shim Y and Amar J G 2009 *Phys. Rev.* E **79** 011602
[91] Amar J G, Popescu M N and Family F 2001 *Phys. Rev. Lett.* **86** 3092–5
[92] Amar J G, Family F and Popescu M N 2002 *Comput. Phys. Commun.* **146** 1–8
[93] Zaki N, Potapenko D, Johnson P D and Osgood R M 2009 *Phys. Rev.* B **80** 155419
[94] Syromyatnikov A G, Saletsky A M and Klavsyuk A L 2018 *JETP Lett.* **107** 766–9
[95] Syromyatnikov A G, Saletsky A M and Klavsyuk A L 2019 *JETP Lett.* **110** 348–51
[96] Gambardella P, Blanc M, Brune H, Kuhnke K and Kern K 2000 *Phys. Rev.* B **61** 2254–62
[97] Chame A and Aarão Reis F 2007 *Physica* A **376** 108–16
[98] Stinchcombe R B and Aar ao Reis F D A 2008 *Phys. Rev.* B **77** 035406

[99] Tokar V I and Dreyssé H 2008 *Phys. Rev.* E **77** 066705
[100] Tokar V I and Dreyssé H 2015 *Phys. Rev.* E **92** 062407
[101] Sánchez J A, González D L and Einstein T L 2019 *Phys. Rev.* E **100** 052805
[102] Tokar V I and Dreyssé H 2007 *Phys. Rev.* B **76** 073402
[103] Dubrovskii V G, Berdnikov Y S and Sokolova Z V 2015 *Tech. Phys. Lett.* **41** 242–5
[104] Ganapathy R, Buckley M R, Gerbode S J and Cohen I 2010 *Science* **327** 445–8
[105] Rupich S M, Castro F C, Irvine W T and Talapin D V 2014 *Nat. Commun.* **5** 5045
[106] Singh N, Vladisavljević G T, Nadal F m c, Cottin-Bizonne C, Pirat C and Bolognesi G 2020 *Phys. Rev. Lett.* **125** 248002
[107] Villada-Balbuena A, Ortiz-Ambriz A, Castro-Villarreal P, Tierno P, Castaneda Priego R and Méndez-Alcaraz J M 2021 *Phys. Rev. Res.* **3** 033246
[108] Hermes M, Vermolen E C M, Leunissen M E, Vossen D L J, van Oostrum P D J, Dijkstra M and van Blaaderen A 2011 *Soft Matter* **7** 4623–8